

Ingebjørg Eggen Skarbøvik

# Evaluation of On-site Wind Pressure Coefficients Compared to Standard Coefficients

A case study of the natural ventilation potential in the ZEB Laboratory

Master's thesis in Energy and Environment Engineering

Supervisor: Hans Martin Mathisen

June 2023



Ingebjørg Eggen Skarbøvik

# **Evaluation of On-site Wind Pressure Coefficients Compared to Standard Coefficients**

A case study of the natural ventilation potential in the ZEB Laboratory

Master's thesis in Energy and Environment Engineering  
Supervisor: Hans Martin Mathisen  
June 2023

Norwegian University of Science and Technology  
Faculty of Engineering  
Department of Energy and Process Engineering





# Preface

This Master's thesis is a part of the subject *TEP4910 - Energy and Indoor Environment, Master's Thesis*, conducted for the Department of Energy and Process Engineering at the Norwegian University of Science and Technology (NTNU) during the spring of 2023. The thesis is a part of the two-year MSc program *Energy and Environment Engineering* and accounts for 30 ECST credits.

This thesis is a continuation of the project thesis, *Evaluating the Method for Measuring and Calculating Wind Pressure Coefficients*, completed in the fall of 2022. I want to thank Tore Kvande, Odne Oksavik, and Thomas Lassen for their help and assistance with the on-site measurements at the ZEB Laboratory. I want to thank my supervisor Professor Hans Martin Mathisen for his guidance and advice during the work throughout the semester. I would also like to thank co-students, friends, and family for their help, support, and encouragement.

**Trondheim, June 11, 2023**

Ingebjørg Eggen Skarbøvik

**Ingebjørg Eggen Skarbøvik**

# Abstract

The building sector is currently the largest energy-consuming sector and a big contributor to CO<sub>2</sub> emissions. A significant amount of this energy is used for heating, cooling, and domestic hot water. By integrating solutions such as PV panels for local electricity production, optimized daylighting, and natural ventilation as air conditioning, buildings can achieve a comfortable indoor environment while also reducing energy costs. Zero emission buildings (ZEB) are buildings where solutions and technology are utilized to compensate for the greenhouse gas emissions of the buildings during their lifetime. The ZEB Laboratory located at the Gløshaugen campus in Trondheim is an example of such a building, and is an office building with permanent working spaces. The building is used for experiments on energy production, ventilation, heating and cooling, and more. This Master's thesis aims to investigate the effect of utilizing on-site wind pressure coefficients compared to standard coefficients in simulations. Natural ventilation is implemented in the building through a window control algorithm.

An important part of this Master's thesis was to evaluate the on-site wind pressure coefficient specific to the ZEB Laboratory. 15 differential pressure sensors and a reference sensor were used to measure the pressure difference between the inside and outside of the building. The measurements were conducted for 10 weeks, and the resulting pressures were used to calculate the specific coefficients of the building. Uncertainties with the equipment and a limited amount of sufficient data available to use in the calculations resulted in varying degrees of reliability with the wind pressure coefficients. Improvement in the results can be achieved by conducting the pressure measurements for a longer period of time to gather more data.

Wind pressure coefficients obtained from the evaluation were incorporated into IDA ICE, and simulations were carried out for one week at the end of July with a simplified model of the ZEB Laboratory. A window control algorithm was implemented in the model to allow for natural ventilation through automatic windows in the building. The simulations revealed minimal differences between the on-site and standard pressure coefficients, and both simulations resulted in an acceptable indoor environment with all parameters within the acceptable range, and no occupational hours where the temperature exceeded 26°C. Furthermore, the draught risk in the building was found to be low during a day with low wind velocities during the summer. The differences between the two sets of coefficients could be attributed to low wind velocities during the simulated week, where the buoyancy effect will be the main contributor to natural ventilation in the building.

The simulation results indicate that the window control algorithm works as intended to allow natural ventilation of the ZEB Laboratory. However, the algorithm was developed for use during the cooling season, and modifications can be made to the setpoints to optimize the use of natural ventilation during the heating season.

# Sammendrag

Byggesektoren er i dag den største energiforbrukende sektoren i tillegg til å være en stor bidragsyter til CO<sub>2</sub> -utslipp. En betydelig mengde av denne energien brukes til oppvarming, kjøling og varmtvann til husholdningsbruk. Ved å integrere løsninger som solcellepaneler for lokal elektrisitetsproduksjon, optimalisert dagslys og naturlig ventilasjon som klimaanlegg, kan bygninger oppnå et komfortabelt innemiljø samtidig som energikostnadene reduseres. Nullutslippsbygg (ZEB) er bygninger der løsninger og teknologi benyttes for å kompensere for bygningenes klimagassutslipp i løpet av levetiden. ZEB-laboratoriet lokalisert på Gløshaugen i Trondheim er et eksempel på et slikt bygg og er et kontorbygg med faste arbeidsplasser. Bygget skal brukes til forsøk på energiproduksjon, ventilasjon, oppvarming og kjøling, med mer. Denne masteroppgaven skal undersøke effekten av å bruke spesifikke vindtrykkskoeffisienter for bygget sammenlignet med standardkoeffisienter i simuleringer. Naturlig ventilasjon er implementert i bygget gjennom en vinduskontrollalgoritme.

En viktig del av denne masteroppgaven var å evaluere vindtrykkskoeffisientene, som er spesifikke for ZEB-laboratoriet. 15 differensialtrykksensorer og en referansesensor ble brukt for å måle trykkforskjellene mellom innsiden og utsiden av bygget. Målingene ble utført i 10 uker, og de resulterende trykkene ble brukt til å beregne koeffisientene til bygget. Usikkerhet med utstyret som ble brukt og begrenset tilgang på tilstrekkelig data til bruk i beregningene resulterte i varierende grad av pålitelighet med vindtrykkskoeffisientene. Forbedring av resultatene kan oppnås ved å gjennomføre differensialtrykkmålingene over lengre tid for å samle mer data.

Vindtrykkskoeffisientene fra evalueringen ble lagt inn i IDA ICE, og simuleringer ble gjennomført i en uke i slutten av juli med en forenklet modell av ZEB-laboratoriet. En vinduskontrollalgoritme ble implementert i modellen for å tillate naturlig ventilering gjennom automatiske vinduer i bygningen. Simuleringene avdekte minimale forskjeller mellom de spesifikke trykkoeffisienter til bygget og standard koeffisienter, og begge simuleringene resulterte i et akseptabelt innemiljø med alle parametere innenfor det akseptable området, og ingen arbeidstimer der temperaturen oversteg 26°C. Videre er trekkrisikoen i bygget vurdert til å være lav i løpet av en typisk dag med lave vindhastigheter om sommeren. Forskjellene mellom de to settene med koeffisienter kan tilskrives lave vindhastigheter i løpet av den simulerte uken, hvor oppdriftseffekten vil være den viktigste bidragsyteren til naturlig ventilasjon i bygget.

Simuleringsresultatene indikerer at vinduskontrollalgoritmen fungerer etter hensikten for å tillate naturlig ventilering av ZEB-laboratoriet. Algoritmen ble imidlertid utviklet for bruk i kjølesesongen, og det kan gjøres endringer i settpunktene for å optimalisere bruken av naturlig ventilasjon i fyringssesongen.

# Contents

<b>Preface</b>	<b>i</b>
<b>Abstract</b>	<b>ii</b>
<b>Sammendrag</b>	<b>iii</b>
<b>Nomenclature</b>	<b>vii</b>
<b>Abbreviations</b>	<b>viii</b>
<b>List of Figures</b>	<b>ix</b>
<b>List of Tables</b>	<b>xii</b>
<b>1 Introduction</b>	<b>1</b>
1.1 Scope . . . . .	1
1.2 Limitations . . . . .	2
1.3 Structure of this Master's thesis . . . . .	2
<b>2 Indoor environment</b>	<b>3</b>
2.1 Thermal environment . . . . .	3
2.1.1 Temperature . . . . .	3
2.1.2 Draught . . . . .	4
2.1.3 Relative humidity . . . . .	4
2.1.4 Activity level . . . . .	5
2.1.5 Clothing level . . . . .	5
2.2 Thermal comfort . . . . .	6
2.2.1 PMV - Predicted mean vote . . . . .	6
2.2.2 PPD - Predicted percentage dissatisfied . . . . .	7
2.2.3 Adaptive thermal comfort model . . . . .	8
2.3 Atmospheric environment . . . . .	8
2.3.1 Carbon dioxide concentrations . . . . .	8
2.3.2 Other pollutions . . . . .	9
2.3.3 Age of air . . . . .	9
2.4 Consequences of poor indoor environment . . . . .	9
<b>3 Building ventilation</b>	<b>10</b>
3.1 Mechanical ventilation . . . . .	10
3.1.1 Control strategies . . . . .	11
3.2 Natural ventilation . . . . .	11
3.2.1 Wind-driven ventilation . . . . .	12
3.2.2 Buoyancy-driven ventilation . . . . .	12
3.2.3 Combined buoyancy and wind-driven ventilation . . . . .	14
3.2.4 Advantages and disadvantages with natural ventilation . . . . .	14
3.3 Natural ventilation in Nordic climate . . . . .	15
3.4 Cooling of buildings with natural ventilation . . . . .	16
3.4.1 Operation of windows . . . . .	17
3.4.2 Night cooling . . . . .	18
3.5 Hybrid ventilation . . . . .	18
3.5.1 Approaches to hybrid ventilation . . . . .	19



3.6	Distribution of ventilated air . . . . .	20
3.6.1	Mixing ventilation . . . . .	20
3.6.2	Displacement ventilation . . . . .	20
<b>4</b>	<b>Principles of natural ventilation</b>	<b>21</b>
4.1	General principles . . . . .	21
4.1.1	Continuity principle . . . . .	21
4.1.2	Bernoulli equation . . . . .	22
4.1.3	Flow through a simple opening . . . . .	22
4.2	Air pressure . . . . .	22
4.2.1	Wind effects . . . . .	23
4.2.2	Pressure gradients . . . . .	24
4.2.3	Wind pressure coefficient . . . . .	25
4.3	Air jets . . . . .	26
<b>5</b>	<b>Zero Emission Buildings</b>	<b>28</b>
5.1	ZEB ambition levels . . . . .	28
5.2	ZEB Laboratory . . . . .	29
5.2.1	Building structure . . . . .	30
5.2.2	Floor plan . . . . .	31
5.2.3	Ventilation strategy in the ZEB Laboratory . . . . .	32
5.2.4	Surroundings of the ZEB Laboratory . . . . .	32
5.3	IDA ICE as a simulation tool . . . . .	33
<b>6</b>	<b>Method</b>	<b>35</b>
6.1	Measurements in the ZEB Laboratory . . . . .	35
6.1.1	Setup of the measurements and equipment . . . . .	35
6.1.2	Reference freestream pressure measurement . . . . .	38
6.1.3	Weather station . . . . .	39
6.2	On-site calibration of the Sensirion sensors . . . . .	39
6.3	Calculations and measurements compensations . . . . .	40
6.3.1	Voltage to differential pressure . . . . .	40
6.3.2	Pressure loss in the tubes . . . . .	41
6.3.3	Height compensations . . . . .	41
6.3.4	Calculation of the wind pressure coefficient . . . . .	43
6.4	Complications during the measurements and missing data . . . . .	45
6.5	ZEB Laboratory as IDA ICE model . . . . .	46
6.5.1	Openings in the ZEB Laboratory model . . . . .	47
6.5.2	Internal gains and schedules . . . . .	48
6.5.3	Mechanical ventilation in the ZEB Laboratory model . . . . .	50
6.5.4	Window control algorithm . . . . .	50
6.5.5	Evaluation of simulations in IDA ICE . . . . .	51
6.6	Evaluation of draught . . . . .	52
<b>7</b>	<b>Results</b>	<b>53</b>
7.1	Calibration of the Sensirion sensors . . . . .	53
7.2	Calculated pressure on the facades . . . . .	54
7.3	Wind pressure coefficients . . . . .	56
7.4	Simulations in IDA ICE . . . . .	59
7.4.1	Simulation with on-site wind pressure coefficients . . . . .	59
7.4.2	Simulation with standard wind pressure coefficients . . . . .	61

7.5	Evaluation of draught . . . . .	64
<b>8</b>	<b>Discussion</b>	<b>67</b>
8.1	Weather data used for calculations . . . . .	67
8.2	Pressure on the facades . . . . .	67
8.3	Wind pressure coefficients . . . . .	68
8.3.1	Calibration of the sensors . . . . .	69
8.3.2	Complications during the measurements . . . . .	70
8.4	IDA ICE model of the ZEB Laboratory . . . . .	71
8.4.1	Simulations with on-site and standard wind pressure coefficients . .	71
8.5	Comparison of the on-site and standard wind pressure coefficients . . . . .	72
8.6	Draught risk in the ZEB Laboratory . . . . .	73
8.7	Improvement of the window control algorithm . . . . .	74
<b>9</b>	<b>Conclusion</b>	<b>76</b>
<b>10</b>	<b>Further work</b>	<b>78</b>
	<b>References</b>	<b>79</b>
<b>A</b>	<b>Facade drawings of the ZEB Laboratory</b>	<b>I</b>
<b>B</b>	<b>ZEB Laboratory floor plans</b>	<b>V</b>
<b>C</b>	<b>Placement of the manual and automatic windows in the ZEB Laboratory</b>	<b>IX</b>
<b>D</b>	<b>Raw output data from the differential pressure measurements</b>	<b>XI</b>
<b>E</b>	<b>Raw output data from the reference sensor</b>	<b>XIII</b>
<b>F</b>	<b>Raw output data from weather station</b>	<b>XIV</b>
<b>G</b>	<b>Calculation of differential pressure</b>	<b>XV</b>
<b>H</b>	<b>Description of the window control algorithm</b>	<b>XVI</b>

# Nomenclature

---

A	Area [ $m^2$ ]
$C_d$	Discharge coefficient [-]
$C_p$	Pressure coefficient [-]
$g$	Acceleration from gravity [ $\frac{m}{s^2}$ ]
$\dot{m}$	Mass flow rate [ $\frac{kg}{s}$ ]
P	Pressure [Pa]
Q	Air flow rate [ $\frac{kg}{h}$ ]
T	Air temperature [ $^{\circ}C$ ]
u	Air velocity [ $\frac{m}{s}$ ]
z	Height [h]
$\rho$	Mass density [ $\frac{kg}{m^3}$ ]
$F_p$	Angle factor [-]
$\dot{V}$	Volume flow [ $\frac{m^3}{s}$ ]
D	Diameter [m]
l	Length [m]
$A_{out}$	Output voltage [V]
VDD	Input voltage [V]
$\eta$	Viscosity [ $\frac{Pa}{s}$ ]

# Abbreviations

---

AHU	Air Handling Unit
AIVC	Air Infiltration and Ventilation Center
BES	Building Energy Simulation
BIPV	Building Integrated Photovoltaic Panels
BRI	Building-Related Illness
CAV	Constant Air Volume
CO	Carbon Monoxide
CO <sub>2</sub>	Carbon Dioxide
DCV	Demand Control Ventilation
HVAC	Heating Ventilation and Air Condition
IAQ	Indoor Air Quality
IDA ICE	IDA Indoor Climate and Energy
MRT	Mean Radiant Temperature
NTNU	Norwegian University of Science and Technology
nZEB	Nearly Zero Emission Buildings
PCM	Phase Changing Material
PM	Particulate Matter
PMV	Predicted Mean Vote
PPD	Predicted Percentage Dissatisfied
PV	Photovoltaic
RH	Relative Humidity
SBS	Sick Building Syndrome
SFP	Specific Fan Power
TEK	Byggtekniske Forskrifter
VAV	Variable Air Volume
VOCs	Volatile Organic Compounds
ZEB	Zero Emission Building

# List of Figures

2.1	The relation between PMV and PPD. . . . .	7
3.1	Illustration of mechanical ventilation with one exhaust fan. . . . .	10
3.2	Illustration of balanced mechanical ventilation with one supply fan and one exhaust fan. . . . .	10
3.3	Principle of single-sided ventilation. The air will enter and exit on the same side of the facade. . . . .	12
3.4	Principle of cross ventilation. The air will enter and exit on two different facades. . . . .	12
3.5	General ventilation concept of buoyancy ventilation. Air will enter at a lower level, heat up and exit at a higher level. . . . .	13
3.6	Illustration of buoyancy-driven ventilation and the airflow with one opening. . . . .	14
3.7	Illustration of buoyancy-driven ventilation and the airflow with two openings. . . . .	14
4.1	Illustration of the wind effect on a building. The wind velocity will be lower closer to the ground, and the wind can be affected by nearby buildings. . . . .	23
4.2	General pressure gradients when the external air temperature is lower than the internal air temperature. . . . .	25
5.1	The ZEB Laboratory seen from the northeast. . . . .	29
5.2	The ZEB Laboratory seen from the southwest. . . . .	29
5.3	Architectural drawing of the floor plans in the ZEB Laboratory. . . . .	31
5.4	Surroundings of the ZEB Laboratory. . . . .	33
6.1	The setup of the differential pressure measurements, identical for all 15 sensors. . . . .	36
6.2	Illustration of the sensor setup and the tube placement, illustrated in blue. It can be seen how the tube barely went through the window gasket. . . . .	36
6.3	Placement of the five sensors on the north facade and their respective sensor number. . . . .	37
6.4	Placement of the five sensors on the south facade and their respective sensor number. . . . .	37
6.5	Placement of the two sensors on the east facade and their respective sensor number. . . . .	38
6.6	Placement of the three sensors on the west facade and their respective sensor number. . . . .	38
6.7	Illustration of the tube inlet connected to the reference sensor. The tube, marked in blue, is placed halfway on the weather station pole. . . . .	39
6.8	Setup of the equipment used to calibrate the Sensirion sensors. . . . .	40
6.9	Illustration of the pressure gradient inside the tube. . . . .	42
6.10	Real example of the pressure in the tube, and the inside pressure, based on pressure gradients. . . . .	43
6.11	Overview of where the different points used for calculating $\Delta P$ were placed according to the building facade. . . . .	44
6.12	The south and west facades of the ZEB Laboratory model in IDA ICE. . . . .	47
6.13	The north and east facades of the ZEB Laboratory model in IDA ICE. . . . .	47

6.14	Occupant schedule used in the first floor in the IDA ICE model. . . . .	48
6.15	Occupant schedule used in the second and third floor in the IDA IE model.	49
6.16	Occupant schedule used in the fourth floor in the IDA IE model. . . . .	49
6.17	The modeled AHU in the ZEB Laboratory model, clipped from IDA ICE.	50
6.18	A flow diagram of the implemented window control algorithm used to allow natural ventilation of the ZEB Laboratory model in IDA ICE. . . . .	51
7.1	Calculated wind pressure acting on the north facade of the ZEB Laboratory, based on pressure measurements. . . . .	54
7.2	Calculated wind pressure acting on the east facade of the ZEB Laboratory, based on pressure measurements. . . . .	55
7.3	Calculated wind pressure acting on the south facade of the ZEB Laboratory, based on pressure measurements. . . . .	55
7.4	Calculated wind pressure acting on the west facade of the ZEB Laboratory, based on pressure measurements. . . . .	56
7.5	Resulting indoor temperatures in the first floor during the simulated week with on-site pressure coefficients. The figure is clipped from IDA ICE. . . .	59
7.6	Resulting indoor temperatures in the third floor during the simulated week with on-site pressure coefficients. The figure is clipped from IDA ICE. . . .	59
7.7	CO <sub>2</sub> concentrations in the first floor during the simulated week with on-site pressure coefficients. The figure is clipped from IDA ICE. . . . .	60
7.8	CO <sub>2</sub> concentrations in the third floor during the simulated week with on-site pressure coefficients. The figure is clipped from IDA ICE. . . . .	60
7.9	Resulting age of air in the first floor with simulation using on-site pressure coefficients. The figure is clipped from IDA ICE. . . . .	60
7.10	Resulting age of air in the third floor with simulation using on-site pressure coefficients. The figure is clipped from IDA ICE. . . . .	60
7.11	PPD and PMV in the first floor from simulation with on-site pressure coefficients. The figure is clipped from IDA ICE. . . . .	61
7.12	PPD and PMV in the third floor from simulation with on-site pressure coefficients. The figure is clipped from IDA ICE. . . . .	61
7.13	Resulting indoor temperatures in the first floor during the simulated week with standard pressure coefficients. The figure is clipped from IDA ICE. . .	62
7.14	Resulting indoor temperatures in the third floor during the simulated week with standard pressure coefficients. The figure is clipped from IDA ICE. . .	62
7.15	CO <sub>2</sub> concentrations in the first floor during the simulated week with standard pressure coefficients. The figure is clipped from IDA ICE. . . . .	62
7.16	CO <sub>2</sub> concentrations in the third floor during the simulated week with standard pressure coefficients. The figure is clipped from IDA ICE. . . . .	62
7.17	Resulting age of air in the first floor with simulation using standard pressure coefficients. The figure is clipped from IDA ICE. . . . .	63
7.18	Resulting age of air in the third floor with simulation using standard pressure coefficients. The figure is clipped from IDA ICE. . . . .	63
7.19	PPD and PMV in the first floor from simulation with standard pressure coefficients. The figure is clipped from IDA ICE. . . . .	64

7.20	PPD and PMV in the third floor from simulation with standard pressure coefficients. The figure is clipped from IDA ICE. . . . .	64
7.21	Duration curve of the air throw length into the zone during one typical day. . . . .	65
7.22	Wind velocity at reference level during the simulated day. . . . .	65
7.23	Duration curve of the air throw length into the zone during the simulated week. . . . .	66
7.24	The calculated velocity of the air jet at 6.8 m into the room during the simulated week. . . . .	66
7.25	Wind velocity at reference level during the simulated week. . . . .	66
A.1	Facade drawings of the ZEB Laboratory of the north facade . . . . .	I
A.2	Facade drawings of the ZEB Laboratory of the east facade . . . . .	II
A.3	Facade drawings of the ZEB Laboratory of the south facade . . . . .	III
A.4	Facade drawings of the ZEB Laboratory of the west facade . . . . .	IV
B.1	Floor plan of the first floor of the ZEB Laboratory. . . . .	V
B.2	Floor plan of the second floor of the ZEB Laboratory. . . . .	VI
B.3	Floor plan of the third floor of the ZEB Laboratory . . . . .	VII
B.4	Floor plan of the fourth floor of the ZEB Laboratory . . . . .	VIII
C.1	Placement of the manual and automatic windows on the north facade. The manual windows are illustrated in green, and the automatic windows are illustrated in red. . . . .	IX
C.2	Placement of the manual and automatic windows on the east facade. The manual windows are illustrated in green, and the automatic windows are illustrated in red. . . . .	IX
C.3	Placement of the manual and automatic windows on the south facade. The manual windows are illustrated in green, and the automatic windows are illustrated in red. . . . .	X
C.4	Placement of the manual and automatic windows on the north facade. The manual windows are illustrated in green, and the automatic windows are illustrated in red. . . . .	X
D.1	Raw data from sensors 1, 2, 3, 4, and 5 placed on the north facade. . . . .	XI
D.2	Raw data from sensors 6 and 7 placed on the east facade. . . . .	XI
D.3	Raw data from sensors 8, 9, 10, 11, and 12 placed on the south facade. . . . .	XII
D.4	Raw data from sensors 13, 14, and 15 placed on the west facade . . . . .	XII
E.1	Raw data from the reference sensor . . . . .	XIII
F.1	Raw data of the wind velocity and wind direction obtained from the weather station. . . . .	XIV
F.2	Raw data of the outdoor temperature obtained from the weather station. . . . .	XIV
H.1	Detailed description of the window control algorithm. . . . .	XVI

# List of Tables

2.1	Recommended values for operative temperature based on activity levels. . .	4
2.2	Metabolic rate of a person with different activities. . . . .	5
2.3	Clothing and the corresponding insulation. . . . .	6
2.4	PMV seven-point thermal sensation scale. . . . .	7
2.5	The different building categories described in NS-EN 15251. . . . .	8
5.1	ZEB ambition levels and their respective system boundaries . . . . .	29
5.2	U-values of the ZEB-laboratory. [70] . . . . .	30
5.3	Pressure coefficients provided by AIVC in IDA ICE for <i>semi-exposed</i> setting. . . . .	34
6.1	The lower limit of wind velocity used to calculate the wind pressure coefficients. . . . .	45
7.1	Overview of the $a$ coefficient and the $R^2$ number obtained from calibrating the Sensirion sensors against a reference pressure logger. . . . .	53
7.2	Calculated wind pressure coefficients on the north facade, based on the measurements from the five sensors placed on this facade. . . . .	57
7.3	Calculated wind pressure coefficients on the east facade, based on the measurements from the two sensors placed on this facade. . . . .	57
7.4	Calculated wind pressure coefficients on the south facade, based on the measurements from the five sensors placed on this facade. . . . .	58
7.5	Calculated wind pressure coefficients on the west facade, based on the measurements from the three sensors placed on this facade. . . . .	58
7.6	Number of occupancy hours within four comfort categories evaluated according to EN-15251. The simulation was done with on-site pressure coefficients. . . . .	61
7.7	Number of occupancy hours within four comfort categories evaluated according to EN-15251. The simulation was done with on-site pressure coefficients. . . . .	63
7.8	Calculated throw length of the air entering an arbitrary window on the third floor. The throw length was calculated with different values of $K_2$ and $\epsilon$ . . . . .	64



# 1 Introduction

According to the Energy Performance of Buildings Directive (EPBD), all new buildings from 2021 must be nearly Zero Emission Buildings (nZEB) [1]. Such legislation will contribute to minimize energy use in buildings and reduce emissions associated with buildings. The building sector today is the main contributor to energy consumption and  $CO_2$  emissions in Europe [2], but energy heating demands has been decreased in recent years through the improvement of U-values and air tightness of the building envelope. Furthermore, cooling demands have been reduced by improved glazing and implementation of shading strategies. Further improvements in energy demands can, however, be made with passive measures. [3]

Implementing natural ventilation in buildings is a measure of providing passive cooling and ventilation by introducing outdoor fresh air without the use of electricity. Natural ventilation is induced either by the buoyancy effect resulting from temperature differences or wind effect due to pressure differences on the building facades. It is a passive building ventilation strategy that can contribute to improve the indoor environment and thermal comfort in a building, in addition to reduce energy consumption. Maintaining a good and healthy indoor environment is essential, as the average person spends about 90% of his time indoors [4]. [5, 6]

Zero Emission Buildings (ZEB) are buildings with high energy performance that compensate for the greenhouse gas emissions during their lifetime by having renewable on-site energy production [7]. The ZEB Laboratory located at the Gløshaugen campus in Trondheim is such a building, with the ambition of reaching the level of ZEB-COM. The building will act as a *living lab* where technical solutions can be investigated and tested in interaction with the occupants. [8]

## 1.1 Scope

NTNU and SINTEF have built a new living lab of 1800 m<sup>2</sup> at Gløshaugen. It is an office building with permanent working spaces, but it will also be used for experiments on energy production, energy supply, ventilation, heating, cooling, lighting, organization of workplaces, and more. The building has both natural and mechanical ventilation. Previous master students have developed models with natural ventilation of the building and done some measurements.

The scope of this Master's thesis is to further develop models on how to combine natural and mechanical ventilation in an optimal way with regard to energy use, indoor climate, and outdoor conditions. Pressure measurements will be done in the building and used to evaluate the wind pressure coefficients on the facades of the ZEB Laboratory. The wind pressure coefficients will be implemented in IDA ICE to develop algorithms for opening the windows, which will further be used to find optimized solutions with the ventilation

system regarding energy use and the indoor environment. The final goal is to make a model to control the hybrid ventilation system of the ZEB Laboratory building.

## 1.2 Limitations

Parts of the scope of the thesis were changed during the semester. Problems with the equipment used for the on-site pressure measurements and challenges with the calculations of the wind pressure coefficients resulted in less time spent developing the IDA ICE model of the ZEB Laboratory. Because of the limited time for the simulations, several simplifications were done to the model, such as using simplified zones in the building, and it was decided to use an algorithm developed by a previous Master's student Sande [9]. As a consequence, the focus of the thesis was shifted towards investigating the impact of on-site pressure wind pressure coefficients compared to standard coefficients. The final goal of the thesis was to make a model to control the hybrid ventilation system and implement this in the building, but this was not done due to lack of time. Instead, a simple evaluation of the draught risk in the building during the summer was done.

## 1.3 Structure of this Master's thesis

The structure of this Master's thesis begins with presenting relevant theory and literature on indoor environment and the parameters that affect indoor air quality in chapter 2. Chapter 3 contains relevant theory on building ventilation, including mechanical, natural, and hybrid ventilation systems. Further, chapter 4 presents the principles and equations that are needed to understand airflows occurring due to natural ventilation. In addition, air pressure, wind effects, and wind pressure coefficients will be presented here. Chapter 5 will describe Zero Emission Buildings, and the ZEB Laboratory will be presented. The theory and literature presented in these chapters are based on the literature study conducted during the project thesis, *Evaluating the Method for Measuring and Calculating Wind Pressure Coefficients*, completed during the fall of 2022 [10]. The theory from the project thesis has since been reviewed, and additional relevant theory has been added.

Chapter 6 presents the method to conduct the differential pressure measurements over the facades of the ZEB Laboratory, information about the equipment used, and the method to calibrate the sensors. Further, the method to calculate the wind pressure coefficients is described, and the compensations done to obtain the results. Lastly, the simplified ZEB Laboratory model in IDA ICE is presented, and the implemented window control algorithm to introduce natural ventilation in the building is described. The method for the differential pressure measurements and calculation of the wind pressure coefficient is based on the work done during the project thesis [10], and additional information has since been added. Chapter 7 and 8 will present the results obtained from the project, and lastly, chapter 9 will present the conclusion and further work from the thesis.

## 2 Indoor environment

Indoor air quality (IAQ) and the effect it has on the well-being and comfort of the occupants is an important aspect to consider with the building environment. Poor indoor environment can affect the comfort and productivity of the occupants and, in some cases, lead to reduced health of the occupants. Two strategies to improve the IAQ are to either increase the ventilation rate and, in this way, reduce air pollutants or reduce the source of pollution affecting the air quality. [11]

In this section, the different parameters affecting the indoor environment will be presented first. Further, building ventilation will be introduced, and the different approaches and strategies to utilize ventilation to achieve an acceptable indoor environment will be presented. Lastly, Zero Emission Buildings will be introduced, as well as the ZEB Laboratory located at Gløshaugen in Trondheim.

### 2.1 Thermal environment

Local environmental parameters such as temperature, air velocity, and relative humidity will impact a person's thermal balance. Thermal balance can be influenced by physical parameters such as activity and clothing level as well. These factors can be measured or estimated and are essential to understand to ensure occupants are thermally comfortable in the indoor environment. This section will present the different parameters that can have an effect on the perceived thermal environment in a building. [12]

#### 2.1.1 Temperature

Mean radiant temperature (MRT) is an important parameter when discussing human energy balance and thermal comfort. MRT is an expression of the average surface temperatures from the surrounding surfaces, based on the angular relationship between the surface and the object in question, for example, a person. MRT,  $\bar{T}_r$ , can be calculated using equation 2.1, where  $F_{P-n}$  is the angle factor between the object and the surface, and  $T_n$  is the surface temperature. [13, 14]

$$\bar{T}_r = F_{P-1} T_1 + F_{P-2} T_2 + \dots = \sum_1^n F_{P-n} T_n \quad (2.1)$$

Operative temperature is a parameter based on air temperature and radiation exchange between the occupant's body and the surrounding surfaces. If the relative air velocity is less than  $2 \frac{m}{s}$  and the difference between the MRT and the air temperature is less than 4 K, the operative temperature can be defined as equation 2.2. [14]

$$T_o = \frac{T_a + \bar{T}_r}{2} \quad (2.2)$$

$T_o$  in equation 2.2 is the operative temperature and  $T_a$  is the air temperature. If there is no significant heating or cooling from surfaces in the room, the operative temperature becomes approximately equal to the air temperature. [14]

*Byggteknisk forskrift*, TEK17, recommends that the air temperature in a room is kept below 22°C during the heating season [15]. The regulation does, however, state that the air temperature should be customized to the function and use of the room. The recommended operative temperatures for typical types of activity are given in table 2.1. During periods with high outside air temperatures, keeping the maximum temperature below the suggested values can be difficult. Temperatures above the limit should be accepted, but not for more than 50 hours during a typical year. [15]

**Table 2.1:** Recommended values for operative temperature based on activity levels. [15]

Activity group	Light work	Medium work	Hard work
Temperature [°C]	19 - 26	16 - 26	10 - 26

### 2.1.2 Draught

Air in motion inside an occupied zone is called *draught* and can affect the thermal comfort of the occupants. Draught is caused by air in movement inside the room and gives a cooling effect. The cooling effect increases with increasing air velocity, as well as in combination with the radiation asymmetry from cold surfaces. Draught created by air jets entering a room will be described further in section 4.3. [14]

### 2.1.3 Relative humidity

Relative humidity (RH) represents the amount of water in the air compared to the saturation point. The value for relative humidity is given in percentage and is calculated from equation 2.3. Here,  $P$  and  $P_{sat}$  are the pressure and the saturation pressure of the air, respectively. [14]

$$RH = \frac{P}{P_{sat}} = \frac{x}{x_{sat}} \quad (2.3)$$

It is recommended to keep the level of relative humidity within the limit of 20-70% during the summer and 20-40% during the winter. The upper limit of relative humidity is based on the risk of microbiological growth, like house dust mites and mold, which can occur if relative humidity levels exceed 70%. The upper limit is also chosen based on the risk of condensation that can damage the building construction. A lower level of relative humidity than recommended should also be avoided, as this can lead to dry mucous membranes and skin. [16, 17]

### 2.1.4 Activity level

The rate of heat production from the human body, or metabolic rate, is dependent on the activity level of the person. The unit of metabolic rate is *met*, where 1 met is equivalent to the heat produced by the body when in a sedentary state, equal to  $58.2 \frac{W}{m^2}$ . The metabolic rate will increase with increasing activity levels. Table 2.2 shows the metabolic rate of a person with different activity levels. [14]

**Table 2.2:** Metabolic rate of a person with different activities [14].

Activity	Heat production	
	$[\frac{W}{m^2}]$	[Met]
Lying down	46	0.8
Seated, relaxed	58	1.0
Standing, relaxed	70	1.2
Sedentary activity (office, residential, school)	70	1.2
Standing, light activity (laboratory, light industry)	93	1.6
Standing, medium activity (shop assistant, housework)	118	2.0
Medium activity (workshop work)	165	2.8
<b>Walking speed:</b>		
$3 \frac{km}{h}$	-	2.0
$5 \frac{km}{h}$	-	3.0
$10 \frac{km}{h}$	-	8.0

### 2.1.5 Clothing level

Different clothes have different thermal resistance and insulation, and the type and amount of clothing worn by occupants can affect their thermal comfort. The heat conduction resistance of the clothing, describing the thermal resistance between the skin and the outer surface of the clothes, is used to evaluate the effect of the clothes. The unit for this is *clo* or  $\frac{m^2K}{W}$ , where 1 clo is equal to  $0.155 \frac{m^2K}{W}$ . Table 2.3 includes typical clothing outfits and their respective clo values. [14]

**Table 2.3:** Clothing and the corresponding insulation in clo and  $\frac{m^2K}{W}$ . [14]

Clothing	[clo]	$[\frac{m^2K}{W}]$
Naked	0.0	0.000
Typical tropical outfit (shorts, t-shirt, sandals)	0.30	0.050
Summer outfit (light dress, tights)	0.45	0.070
Summer outfit (light trousers, short sleeve shirt, shoes)	0.5	0.080
Light work attire (long sleeve shirt, work trousers, wool socks, shoes)	0.70	0.110
Winter outfit for indoor use (long sleeve shirt, trousers, jacket or sweater, thick socks, shoes)	1.00	0.155
Outdoor outfit (coat, jacket, vest, trousers, long sleeve shirt, socks, shoes)	1.50	0.230

## 2.2 Thermal comfort

Thermal comfort is defined as the condition in which a person is neither too warm nor too cold and is an essential factor in evaluating the environmental quality of the building. Occupants can perform optimally in a thermally comfortable space. Parameters that influence thermal comfort are physical parameters, like temperature and air velocity, physiological parameters, like age and gender, and external parameters, like human activity, clothing, and social conditions. [11, 18]

There are two approaches to research on thermal comfort. The first is heat balance models based on laboratory studies. This includes the work of Fanger, who related thermal sensation to heat balance by observing a large number of people in laboratory experiments, leading to the two measures of PPD and PMV. The other approach is the adaptive thermal comfort model, based on field studies in real buildings. [19]

### 2.2.1 PMV - Predicted mean vote

Predicted mean vote (PMV) is an index that aims to predict how the occupants are experiencing the thermal environment. The index is based on standard NS-ISO 7730, and the values are a function of physical activity, clothing, and thermal environment parameters such as operative temperature and relative humidity. PMV is developed from experiments and expresses the mean value of votes from a group of people on a seven-point thermal sensation scale. The scale is presented in table 2.4, where a PMV of 0 means there is thermal equilibrium, where the internal heat production of the occupant and his heat loss is the same. This means the occupant is thermally comfortable. [12, 14, 20]

**Table 2.4:** PMV seven-point thermal sensation scale. [12]

Scale	Thermal sensation
+3	Hot
+2	Warm
+1	Slightly warm
0	Neutral (comfortable)
-1	Slightly cool
-2	Cool
-3	Cold

### 2.2.2 PPD - Predicted percentage dissatisfied

Suppose the PMV is considered to be 0, meaning the average perception of the thermal environment is that the group of occupants is comfortable. In this case, individual votes will still be scattered around the mean vote. The predicted percentage dissatisfied (PPD) is an index predicting the percentage of occupants experiencing local discomfort with the thermal environment. The main factors causing discomfort are unwanted cooling or heating of the occupant. Using the determined PMV value, the PPD can be calculated by equation 2.4. [12, 14, 20]

$$PPD = 100 - 95 \cdot e^{-0.03353 \cdot PMV^4 - 0.2179 \cdot PMV^2} \quad (2.4)$$

The PPD will predict the number of people among a large group to be dissatisfied with the thermal environment. The remaining part of the group will either feel neutral, slightly warm, or slightly cool. Figure 2.1 illustrates the relation between PMV and PPD. [12]

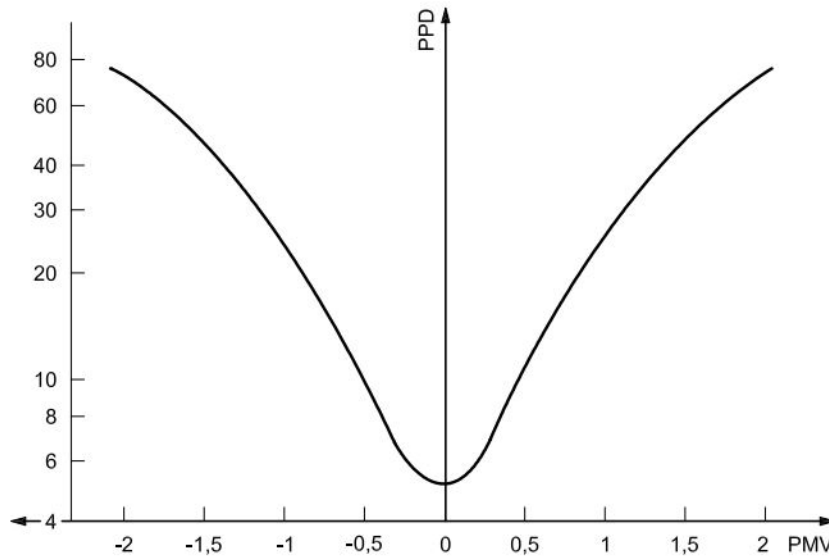


**Figure 2.1:** The relation between PMV and PPD. [12]

The acceptable levels of PPD and PMV in a building depend on what *building category* the building belongs to. The different categories are described in standard NS-EN 15251:2007 and are given in table 2.5 [21].

**Table 2.5:** The different building categories described in NS-EN 15251 [21].

Category	Explanation
I	High expectation level. Recommended in rooms with sensitive and vulnerable occupants
II	Normal expectation level. Should be used in new and renovated buildings
III	Acceptable, moderate expectation level. Can be used in existing buildings

ZEB Laboratory is categorized as building category II, based on the descriptions in table 2.5. For a building in this category, the PPD levels should be below 10%, and the average PMV index should be in the range of  $\pm 0.5$ . [21]

### 2.2.3 Adaptive thermal comfort model

The adaptive thermal comfort model is based on findings from field measurements in buildings. The researchers collected data on the thermal environment and the thermal response of the subjects occupied in the room. This method assumes that people will react in ways that make them more comfortable with the environment if they experience discomfort, like adding or removing clothes. The model states that the perception of comfort is not a fixed condition as it depends on both physiological and non-physiological factors. During the experiments, it was observed that people in a real building were more tolerant to the thermal environment than Fanger's method suggests. This model also concludes that the preferred temperatures in the building are variable and change with the seasons. [19]

## 2.3 Atmospheric environment

The atmospheric environment can be used to indicate the quality of the indoor air. The atmospheric environment is important for the level of comfort and the risk of diseases.

### 2.3.1 Carbon dioxide concentrations

Carbon dioxide ( $\text{CO}_2$ ) concentration is often used as an indicator of the air quality in a building.  $\text{CO}_2$  is, however, not itself regarded as a hazardous component. The level of  $\text{CO}_2$  can be used to indicate how many occupants are present in a zone and how long they have been present in the zone. [22, 23]



According to the standard NS-EN 15251, the CO<sub>2</sub> concentration should not exceed the outdoor concentration levels by more than 500 ppm [21]. The CO<sub>2</sub> concentration in Norway is found to be in the range of 400 to 450 ppm [24]. Consequently, CO<sub>2</sub> concentrations in a building should not exceed 900 ppm.

### 2.3.2 Other pollutions

Other outdoor pollutions can affect the indoor environment and include, among others, carbon monoxide (CO), volatile organic compounds (VOCs), particulate matter (PM), and aerosol. The pollutants are normally a complex mixture of particles and gaseous components, and the effect of them depends on the sources and emission rates. The sources of the pollutants can be from human daily activities such as cooking, cleaning, and smoking, equipment such as computers or printers, or common building materials. It is also known that outdoor contaminants can have a great effect on the IAQ due to the transportation of the contaminants from outside to inside air via ventilation. Therefore, the design and operation of the ventilation system are important to create a healthy indoor environment by exchanging indoor air with fresh outdoor air. Filters in the air handling units (AHU) are important as well to avoid bringing contaminants from one place to another. [4]

### 2.3.3 Age of air

Building ventilation contributes to supply fresh air and extracting the contaminated air in a room. *Age of air* is a useful tool to classify the efficiency of the ventilation system. The age of air refers to the time it takes for the air within a space to be completely replaced by fresh air. The average age of air in a room depends on the volumetric flow rate and its airflow pattern, and the value can be used to determine the air change efficiency of the room. [25]

## 2.4 Consequences of poor indoor environment

Poor IAQ can have an effect on human health by causing building-associated illnesses. Building-associated illnesses are illnesses caused by indoor environmental factors and are divided into two categories: sick building syndrome (SBS) and building-related illness (BRI). SBS refers to a group of symptoms related to the physical environment of buildings, and the effects will occur after the occupant has spent a certain amount of time in the building. The symptoms of SBS include mucous membrane irritation, neurotoxic effects such as headaches, mental fatigue and nausea, asthma and asthma-like symptoms, and skin irritation. Low ventilation rates, high relative humidity in the building, and high room temperatures tend to increase the risk of SBS to occur. BRI are illnesses directly related to exposure to poor air quality in buildings. BRI can be caused by chemicals such as formaldehyde and benzene or by biological contaminants. The illnesses have been associated with the flu, fever, muscle aches, and cough. [4]

### 3 Building ventilation

Building ventilation can be sectioned into three categories. The system can be a mechanical ventilation system using fans and ducts, a system using ventilation occurring due to natural forces like wind and temperature, or a hybrid solution combining the two.

#### 3.1 Mechanical ventilation

Mechanical ventilation includes the use of fans and ducts to ensure sufficient IAQ. The system can be a simple exhaust system or a more complicated balanced system. Exhaust systems use fans to exhaust the air through ducts, while fresh air will leak into the building through intentional vents or unintentional cracks in the building shell. Such a system is illustrated in figure 3.1. A negative aspect of exhaust systems is the lack of control over the incoming air to the room. As a consequence, larger heat emitters to regulate the air temperature in the room can be required [3]. A balanced system uses fans to secure both supply and exhaust air in the building through ducts to the respective rooms, and an illustration of a building with balanced mechanical ventilation can be seen in figure 3.2. This type of system can also integrate filters to filter the outside air of pollutants before it enters the building. Mechanical ventilation systems can also utilize heat recovery to save energy used to heat the ventilation air. [14, 26]

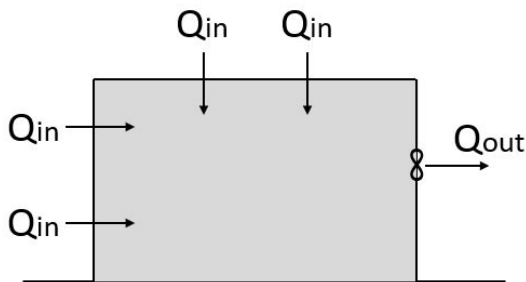


**Figure 3.1:** Illustration of mechanical ventilation with one exhaust fan. The air will enter the building through cracks or openings in the envelope.



**Figure 3.2:** Illustration of balanced mechanical ventilation with one supply fan and one exhaust fan.

Figure 3.1 illustrates how, when an extract fan is turned on, the fan blades start to rotate and will initiate airflow out of the building,  $Q_{out}$ . With the use of only one extract fan, airflow into the building,  $Q_{in}$ , will be induced because of reduced internal pressure and will enter through cracks and openings in the building. Using a supply fan instead of an extract fan will increase the internal pressure, hence creating outflow through openings in the envelope. If an exhaust fan and a supply fan are used simultaneously, and they generate the same flow rates, no pressure differences will occur, and the system will be balanced, illustrated in 3.2. [26]

### **3.1.1 Control strategies**

Mechanical ventilation systems can be managed by different control strategies. The strategies include controlling the system by varying the amount of supplied air, the temperature of the air, or the demand for air in the room.

#### **Constant air volume**

With constant air volume (CAV), the air is supplied to the room at a constant volume, and the fans and dampers in the system are not regulated. For systems with CAV, the air supply volume is calculated based on the dimensioning pollution load. In office buildings, the number of people varies, and the design air volume is based on the maximum person load in the room. CAV as the control strategy is still widely used in buildings because of the airflow requirements, the simple system design, and the costs. [27, 28]

#### **Variable air volume**

Variable air volume (VAV) is a control strategy that includes all ventilation systems where the amount of supply air can be varied. This ventilation system uses sensors in the rooms to detect whether people are present. When the sensors detect occupants in the room, dampers will change to predetermined positions to allow supply of fresh air. [28]

#### **Demand controlled ventilation**

The last control strategy is demand controlled ventilation (DCV), where the amount of air supplied to the room is controlled by demand, which varies with time. With this control strategy, the ventilation rate and the heating and cooling effect of the ventilation air are automatically controlled. DCV systems use a feedback loop in the form of a signal to display the achieved quality of the indoor air. The achieved and desired air quality is then compared, and the DCV system is regulated to minimize any deviations that occur. [28]

## **3.2 Natural ventilation**

Natural ventilation is the supply and exhaust of airflow through doors and openings in a building established due to pressure differences created by wind or buoyancy forces. Natural ventilation includes infiltration and exfiltration through cracks in the building, so-called unintended or passive ventilation, and intended ventilation by opening windows, doors, and hatches. This type of ventilation has been utilized in enclosures occupied by humans prior to the use of mechanical ventilation, which has been developed for the last 150 years. With an increasing demand for IAQ and the low requirements for energy consumption and sustainability in buildings, natural ventilation is an interesting solution to implement in buildings. [29]

Buoyancy and wind are the driving forces for natural ventilation. Differences between the indoor and outdoor temperature and differences in wind pressure along the building

facade create a natural air exchange between indoor and outdoor air. The airflow rate depends on the strength and direction of these forces and whether any objects in the flow path create resistance. Since several unpredictable and fluctuating factors act on natural ventilation, it is challenging to accurately predict the airflow rate and control the ventilation to obtain the required indoor environment. Wind pressure coefficients are used to determine the amount of pressure exerted on a building facade due to the wind, which impacts the ventilation and airflow patterns. Wind pressure coefficients will be further described in section 4.2.3. [30, 31]

### 3.2.1 Wind-driven ventilation

Wind-driven ventilation is mainly caused by static pressure induced by wind on the building facades, and the static pressure differences across openings determine the airflow rates of the building. Wind-driven ventilation can be classified into two common types based on the relative location of the openings used, called single-sided ventilation and cross ventilation. The principle of single-sided ventilation can be seen in figure 3.3, where it is shown how the air will enter and exit the building through openings placed on the same facades. Figure 3.4 illustrates the principle of cross ventilation where the air will enter through openings on one facade and will exit through openings on another facade. The openings used for ventilation are usually windows. To ensure sufficient ventilation flow, there must be a significant wind pressure difference between the inlet and outlet openings and a minimal internal resistance to flow. [5, 32]

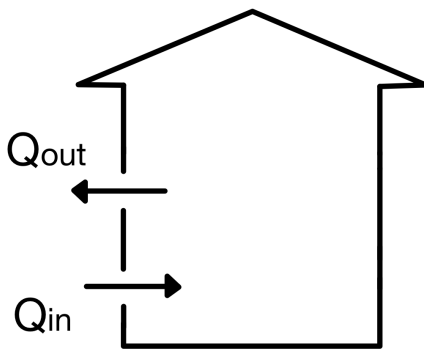


**Figure 3.3:** Principle of single-sided ventilation. The air will enter and exit on the same side of the facade.

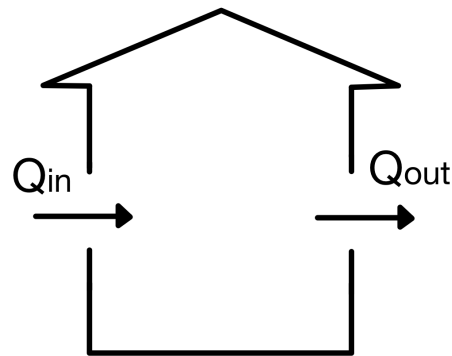


**Figure 3.4:** Principle of cross ventilation. The air will enter and exit on two different facades.

### 3.2.2 Buoyancy-driven ventilation

Buoyancy-driven ventilation, also called stack ventilation, occurs when there is a temperature difference between the inside and outside of the building. This temperature difference creates a density difference, where warm air is less dense than cold air. When a space has

one upper and one lower opening, the higher pressure at the upper opening will create an outflow of air, and the lower pressure at the bottom opening will create an inflow of air. The air will heat up after entering the building and rise to the upper opening. This creates a temperature stratification within the space, also referred to as displacement ventilation. Figure 3.5 illustrates the concept of buoyancy ventilation, where cold air will enter the openings on the lower floors, heat up and exit at the opening at the top of the building. [30]

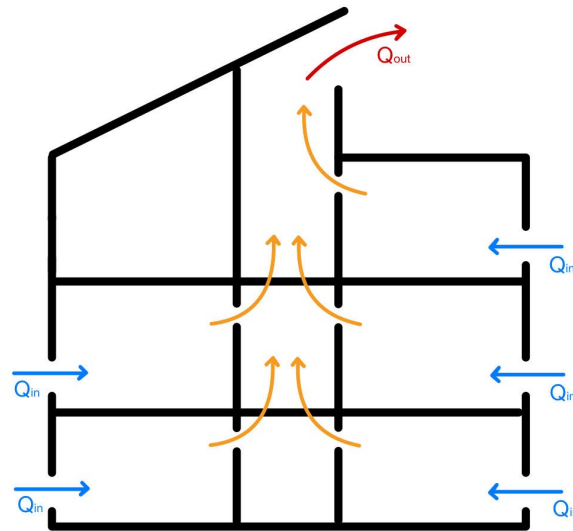


**Figure 3.5:** General ventilation concept of buoyancy ventilation. Air will enter at a lower level, heat up and exit at a higher level. (inspired by [33])

Buoyancy-driven ventilation can occur in a space that has one large opening as well, but the effect will not be as strong as with two openings on different levels. An illustration of buoyancy ventilation and the effect on the airflow is illustrated in figure 3.6. With one opening, the ventilation flow will be lower, and the air will not penetrate as far into the zone. In the case of two openings, illustrated in figure 3.7, where there is a significant vertical separation between the inlet and outlet, stronger airflow will occur, given that there is a difference between the indoor and outdoor temperatures. In a space with two openings, the cool air will enter at the bottom opening, heat up as it enters the room, and exit at the upper opening. [30]

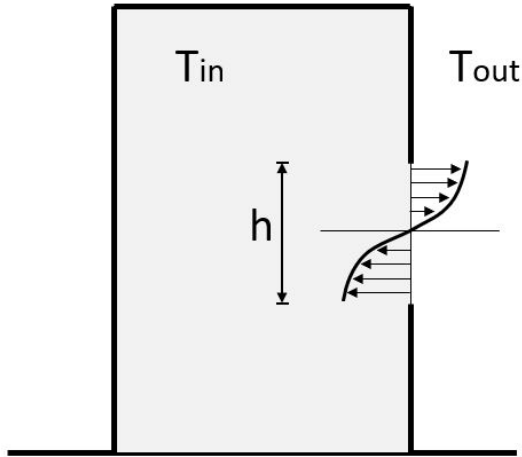


**Figure 3.6:** Illustration of buoyancy-driven ventilation and the airflow with one opening. The figure is inspired by [30].

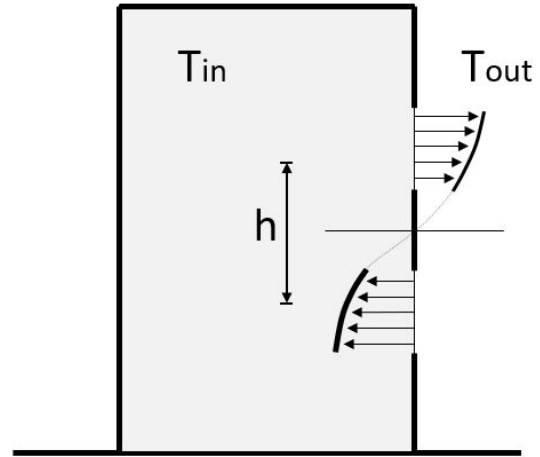


**Figure 3.7:** Illustration of buoyancy-driven ventilation and the airflow with two openings. The figure is inspired by [30].

Buoyancy ventilation can create uncontrolled vertical air movement in buildings if there are strong forces present. The air movement can create noise and draft when moving over the building envelope and internal parts of the building. The stack effect is usually stronger during colder periods due to bigger temperature differences between the inside and outside air, and the vertical movement will often be the strongest in stacks or stairwells, as well as other vertical openings. [34]

### 3.2.3 Combined buoyancy and wind-driven ventilation

Pressure drops around the building body due to the wind will create positive pressure on the wind side and negative pressure on the lee side. Consequently, the air in the room will ventilate through openings in the facades. When there is a heating source inside the room, the air will be subjected to both wind-associated pressure forces and buoyancy forces, and combined buoyancy and wind-driven ventilation will occur. The ventilation rate depends on the strength and direction of the wind, the temperature difference between the internal and external environment, and the size and location of the openings on the facade. The effects of the wind and temperature differences will reinforce and counteract each other. [30, 35]

### 3.2.4 Advantages and disadvantages with natural ventilation

Natural ventilation systems have the potential to contribute to considerable energy savings from cooling needs and reduce the energy cost required for mechanical ventilation if the system is designed properly. The system needs less space, as there are no ducts and AHU, and less maintenance because no mechanical devices are needed. As a result, the

maintenance cost for a natural ventilation system is lower than for a mechanical system. The investment cost is also generally lower. [11, 29]

Utilizing natural ventilation is a tool to improve IAQ, increasing occupant productivity by reducing absenteeism and reducing health risks. Research indicates that occupants of buildings with natural ventilation have fewer SBS symptoms than those of mechanically air-conditioned buildings [36]. Natural ventilation systems also allow the occupant to control their local thermal environment by opening and closing the windows. This is a solution to several user complaints concerning mechanical ventilation, such as noise. However, natural ventilation can also be harmful in cities with high outdoor air pollution since high exposure to PM can negatively impact the health of the occupant. This matter will generally be filtered out before the air enters the building with a mechanical ventilation system. [11, 37, 38]

The efficiency of natural ventilation is directly related to ambient conditions. No airflow rate will occur if there is no wind and if the indoor temperature is close to the ambient temperature. On the other hand, if there are big pressure differences, there will be a large airflow rate, which can create a draught. Draught can occur especially in colder climates with big differences between the inside and outside temperatures. As the airflow rate varies, so will the air quality. This can give unacceptable temperature or accumulation of contaminants in the room. [37, 38]

Mechanical ventilation systems ensure low energy consumption by heat recovery in the AHU before the fresh air enters the respective rooms. A disadvantage of natural ventilation is the lack of this heat recovery, leading to a colder temperature of the supplied air. Consequently, if the ambient temperatures are low this will result in cold air supply air, which can lead to higher space-heating demands. [39]

### **3.3 Natural ventilation in Nordic climate**

Nordic climates are affected by long, cold winters with short days and a lack of sunlight. The peak energy demand happens during the winter due to increased heating requirements, and the demand is the lowest during summer. Because of the low ambient temperatures during the winter, it can be challenging to implement natural ventilation in this climate. The challenges arise due to the cold temperatures of the supplied air and no heat recovery. This can lead to increased heating demand in the building. However, it is possible to implement natural ventilation in cold climates, but research has shown that it has the biggest potential during the cooling season. [3]

Wind-induced ventilation is a concept widely used in buildings in warm climates [40]. However, these systems can cause draught in cold climates and are therefore not applicable. To utilize natural ventilation in cold climates, wind towers and wind catchers can be introduced. Such a system can give a centralized source of airflow, which can

be distributed and used to create a system with a regulated airflow rate. However, these systems have limitations such as the height of the building, the number of floors, and local weather conditions. Operation of wind towers is, however, generally limited to summer seasons, as the outdoor temperature is too cold during the majority of the year, leading to cold supply air temperature [41]. [42]

Thermally induced ventilation can also be used in cold climates by using passive stack ventilation systems such as solar chimneys and double-skin facades. Solar chimneys can create controllable centralized air distribution, but this technology requires a significant amount of solar radiation and is, therefore, most applicable during the summer [43]. Solutions like double skin facades can be introduced during the cold season, where the air is heated in the cavity between the two facades with solar radiation [44]. Passive stack ventilation is used to create underpressure in the building, thus creating ventilation by infiltration through the envelope. [42]

Another solution is a system with ventilated double windows that can preheat the ventilation air through air channels where the air collects heat from solar radiation or heat loss through the system from the inside. A ventilated double window consists of two parallel windows, where the air is passively heated after entering a vent or an air inlet at the bottom of the outer window. An additional air vent is installed at the top of the inner window, where the heated air will exit the building. The channel between the two windows acts as an air path for the air. A study by Carlos et al. [45] did simulations to evaluate the performance of ventilated double windows during the winter in Oslo. The study showed that this type of window system did heat the incoming air slightly before entering the room. The main source of heat to the incoming air was thermal losses from the inside due to lack of solar radiation. Simulations were done on the north and south orientation of the facade to get the effect of the lowest and highest solar radiation available. [45]

### **3.4 Cooling of buildings with natural ventilation**

Natural ventilation can be used to cool buildings by removing excess heat. Cooling can be done by opening windows, either automatically or manually, or by utilizing night cooling of the buildings. The cooling potential from using natural ventilation is greatly dependent on window control and the ambient climatic parameters. Using the same method for ventilative cooling of buildings in different climatic locations will have varying degrees of effect. The cooling potential is additionally dependent on the internal gains in the building, as this impacts the thermal performance. In hot climates, more than natural ventilation will be required to cover the cooling needs of the building, as high ambient temperatures and high outdoor humidity make it hard to extract any cooling. In colder climates, however, natural ventilation can offer high ventilation rates when the natural forces are strong and contribute to summer cooling and removal of indoor contaminants. [29, 46]



### 3.4.1 Operation of windows

In order to fully utilize the benefits of natural or hybrid ventilation systems in buildings, it is crucial to control the opening of windows and the heating, ventilation, and air conditioning (HVAC) system. Window operations can be accomplished manually or automatically, and the level of automation can vary. Manual window operation is dependent on occupant skill and behavior and can result in sub-optimal indoor conditions. Therefore, the integration of automatic windows and control systems for vents is often advisable. While individual control of windows should be maintained as far as possible, advanced automatic control strategies for window opening can provide a better indoor environment and greater energy savings, particularly when ambient conditions and internal occupancy and activities vary. [39, 47]

A study by Andersen et al. [48] investigating window opening behavior in Danish buildings found that there was a pattern between the opening behavior and IAQ. Firstly, indoor CO<sub>2</sub> concentration, indoor temperature, and solar radiation were correlated with the probability of opening the windows. Further, outdoor temperatures were correlated with the probability of closing the windows. Low outdoor temperatures are also the main reason not to open the windows [49]. In the study, the probability of both opening and closing the windows was also found to be affected by the season and the time of day. [48]

#### Window opening control schemes

To operate windows for ventilation and cooling purposes, it is important to consider controlling strategies. The opening strategy can either be simple, where the occupants control everything, or highly advanced and fully automatic systems. Four different control schemes are commonly used as control strategies. The first is spontaneous control, which is the simplest control scheme where the occupant can control the windows freely. This strategy is both low in investment and maintenance cost but is shown to have limited energy saving and improvement in thermal comfort. The second strategy is informed occupant control, where a signal to either open or close the window notifies the occupant to take appropriate action. [50]

The next control scheme that can be utilized is a heuristic control strategy, where rule-based criteria decide when the windows should be opened automatically and regulate the window opening position accordingly. Heuristic control uses IF-THEN rules, where parameters like temperature, wind, and relative humidity are used to decide when the windows should be opened and the mechanical HVAC system should be turned off. The last control strategy is Model Predictive Control (MPC), which is an advanced control scheme applying a prediction-based modeling approach to evaluate the best action with regard to thermal comfort and energy consumption. [6, 50]

According to the findings of Chen et al. [50], the use of automatic control strategies, including heuristic control and MPC, along with mechanical window actuators and coordinated HVAC control, led to considerable cooling energy savings while maintaining indoor temperatures throughout the year in the studied buildings. Overall, the cases with MPC indicated better performance in thermal comfort and energy savings than the heuristic control cases. Further, the study indicated that control strategies using spontaneous and informed occupant control was not able to maintain the indoor temperatures within the comfort range at all times and showed lower cooling energy savings. The study also discusses how improper use of windows when using occupant control could lead to frustration with thermal comfort outside the acceptable range, which can cause occupants to become reluctant to follow the signals from the system and convert to mechanical cooling instead. [50]

### 3.4.2 Night cooling

One approach to cooling buildings and reducing energy demand without reducing occupant comfort is passive cooling by night ventilation, where the cold outdoor air is used to cool down the construction and the interior during the night. The efficiency of night cooling is affected by the ambient temperature, and it is shown that night ventilation can be effective in colder climates where the temperature is below 20 °C most of the nights during the summer [46]. In warmer climates, night cooling is not always sufficient to cool the building due to the high ambient temperatures. Night cooling as a passive ventilation strategy is, however, generally found to be an effective measure to reduce cooling requirements and can contribute to reducing energy consumption and greenhouse gas emissions of the building. [46, 51]

## 3.5 Hybrid ventilation

Hybrid ventilation is a solution combining natural and mechanical ventilation. An intelligent control system can be implemented to minimize energy consumption and use solutions for optimizing the balance between indoor air quality, thermal comfort, and energy use. Hybrid ventilation provides opportunities for innovative solutions to the ventilation system and can improve the overall quality of the ventilation. Different system features can be used at different times of the day or the season to achieve an acceptable indoor environment and to take maximum advantage of the ambient conditions. There is also a financial motivation with lower investment and operational costs. [37, 52]

Ventilation control needs to be an equilibrium between IAQ, thermal comfort, energy use, and environmental impact during the heating and cooling seasons. This includes, among other things, utilizing heat recovery to reduce the heating and cooling demands, passive heating or cooling of the ventilation air, and reducing the need for fan energy by using low-pressure ducts and other components and optimizing the natural driving forces. [37]

Hybrid ventilation systems are tailored to each building and need to be integrated in the early design phase. It is also important to consider night cooling potential, noise, and air pollution from the surroundings early when designing the system. When designing the building, the location and size of the openings and the different features to enhance the driving forces, such as stacks or solar chimneys, need to be considered to optimize ventilation during the day as well as at night time. The level of automatic and manual control, or user interaction, also needs to be decided. [37, 52]

### **3.5.1 Approaches to hybrid ventilation**

There are three different approaches to a hybrid ventilation strategy. The first is fan-assisted natural ventilation, where natural ventilation is combined with the use of an extract or supply fan when the driving forces are too weak or in periods of high demand. The second approach is stack and wind-assisted mechanical ventilation, where mechanical ventilation is optimized with the use of natural forces. The last approach is a mixed mode strategy where the system can switch between using either mechanical or natural ventilation or a combination of the two. An example of this approach is a system that provides mechanical ventilation during occupied hours and natural ventilation for night cooling. [37]

A building using mixed mode approach integrates fan-assisted ventilation when and where necessary, utilizing natural ventilation when possible to maximize comfort while avoiding significant energy use. There are three different classifications of the mixed mode strategy based on whether they exist in the same place or operate simultaneously. The first classification is the concurrent mode, where the air-conditioning system and the operable windows operate simultaneously in the same place. The occupants are able to open the windows as they prefer, and the HVAC system will supplement with ventilation and cooling as needed. The second classification is change-over, where the mechanical and natural systems operate in the same space but not simultaneously. The building will, in this mode, change between the two ventilation strategies on a seasonal or even daily basis. The last classification is a zoned mode where different strategies are used in different spaces at the same time. With this mode, one room in the building can be ventilated by operable windows, and the HVAC system can ventilate the neighboring room. [53]

## 3.6 Distribution of ventilated air

There are several principles for the distribution of ventilated air through a room, and mixing ventilation and displacement are the two main types. The choice of which principle of distribution to use, the geometry of the room, air temperature, and contamination sources, among others, needs to be considered in the building design phase. [14]

### 3.6.1 Mixing ventilation

Mixing ventilation is the most common principle of ventilation in schools and offices. With this type of distribution, the supply air enters the room with high velocity with the purpose of mixing the fresh supply air with the room air. Mixing the supply air with the room air dilutes the contaminants in the air and provides the set temperature in the space. The supply inlet is normally located close to the ceiling in an unoccupied room area. The disadvantage of this type of system is that it needs a higher airflow to ventilate the room and remove contaminants compared to other systems. The system is, however, easy to design and works well if integrated correctly. [54, 55]

### 3.6.2 Displacement ventilation

Displacement ventilation is categorized as stratified ventilation systems. The air is supplied close to the floor at relatively low velocities, and the fresh air is supplied at a lower temperature than the mean air temperature in the room. The air will start to heat up by surrounding objects giving off heat and rise upwards due to the buoyancy effects. As the air rises, contaminants and excess heat will move toward the ceiling-level exhaust points. A downside with this system is that occupants can feel discomfort if there is a big difference between ankle and head level temperatures. The standard NS-ISO 7730 states that the maximum accepted temperature difference between the ankle and head level is 3 K [12]. [14, 54]

## 4 Principles of natural ventilation

Airflows and the strength of natural ventilation are difficult to predict because of the variability of the ambient conditions, uncertainties around internal loads in the building, and complex airflow patterns. This section will present the fundamental physics and equations needed to understand the basic principles of natural ventilation. The general mathematical principles will be presented first. Further, air pressure, wind effects, and the wind pressure coefficient will be introduced. Lastly, the throw length and velocity of air jets into a room will be presented.

### 4.1 General principles

This section will describe the general principles, equations, and coefficients needed to understand how natural ventilation occurs.

#### 4.1.1 Continuity principle

The continuity principle, presented in equation 4.1, expresses how a physical property like air is preserved, or in other words, how mass flow between two points in steady-state will remain constant.  $\dot{m}$  in the equation is the mass flow in  $\frac{kg}{s}$ ,  $\rho$  is the density of the fluid in  $\frac{kg}{m^3}$  in the investigated points 1 and 2. Further,  $A$  is the cross-sectional area in  $m^2$ , and  $u$  is the fluid velocity at the respective points. According to the continuity principle, the product of the density, cross-sectional area, and velocity at any given point must be equal to the product at any other point along the flow. This means that an increase in the area of the flow will result in a decrease in velocity in order to maintain the same mass flow rate. [14]

$$\dot{m} = \rho_1 A_1 u_1 = \rho_2 A_2 u_2 \quad (4.1)$$

In most cases, when it comes to calculations with ventilation systems, the pressure and temperature differences are so small that the density in the two points can be assumed to be equal. In these cases, the volume flow,  $\dot{V}$  measured in  $\frac{m^3}{s}$ , can be calculated using equation 4.2, based on the continuity principle. [14]

$$\dot{V} = A_1 u_1 = A_2 u_2 \quad (4.2)$$

### 4.1.2 Bernoulli equation

The Bernoulli equation, given in equation 4.3, is a fundamental principle in fluid dynamics that relates pressure, relative height above a reference point, and the velocity of a flow. The equation is based on the conservation of energy. The Bernoulli equation is fundamental to understanding and predicting the behavior of airflows in a building in terms of its natural environment. Here,  $P$  is the pressure of the fluid at a given point,  $g$  is the gravitational constant, and  $z$  is the relative height. The Bernoulli equation indicates that when the velocity of a fluid increases, the pressure and elevation of the fluid change correspondingly to maintain the constant sum of energy. [14, 18]

$$P + \frac{1}{2}\rho_1 u_1^2 + \rho_1 g z = \text{constant} \quad (4.3)$$

### 4.1.3 Flow through a simple opening

Using the Bernoulli equation in equation 4.3, the expression for the velocity of a flow through a simple crack or opening with area  $A$  can be derived. This flow will be induced by the pressure difference occurring over the opening. Equation 4.4 shows the flow rate as a function of the pressure drop through the crack or opening, where  $C_d$  is the discharge coefficient, relating the real airflow,  $Q$ , to the theoretical one. [18]

$$Q = C_d \rho A \sqrt{\frac{2\Delta P}{\rho}} \quad (4.4)$$

## 4.2 Air pressure

Pressure from a fluid or a gas is either referred to as static pressure or dynamic pressure, depending on the state of motion of the fluid. Static pressure is the pressure a gas or fluid exerts on its surroundings if it is not moving. Static pressure is measured compared to atmospheric pressure, and the pressure is uniform in all directions. Dynamic pressure is the result of the density and velocity of the fluid. According to Bernoulli's principle, given in equation 4.3, there is an inverse relationship between the pressure and velocity of a fluid. If the velocity of the fluid increases, the pressure decreases, and vice versa. The dynamic pressure is always positive and in the direction of the fluid. The dynamic pressure of a gas or fluid can be found in equation 4.5. The total pressure is the sum of the static and the dynamic pressure and can be zero, positive, or negative. [14]

$$P_{dyn} = \frac{1}{2}\rho u^2 \quad (4.5)$$

### 4.2.1 Wind effects

Wind flow around a building will cause a pressure drop across the envelope. The wind pressure will be positive on the windward side with an increase in pressure and negative on the lee side of the building with lower air pressure. As a result of the pressure differences between the two sides, the air will flow from the windward side to the lee side of the building. Parameters deciding the effect of wind on the building are climatic parameters, such as wind velocity and incidence angle, environmental, such as plan area density and building height, and the building body. [56]

The local wind flow field is complex and can be very different in urban areas from that in rural areas. The wind is affected by local topography and the size, shape, and distribution of surrounding buildings. The wind velocity in urban areas can also be lower than in rural areas due to wind shielding effects. [57]

When the wind moves towards a building, the wind will either flow through it or around it. The velocity of the approaching wind is affected by the surrounding topography and buildings. Figure 4.1 illustrates how the wind velocity is relative to the building height and how surrounding buildings can act as a shield and interfere with and decrease the wind velocity. The wind velocity will be reduced closer to the ground and will increase with height. [58, 59]

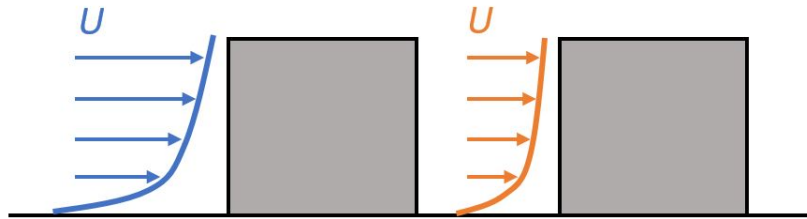


**Figure 4.1:** Illustration of the wind effect on a building. The wind velocity will be lower closer to the ground, and the wind can be affected by nearby buildings. Surrounding buildings will act as a shelter and decrease wind velocity. (Inspired by [58])

Air pressure caused by the wind is found in equation 4.6, where  $P_{wind}$  is the pressure induced by the wind,  $C_p$  is the pressure coefficient,  $\rho_e$  is the external air density and  $u_{ref}$  is the reference wind velocity. The pressure coefficient used in this calculation is described in section 4.2.3. [35]

$$P_{wind} = C_p \frac{1}{2} \rho_e u_{ref}^2 \quad (4.6)$$

The pressure difference between the internal and external air,  $\Delta P_{wind}$ , can be derived from this equation.  $\Delta P_{wind}$  can be found in equation 4.7, where  $P_i$  is the internal air pressure.

$$\Delta P_{wind} = C_p \frac{1}{2} \rho_e u_{ref}^2 - P_i \quad (4.7)$$

### 4.2.2 Pressure gradients

The density of air varies with the temperature. Warm air has a lower density than cold air and is, therefore, lighter. The stack effect occurs due to this, where warm air will rise to higher levels. The density of air can be calculated from equation 4.8, where  $T$  is the temperature. [60]

$$\rho = \rho_0 \frac{T_0}{T} \quad (4.8)$$

The pressure occurring because of the stack effect,  $P_s$ , at a height  $z$ , is described in equation 4.9.  $P_0$  is the static pressure at the reference height in the zone. [26]

$$P_s = P_0 - \rho g \Delta z \quad (4.9)$$

The pressure difference between two zones because of the stack effect is described in equation 4.10. [26]

$$\Delta P = P_{1,0} - P_{2,0} + (\rho_1 - \rho_2)gz \quad (4.10)$$

The pressure differences can be translated into pressure gradients and described graphically. Pressure gradients deciding the inflow or outflow of air in the building result from free convection flow due to density differentials from the temperatures on each side of the enclosure and the forced convection flow due to wind. Figure 4.2 shows the general principle of pressure gradients with the gradient for internal air in red and external air in blue, given that the outdoor air temperature is lower than the indoor air temperature. At a specific height, the neutral plane can be found, where the two pressure gradients are equal. At this point, the pressure difference is zero, and there will be no air movement into or out of the zone. Pressure differences cause air to exit the building above the neutral plane and enter the building below this height. [60]



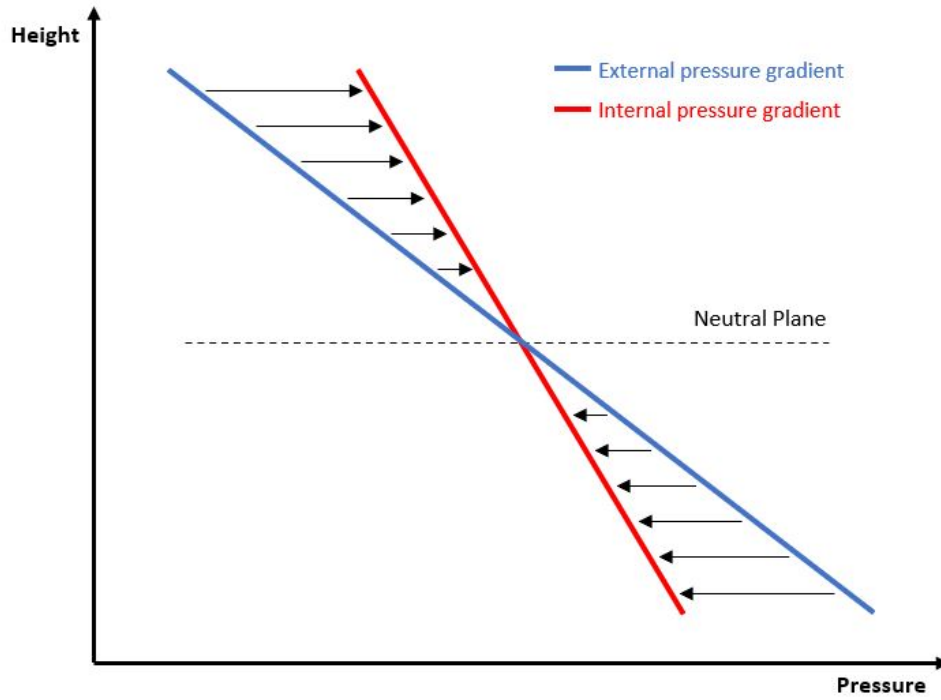


**Figure 4.2:** General pressure gradients when the external air temperature is lower than the internal air temperature. (inspired by [61])

### 4.2.3 Wind pressure coefficient

The wind pressure coefficient,  $C_p$ , is a dimensionless ratio of wind pressure on the building surface to the dynamic pressure in the upstream undisturbed flow and are key inputs for natural ventilation calculations. It is a useful parameter that allows the effects of directional fluctuation and wind velocity fluctuation to be easily identified. Several factors, such as building geometry, position on the facade, degree of exposure, and wind direction, affect the coefficient. The coefficient can be found by arranging equation 4.6, resulting in equation 4.11. Here,  $\Delta P$  is the pressure difference between the point of evaluation and the freestream static pressure, and  $u_\infty$  is the wind velocity in freestream. All the parameters are at the same height, where the pressure coefficient is being evaluated. [31, 58, 62]

$$C_p = \frac{\Delta P}{\frac{1}{2}\rho u_\infty^2} \quad (4.11)$$

Pressure coefficients on a building body can be estimated by full-scale testing, a model test in a wind tunnel, or parametric equations derived from experiments. To determine the pressure coefficient for a specific building, it is necessary to conduct a full-scale measurement or a model test of the building. Full-scale measurements can, however, be expensive, difficult, and require a lot of knowledge. [63]

Standard wind pressure coefficients can be used to examine the natural ventilation potential in buildings in most building energy simulations (BES) as well. The standard coefficients are obtained from databases and are mean values generated from data from full-scale or wind-tunnel measurements. One of the databases used in BES tools is provided by Air Infiltration and Ventilation Center (AIVC), which is based on wind-tunnel measurements. [62]

Because wind pressure coefficients are highly dependent on several factors, the pressure coefficients found in current codes and standards can suffer from inaccuracy to the specific building and lead to uncertainties when calculating the natural ventilation potential and estimating indoor overheating risk and energy consumption. Typically, the pressure coefficient data is calculated as the average value across the building facing the flow to find the ventilation rates. Their errors are assumed to be relatively small for openings located in the facade center instead of the edges where extreme values can occur, and the error increases. [58]

The wind pressure coefficients are also affected by the vertical wind profile modified by the surrounding buildings. Often, the disturbed urbanized wind velocity is used for the calculations instead of undisturbed freestream wind velocities. As explained in section 4.2.1, the wind velocity is lower closer to the ground level. Using a reference freestream wind that is closer to the ground and affected by surrounding buildings and topography can cause biases in the calculated results. Inconsistency in the use of the freestream wind velocity and the local wind velocity will cause biases in the wind pressure coefficient calculation. [58]

The inaccuracy with the used pressure coefficients and the reference wind conditions are regarded as the biggest sources of uncertainty in multi-zone airflow models. Because of this, applying the pressure coefficient data correctly is important to achieve a more accurate estimation of the airflow rate from wind-induced natural ventilation. [58]

### 4.3 Air jets

The velocity of the air entering an opening can be evaluated at a given point in the room. High velocities in the room can create draught that can be perceived as uncomfortable by the occupant. Given that the air enters through a window, it can be assumed that the air enters as a plane. To evaluate the throw distance of the air into the room, equation 4.12 can be used.  $U_m$  is the air velocity at the throw distance  $x$  into the room, and  $U_0$  is the air velocity at the beginning of the plane jet.  $\rho_0$  is the air density at the beginning of the plane jet, and  $\rho_r$  is the air density at a distance  $x$ .  $K_2$  is a coefficient based on the shape of the opening and is normally between 3 and 6, and  $h_0$  is the height of the window column. Lastly,  $\epsilon$  is the contraction coefficient, which varies between 0.7 and 0.9. [64]

$$\frac{U_m}{U_0} = \sqrt{\frac{\rho_0}{\rho_r} K_2 \frac{h_0}{\epsilon x}} \quad (4.12)$$

The throw length of the jet is the distance from the inlet to the place where the velocity in the jet has decreased to  $0.2 \frac{m}{s}$ . To calculate the throw length from the plane jet, equation 4.12 can be rearranged to equation 4.13. [64]

$$x = \frac{\rho_0}{\rho_r} K_2 \frac{h_0}{\epsilon} \frac{U_m^2}{U_r^2} \quad (4.13)$$

If the window is placed less than 30 cm from the roof,  $U_0$  has to be multiplied with  $\sqrt{2}$  because of the *coanda effect*. The Coanda effect is the phenomenon where an air jet adheres to and flows alongside a surface instead of continuing in its original direction. This happens because of a fall in pressure between the air jet and the adjacent surface as the air velocity increases, resulting in inwards suction of the jet towards the wall. The Coanda effect results in an initial free jet transforming into a wall jet. The phenomena can ensure the air does not descend into the room too early and consequently make the occupants of the room feel uncomfortable. [65, 66]

## 5 Zero Emission Buildings

The research center on zero emission buildings (ZEB) is a national research center focusing on eliminating greenhouse gas emissions in buildings. The research center focuses on developing competitive products and solutions for new and existing buildings to lead the market towards zero emission of greenhouse gases through the building phases of production, operation, and demolition. [67]

A zero emission building is a building that compensates for its greenhouse gas emissions during its lifetime by on-site energy production from renewable sources, such as photovoltaic (PV) panels and solar collectors. A net zero emission building (net ZEB) produces the same amount of energy as the energy needed for its operation. In this thesis, the term ZEB will be used about zero emission buildings, and the research center on zero emission buildings will be referred to as the ZEB research center. [7]

### 5.1 ZEB ambition levels

The Norwegian ZEB research center has defined six ambition levels, depending on the number of phases of the building's lifecycle that are accounted for. The ambition levels rank from ZEB-O÷EQ as the lowest level to ZEB-COMPLETE as the highest. A building with the ambition level of ZEB-O÷EQ will have enough renewable energy production to compensate for the greenhouse gas emissions from the operational phase of the building, except for the emissions related to equipment and appliances. With the ambition level of ZEB-COMPLETE, the building will generate enough renewable energy to compensate for the greenhouse gas emissions from the entire lifecycle of the building. This includes the production stage, construction stage, use stage, and the end-of-life stage. The six ambition levels and their respective system boundaries are presented in table 5.1. [7]

**Table 5.1:** The six Norwegian ZEB ambition levels and their respective system boundaries. Each level represents the amount of greenhouse gases the building should compensate for. O represents operation, EQ represents equipment and appliances, M represents materials, C represents construction, and E represents end-of-life. [7]

Ambition level	System boundaries
ZEB-O÷EQ	Compensating for emissions related to the energy use for operation of the building, except for energy used for equipment and appliances.
ZEB-O	Compensating for emissions related to all operational energy.
ZEB-OM	Compensating for emissions related to all operational energy plus embodied emissions from materials.
ZEB-COM	Compensating for emissions related to operational energy, materials, and the construction phase.
ZEB-COME	Compensating for emissions related to operational energy, materials, construction, and the end-of-life phase.
ZEB-COMPLETE	Compensating for emissions from the complete life cycle of the building.

## 5.2 ZEB Laboratory

The ZEB Laboratory is a full-scale office building located in Trondheim at the NTNU Gløshaugen campus. The building is four floors high with an area of  $1800m^2$  and works as a *living laboratory* where the facades, technical system, and other components of the building can be modified and replaced to investigate new and innovative solutions and materials. The solutions used in the building are investigated and tested in interaction with the occupants. The building is planned to achieve the ambition of ZEB-COM over 60 years [8], as a climate adapted building with future-oriented construction techniques, material use, and technology. Pictures of the ZEB Laboratory can be seen in figure 5.1 and 5.2. [8, 68]



**Figure 5.1:** The ZEB Laboratory seen from the northeast.



**Figure 5.2:** The ZEB Laboratory seen from the southwest.

In terms of energy supply, the ZEB Laboratory utilizes a range of renewable energy sources, including electricity, solar panels mounted on the facades and roof, and heat pumps. The heat generated is mainly distributed through waterborne floor heating and radiators, representing an energy-efficient approach that also ensures optimal comfort levels for its occupants. [68]

Of the four floors in the building, half are utilized as office spaces, and the other half are designated for educational purposes. The educational areas comprise lecture rooms and collaborative study spaces. The second floor features two identical office spaces referred to as twin rooms. The two rooms are equipped with independent HVAC systems and a dedicated control room. The twin rooms offer several research opportunities allowing for specific tests in a controlled environment, as the facade materials and components in the rooms can be replaced. The comfort of the occupants is carefully monitored with several installed sensors monitoring factors such as temperature, relative humidity, CO<sub>2</sub> concentrations, and air change rates. [8, 69]

### 5.2.1 Building structure

The load-bearing design of the ZEB Laboratory features columns made of glued laminated timber, cross-laminated timber floors, stiffening inner walls, and wooden frameworks with insulation in the outer walls. The roof is constructed with an innovative compact wooden design that incorporates a smart vapor barrier. U-values of the building components are summarized in table 5.2. Additionally, the normalized leakage rate,  $n_{50}$ , is set to  $0.3h^{-1}$  and the thermal bridge value is set to  $0.03\frac{W}{m^2K}$ . Architectural drawings of the facades of the ZEB Laboratory can be found in appendix A. Permission was given by LINK arkitektur to display the architectural drawings. [69, 70]

**Table 5.2:** U-values of the ZEB-laboratory. [70]

Component	U-value [ $\frac{W}{m^2K}$ ],
Roof	$\leq 0.10$
Outer wall	$\leq 0.16$
Window and door	$\leq 0.80$
Floor	$\leq 0.10$
Inner wall	$\leq 0.16$

Building integrated photovoltaic panels (BIPV) are integrated into the entire roof, most of the east, west, and south facades, as well as the upper part of the north facade. To provide natural light to the first floor, a combination of opaque and semi-transparent photovoltaic (PV) panels arranged in a chessboard pattern has been installed. The total area of installed solar panels is  $963.4 m^2$ , corresponding to 701 panels. The building has two air-to-air heat pumps for heating and hot water systems, as well as an innovative heat storage tank that utilizes phase-changing materials (PCM) to minimize peak heating demands. The building is not equipped with a cooling system, as the intention was to

evaluate to what extent the building can be cooled by using passive means and ventilation strategies. [8, 69]

The windows are three-pane windows, where each pane is 4 mm thick with a 17 mm gap filled with argon gas. The windows have a solar heat gain coefficient of 0.56 and a frame factor of 0.1, and a U-value of  $2.0 \frac{W}{m^2K}$ . Solar shading is implemented on all facades. On the east facade, automatically controlled internal shading is used to ensure the shading is drawn in the morning to prevent unwanted heating. The South facade has implemented automatically controlled external shading. The shading chosen is a zip screen with overall shading of approximately 0.10. The occupants are, however, able to override both the internal and external automatic shadings. The west and north facades have manually controlled internal shading implemented, primarily to be used for preventing glare. [70]

### 5.2.2 Floor plan

ZEB Laboratory is an office and educational building containing four floors. The floors and the zonal division can be found in figure 5.3. The first floor consists of an entrance area, toilets, wardrobes, a cafeteria with seating, and an energy plant. The second floor contains the twin rooms, working spaces, meeting rooms, and toilets. The third floor consists of both open and closed working spaces, meeting rooms, and toilets. Touch-down rooms that can be used as a flexible area is found on both the second and third floor. On the fourth floor, there is a classroom, working spaces, toilets, and a technical room. Larger images of the floor plans can be found in appendix B. Permission was given by LINK arkitektur to display the architectural drawings.

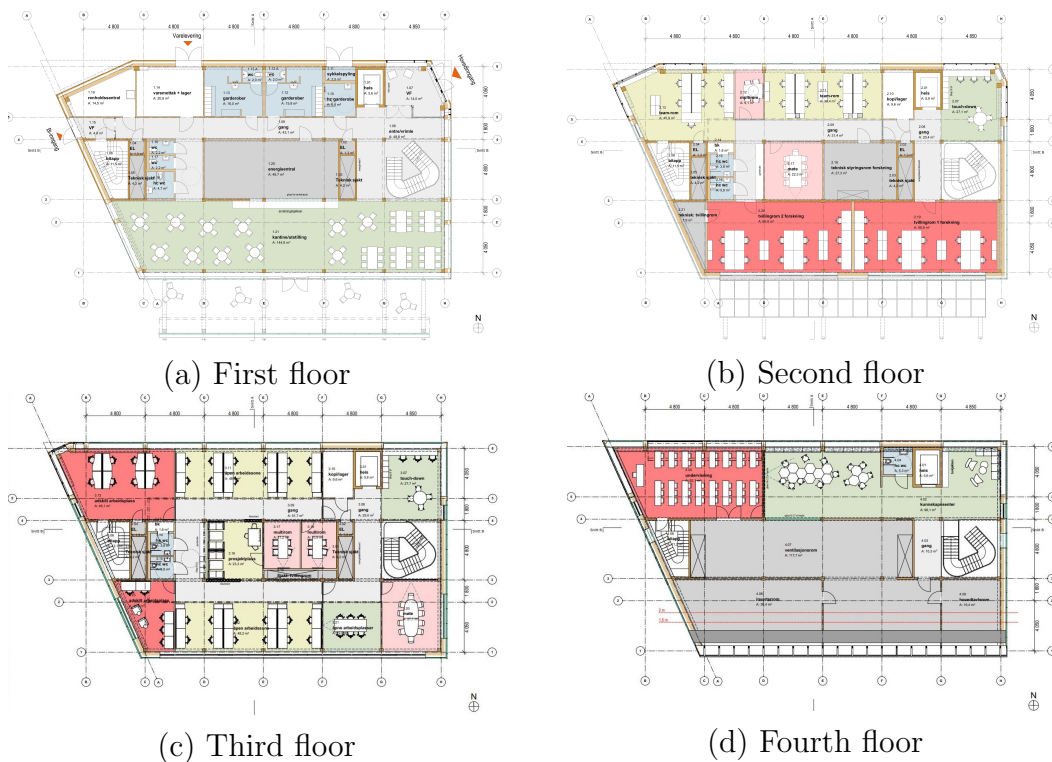


**Figure 5.3:** Architectural drawing of the floor plans in the ZEB Laboratory.

### 5.2.3 Ventilation strategy in the ZEB Laboratory

The ventilation system in the ZEB Laboratory is a hybrid system with both mechanical and natural ventilation. The mechanical ventilation system installed in the building is dimensioned as displacement ventilation with a supply air temperature of 19 °C. The system is dimensioned to deliver  $26 \frac{m^3}{h/person}$  and  $2.5 \frac{m^3}{h/m^2}$  of air. Other demands for the mechanical ventilation system are that it has heat recovery with an efficiency of at least 80% and specific fan power (SFP)  $< 1 \frac{kW}{m^3/s}$ . The two AHUs operating the mechanical ventilation system are placed on the fourth floor and have a total air volume of  $16\ 000 \frac{m^3}{h}$ . The system uses VAV regulated by CO<sub>2</sub> and temperature. [70, 71]

Distribution of air in the ZEB Laboratory is achieved through implementation of the displacement principle, and different methods for ventilation are used on each floor of the building. The first floor employs supply valves positioned on the floor in the canteen and kitchen and a grate located on the wall supplying air to the entrance area. The second floor utilizes ceiling-mounted panels with pressurized chambers located above to supply air, employing displacement ventilation from the roof. The twin rooms located on this floor have individual HVAC systems. On the third floor, the air is supplied from slit valves with pressurized chambers located above. The fourth floor utilizes air supply from terminals located close to the walls near the floor. [71]

The air is extracted centrally on the fourth floor, using the open stairs as shafts. To optimize the functionality of the ventilation system, the closed rooms, like meeting rooms, have overflow valves that are connected to the central exhaust. The toilets and wardrobes have a separate extraction system with CAV regulation and are supplied with air from overflow valves from rooms with higher air quality. [71]

Natural ventilation is provided by a combination of manually and automatically operable windows and will provide the building with fresh air and cooling. The automatic windows can be operated at all hours, while the manual windows can only be operated during working hours. The opening of the manual windows is limited to 20% of the geometric area of the window, and the automatic is limited to 60% of the area. An illustration of the placement of the manual and automatic windows in the ZEB Laboratory can be found in appendix C. [70]

### 5.2.4 Surroundings of the ZEB Laboratory

ZEB Laboratory is located in an area with surrounding buildings and vegetation. The surroundings of the building can be seen in figure 5.4. To the north of the building, the NTNU campus is placed. The topography to the east of the building consists of a semi-open space with limited buildings and vegetation. A railway is placed to the south of the building, and a few buildings are placed behind the railway. There are, however, open spaces located directly to the south of the building. Lastly, the Nina building is placed to the west of the ZEB Laboratory.





(a) The NTNU campus placed to the north of the building.



(b) A semi-open space with buildings and vegetation placed to the east of the building.



(c) Buildings placed to the south of the building.



(d) The Nina building placed to the west of the building.

**Figure 5.4:** Surroundings of the ZEB Laboratory.

### 5.3 IDA ICE as a simulation tool

IDA Indoor Climate and Energy (IDA ICE) is a dynamic simulation tool that can analyze a building's energy consumption, thermal comfort, and indoor environment. The program is a three-dimensional tool that allows for simulation in a multi-zonal building and is based on modules describing the behavior of different parameters and building components. The program provides the opportunity to run detailed simulations by including the intensity of different internal loads, specifying user patterns in each building zone, and implementing technical specifications like HVAC and energy systems. IDA ICE uses equation-based technology, allowing the user to inspect how the model was created. Therefore, no *black box* must be trusted, which gives the user extensive control over the model. IDA ICE is a complex simulation tool that takes time to understand and master. Complex simulations also take large computational power and can take a long time. [72]

Wind pressure coefficients can be implemented in IDA ICE for evaluation of the indoor environment with the use of natural ventilation. Standard wind pressure coefficients used for *semi-exposed* buildings in IDA ICE are given in table 5.3. The coefficients are provided by AIVC and are given for eight different cardinal wind directions on each facade of the building.

**Table 5.3:** Pressure coefficients provided by AIVC in IDA ICE for *semi-exposed* setting.

Wind direction	North facade	East facade	South facade	West facade
0°	0.25	-0.35	-0.50	-0.35
45°	0.06	0.06	-0.60	-0.60
90°	-0.35	0.25	-0.35	-0.50
135°	-0.60	0.06	0.06	-0.60
180°	-0.50	-0.35	0.25	-0.35
225°	-0.60	-0.60	0.06	0.06
270°	-0.35	-0.5	-0.35	0.25
315°	0.06	-0.6	-0.60	0.06

## 6 Method

This section will describe the method used to measure the pressure difference between the inside and outside of the facade, how the data is processed, and the compensations needed to adjust the data. The calculations to find the wind pressure coefficients will also be presented, and the issues that arose with the measurements and the equipment used, as well as the simplifications made. Further, the ZEB Laboratory model in IDA ICE will be presented, and the window control algorithm used to implement natural ventilation in the building will be described. Lastly, the method for evaluating draught in the building is given.

### 6.1 Measurements in the ZEB Laboratory

Full-scale measurements conducted to find specific wind pressure coefficients over a longer period of time will provide more reliable data and give a better representation regarding the sheltering effects from neighboring buildings and vegetation, as well as the structure's geometry, as explained in section 3.2. Full-scale measurements were therefore conducted in the ZEB Laboratory to get the best representation of the forces acting on the facades and their effects on the airflow through the building. The equipment used for the differential pressure measurements were 15 differential pressure sensors, a reference sensor to measure the freestream static pressure, and the weather station located on-site at the ZEB Laboratory.

#### 6.1.1 Setup of the measurements and equipment

Measurements to determine the differential pressure over the facades of the ZEB Laboratory were conducted for 10 weeks from the beginning of February to the middle of April. 15 differential pressure sensors were utilized to measure the pressure difference between the interior and exterior of the building. Specifically, the Sensirion SDP816-125Pa analog sensors were utilized, with a pressure range of  $\pm 125 Pa$ . The sensors use flow-through technology to measure the differential pressure by a thermal sensor element. The sensors have a span accuracy of 3% of the reading and zero-point accuracy of  $0.08 Pa$ . The datasheet for the Sensirion sensors can be found in the references [73].

The overall setup of the measurements is illustrated in Figure 6.1, and was identical for all 15 sensors. In addition to the sensors, the setup consisted of a data logger, a power supply connected to the building's ordinary power outlet, and a tube. The inside pressure was measured at one of the sensor tips, and the outside pressure was measured at the other sensor tip connected to the tube. The tube was placed in the window frame parallel to the outer part of the window. To achieve this, the window was opened, and the tube was positioned in the window frame as parallel to the outer frame as possible, after which the window was closed while holding the tube in place. Figure 6.2 illustrates how the tube was placed and how it barely went through the window gasket. The tube had a diameter

of 2.5 mm and a length of 0.35 m and was relatively stiff. Because of the stiffness of the tube, it is assumed that minimal deformation occurred when closing the window, and sufficient airflow through the tube was maintained. The tube was placed parallel to the outer part of the window to minimize local turbulence around the tube tip. This approach is assumed to enable the sensor only to measure the desired stagnation pressure. However, it should be noted that this is a simplification, and there is no guarantee of no turbulence or perpendicular airflow impacting the results of the measurements.

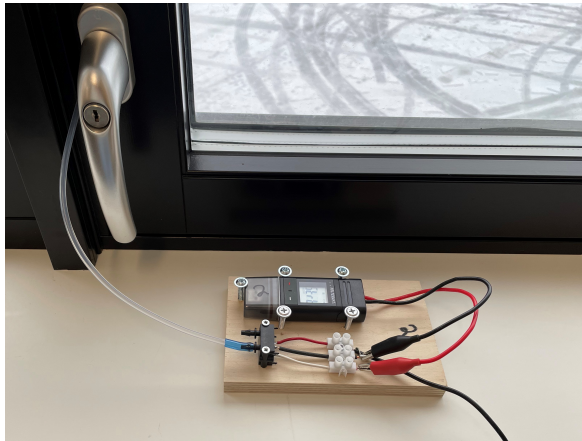


**Figure 6.1:** The setup of the differential pressure measurements consisted of a sensor, a data logger, a power supply, and a tube. The setup was identical for all 15 sensors.

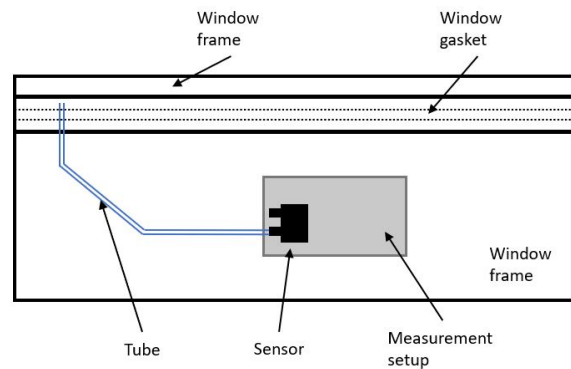


**Figure 6.2:** Illustration of the sensor setup and the tube placement, illustrated in blue. It can be seen how the tube barely went through the window gasket.

The data logger used in the setup was a Voltcraft DL250V measuring the voltage between 0.01 V to 30 V, with an accuracy of  $\pm 0.5\%$ . The sampling rate of the data logger is between 1 min and 24 hours, and it can save up to 31 320 measurements. The datasheet for the datalogger can be found in the references [74].

Five Sensirion sensors were placed on the north facade during the differential pressure measurements. The placement of the sensors on this facade and the corresponding sensor number can be seen in figure 6.3. Further, the placement of the five sensors on the south facade is shown in figure 6.4. Two sensors were placed on the east facade, illustrated in figure 6.5, and lastly, the placement of the three sensors on the west facade can be seen in figure 6.6.



**Figure 6.3:** Placement of the five sensors on the north facade and their respective sensor number.

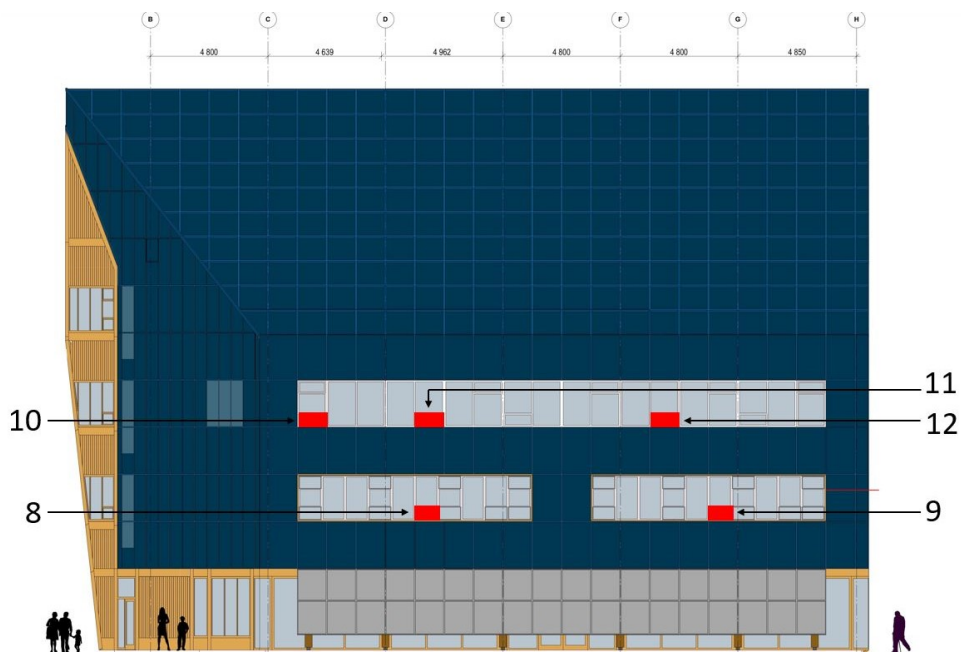


**Figure 6.4:** Placement of the five sensors on the south facade and their respective sensor number.

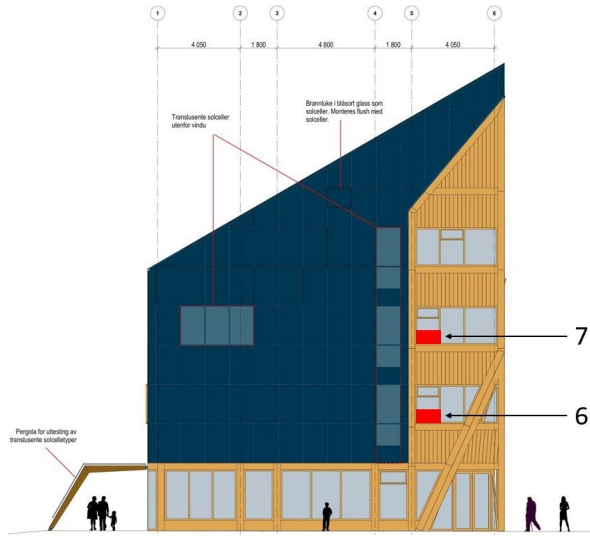


**Figure 6.5:** Placement of the two sensors on the east facade and their respective sensor number.

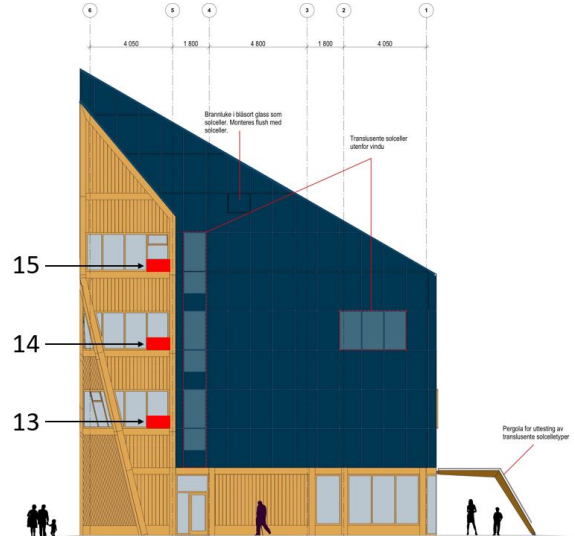


**Figure 6.6:** Placement of the three sensors on the west facade and their respective sensor number.

### 6.1.2 Reference freestream pressure measurement

An additional sensor was used to measure the static freestream pressure, which was used as a reference measurement. This sensor is referred to as the reference sensor throughout the thesis. The sensor used was a DPT-Priima-MOD-az-d sensor. This sensor is a high-accuracy transmitter for measuring differential pressure. It measures the pressure difference of  $\pm 120 Pa$  and with an accuracy of  $0.4\% \pm 0.4 Pa$ . A link to the datasheet can be found in the references [75]. The sensor was placed on the fourth floor in the northeast corner 6.20 meters above floor level, or 18.35 meters above ground level. The tube connected to the sensor inlet measuring the outside pressure was mounted in the middle of the weather station pole. The tube inlet was mounted to a horizontal plate to minimize the impact of stagnation pressure from the horizontal wind and only measure the static pressure. It is assumed that the tube inlet was situated at a height that remains undisturbed by nearby buildings and vegetation, making it in freestream. Figure 6.7 illustrates how the tube inlet was installed.

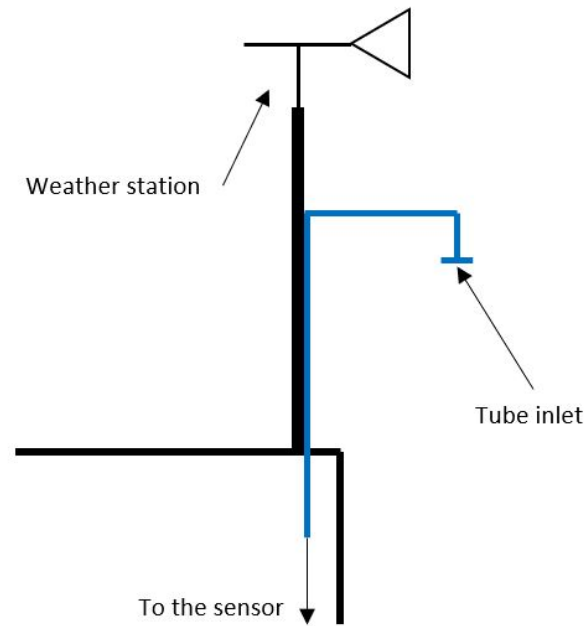


**Figure 6.7:** Illustration of the tube inlet connected to the reference sensor. The tube, marked in blue, is placed halfway on the weather station pole.

### 6.1.3 Weather station

The weather station is placed on the roof of the ZEB Laboratory in the northeast corner. The weather station measures, among other things, the ambient temperature, freestream wind speed, and wind direction. The acquired data was used to determine the wind pressure coefficients. Using the ambient parameters from the weather station located on-site at the building where the measurements are taken gives a higher degree of precision in the variables utilized in the calculations, improving the accuracy of the results.

## 6.2 On-site calibration of the Sensirion sensors

Calibration of the Sensirion sensors was performed as a crucial step during the experimental procedure to adjust the measured pressure values from the installed sensors. The outputs from the sensors were compared to a reference pressure logger with a known standard value to ensure the accuracy of the sensors and their reliability. The calibration setup is illustrated in figure 6.8, where the Sensirion sensors and a TSI VelociCalc 9565-P meter were interconnected via a T-connection to the tube measuring the ambient pressure. The VelociCalc logger was used as a reference pressure logger. In the ideal scenario where the sensors are calibrated, the pressure readings from the two loggers should be identical. Calibrations were done on-site in the ZEB Laboratory, and involved logging pressure readings from the installed sensors every 10 seconds and manually recording the pressure from the VelociCalc pressure logger simultaneously. The data collected from the two loggers were used to establish a trend line and subsequently adjust the pressure measurements obtained from the Sensirion sensors.

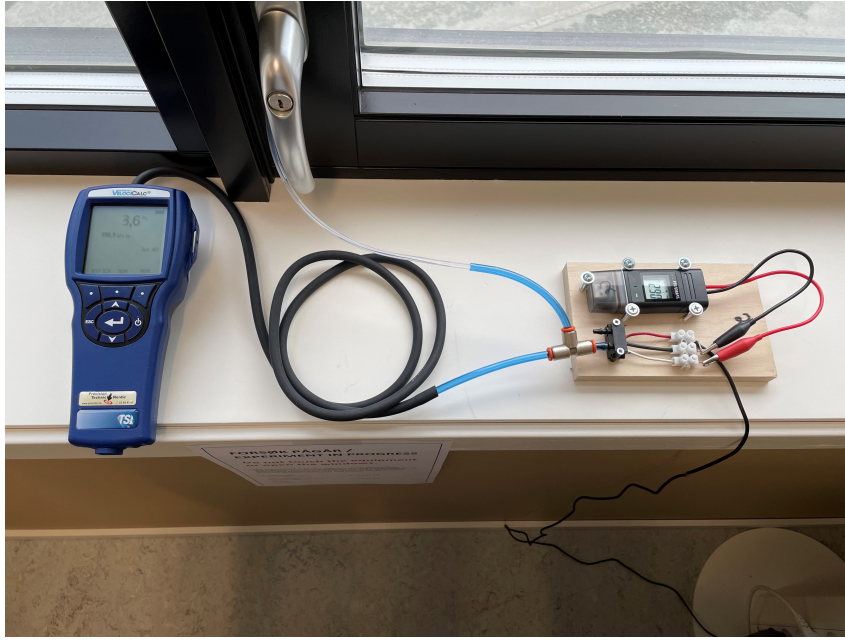


**Figure 6.8:** Setup of the equipment used for calibration of the sensors. The Sensirion sensor was placed to the right, and the VelociCalc differential pressure logger to the left. The two loggers were interconnected through a T-connection to the tube measuring the ambient pressure.

### 6.3 Calculations and measurements compensations

This section will present the equations used to calculate the wind pressure coefficients and how the measurement compensations were done. Measurement compensations were done with regard to the height differences between the reference sensor placed on the fourth floor and the respective sensor measuring the pressure over the facades. In addition, pressure losses in the tube connected to the sensors were taken into account.

#### 6.3.1 Voltage to differential pressure

The data logger connected to the sensors measured the raw data in Voltage. The sensor's output data was configured in *square-root*, as this gives a fully bidirectional output. A benefit of this configuration is that the bidirectional output has a more stable zero point and higher sensitivity at lower pressures [73]. To convert the raw data from Voltage to Pascal, equation 6.1, provided by the manufacturer of the sensors, was used. [73]

$$\Delta P_{sensor} = \left( \frac{A_{out}}{VDD} - 0.5 \right) \cdot \left( \frac{A_{out}}{VDD \cdot 0.4} - 1.25 \right)^2 \cdot 133 \quad (6.1)$$

$\Delta P_{sensor}$  is the output differential pressure in Pa,  $A_{out}$  is the output voltage, and  $VDD$  is the input voltage.



### 6.3.2 Pressure loss in the tubes

A pressure loss in the tubes connected to the sensors will occur. This is because the Sensirion sensors have a small mass flow through the sensors to operate as expected. To calculate the total pressure difference over the facade, including the pressure drop in the tube, equation 6.2 was used. The manufacturer provides this equation in an application note with the sensors [76].  $\Delta P_{eff}$  is the calculated effective differential pressure at the beginning of the tube.

$$\Delta P_{eff} = \frac{\Delta P_{sensor}}{1 + \epsilon} \quad (6.2)$$

To calculate the effective differential pressure in equation 6.2,  $\epsilon$  was calculated using equations 6.3 and 6.4. The manufacturer provides these equations in the same application note [76]. Here, T is the temperature in °C, L is the length, and D is the tube diameter in m. Further,  $\eta_{air}$  is the viscosity of the air at temperature T given in  $\frac{Pa \cdot s}{m}$  and  $\rho_{air}$  is the density of the air in  $\frac{kg}{m^3}$ .  $m_c$  is equal to  $6.17 \cdot 10^{-7} \frac{kg}{s}$  and  $\Delta p_c$  is equal to  $62 Pa$  and are constants provided by the manufacturer.

$$\eta_{air} = (18.205 + 0.0484 \cdot (T - 20)) \cdot 10^{-6} \quad (6.3)$$

$$\epsilon = -\frac{64 \cdot L \cdot \eta_{air} \cdot m_c}{\pi \cdot D^4 \cdot \rho_{air} \cdot \Delta P_{sensor}} \left( \sqrt{1 + \frac{8 \cdot \Delta P_{sensor}}{\Delta p_c}} - 1 \right) \quad (6.4)$$

### 6.3.3 Height compensations

Height compensations were done as a part of the calculation for the wind pressure coefficient in consideration of the height differences between the reference sensor and the respective sensors measuring the pressure over the facades. The reason for doing this was to examine what the measured pressure at a certain height is equivalent to at a different height due to the stack effect. The measured pressure data was compensated to the desired height following pressure gradients due to the temperatures. Equation 4.8 was used to find the density of the air, and equation 4.9 was used to calculate the pressure at the desired height  $z$ , described in section 4.2.2.

The method of height compensation was used to find the static freestream pressure at the intake of the tube connected to the reference sensor or, in other words, the static reference pressure at the roof. The reference sensor measured the pressure at a height of 18.35 meters above the ground. Figure 6.9 illustrates the pressure gradient used to find the pressure at other heights. The figure illustrates how the pressure gradient that occurs in the tube, illustrates in green, follows the outside pressure gradient in blue until

it enters the building and follows the inside pressure gradient in red. It is assumed that the temperature in the tube is equal to the outside in the part of the tube placed outdoors, and the temperature is equal to the inside temperature once the tube enters the building. It is also assumed that the outside temperature is lower than the inside temperature.

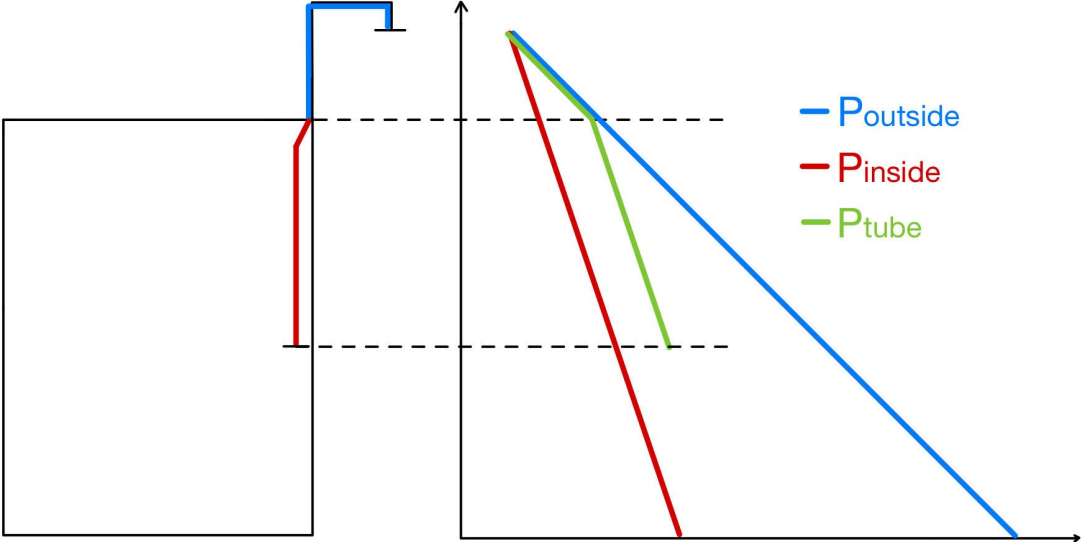


**Figure 6.9:** Illustration of the pressure gradient inside the tube, in green, which follows the outside pressure gradient in blue first and the inside pressure gradient illustrated in red when entering the building.

Figure 6.9 is an exaggerated example to illustrate the principle of the pressure in the tube. Figure 6.10 shows an example of the real pressure in the tube in addition to the inside pressure, as a function of the height above the ground. The parameters for this illustration are from one of the data points gathered during the measurements. The real inside pressure gradient is illustrated in dotted red based on an indoor temperature of  $20^{\circ}\text{C}$ , and the outside pressure gradient is illustrated in dotted blue based on an ambient temperature of  $-6.45^{\circ}\text{C}$ . It can be observed how the pressure in the tube, illustrated in green, follows the outside pressure gradient until it enters the building and starts to follow the inside pressure gradient. The indoor pressure from the reference sensor is illustrated with a solid red line, and it can be observed how it follows the indoor pressure gradient. The pressure found at the facade is given as a yellow dot.

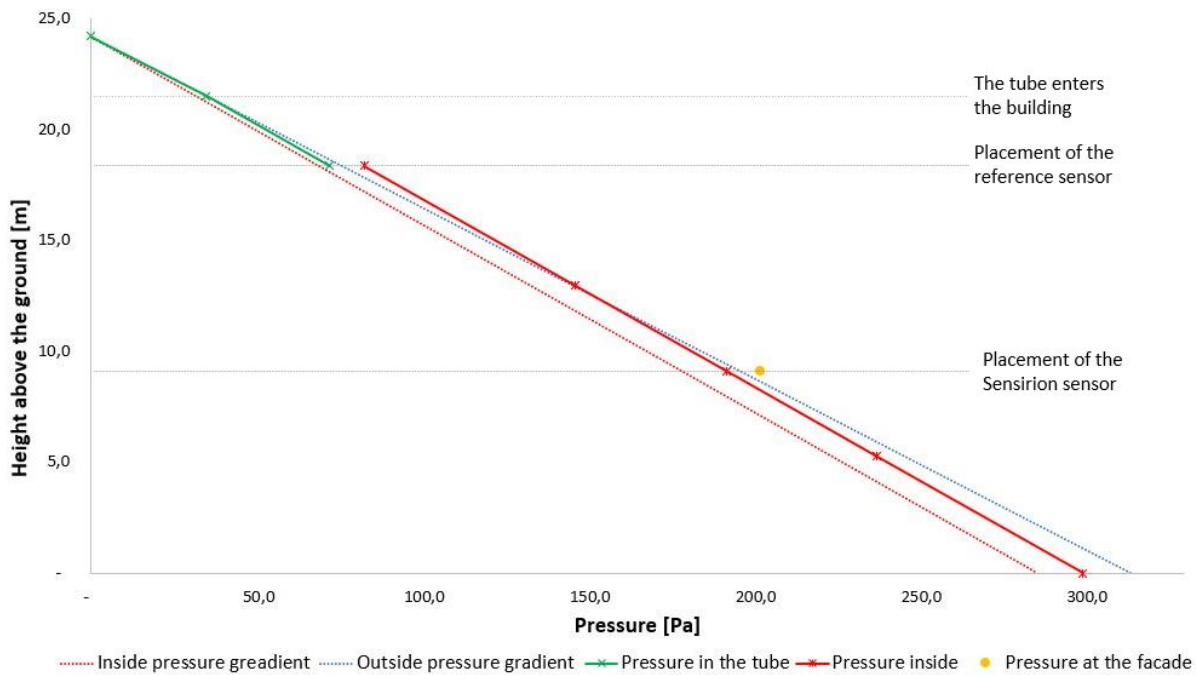


**Figure 6.10:** Real example of the pressure in the tube, and the inside pressure, based on pressure gradients.

The same method was used to find the freestream static pressure and the inside pressure at the same height as the pressure measurements over the facades. The freestream pressure was found by following only the outside pressure gradient with the measurement at the reference sensor tube inlet as the starting point, or in other words, the tube inlet on the roof, and the inside pressure was found by following only the inside pressure gradient with the reference sensor placement as starting point. The ZEB Laboratory is an open building with most zones sharing the same airpath connected to the stairwells. Because of this, the whole structure can be considered one single zone. This means that the assumption can be made that the building is one isothermal zone, where the indoor air temperature is the same throughout the entire building. Hence, one pressure gradient will apply to the inside of the building, decided by the indoor temperature, and a different pressure gradient will apply to the outside of the building, decided by the outdoor temperature.

### 6.3.4 Calculation of the wind pressure coefficient

This section will describe in more detail how the data was used and how the calculations were done to find the pressure coefficients for the ZEB Laboratory. A summary of the raw data output in voltage from the 15 Sensirion sensors can be found in appendix D, the raw data from the reference sensor can be found in appendix E, and the raw data from the weather station can be found in appendix F.

The outside and inside air density was calculated using equation 4.8, with the respective measured outdoor and indoor temperatures measured by the weather station and indoor sensors. Further, the raw data in voltage from the 15 sensors were converted to pressure

in Pascal, using equation 6.1 as described in section 6.3.1. The pressure drop in the tubes was calculated following the method in section 6.3.2 for all 15 sensors. The method was followed for every logged reading from the sensors.

The indoor reference pressure,  $P_i$ , was set to 0 Pa at the height of the reference pressure sensor. The indoor pressure difference,  $\Delta P_i$ , at the second and third floors was calculated using equation 4.9, with  $P_0$  as the indoor reference pressure at this height. Next, the height compensation in the tube,  $\Delta P_{tube}$ , was calculated, as well as the height compensation for the freestream pressure,  $\Delta P_{out}$ , explained in section 6.3.3.

To calculate the desired differential pressure,  $\Delta P$ , equation 6.5 was used,

$$\Delta P = P_v - P_f = \Delta P_{m,v} + \Delta P_{m,t} + \Delta P_i + \Delta P_{tube} - \Delta P_{out} \quad (6.5)$$

where  $P_v$  is the pressure against the outside of the window and  $P_f$  is the freestream pressure at the reference height.  $\Delta P_{m,t}$  is the static pressure measured by the reference sensor, and  $\Delta P_{m,v}$  is the differential pressure over the windows measured by the 15 Sensirion sensors. The calculated differential pressure from equation 6.5 was used to find the wind pressure coefficients by using equation 4.11. An overview of where the different points used in the calculations were placed according to the building facade can be found in figure 6.11. The derivation for equation 6.5 can be found in appendix G.

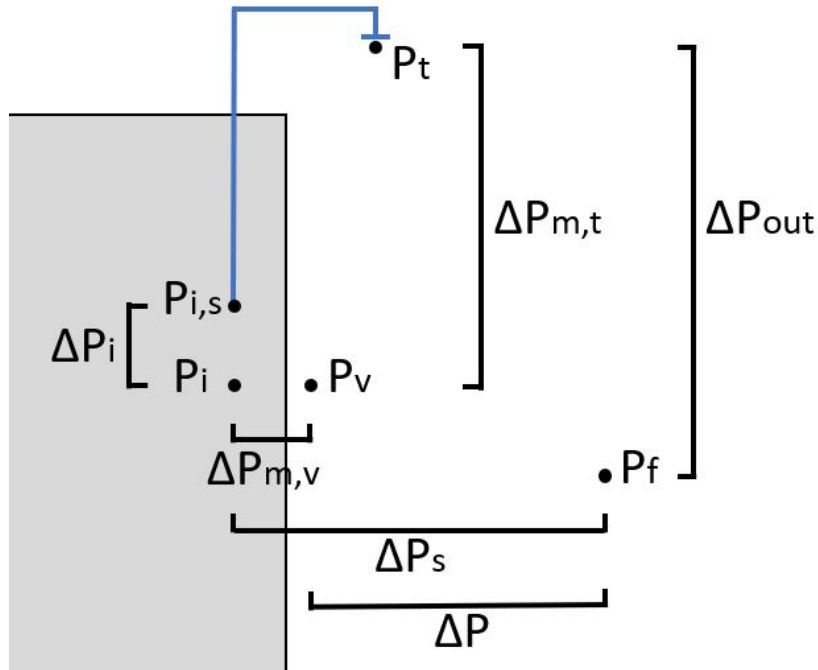


**Figure 6.11:** Overview of where the different points used for calculating  $\Delta P$  were placed according to the building facade. The tube connected to the reference sensor is illustrated in blue.

The resulting pressure coefficients from each measuring point were used to find an average from each sensor and the eight cardinal wind directions. This was done by sorting the data by wind direction, from lowest to highest. The values were divided according to the wind directions used for pressure coefficients in IDA ICE, with an interval of  $\pm 22,5^\circ$ . To achieve the most accurate results, it was desirable to utilize the pressure measurements with the highest wind velocities possible. However, due to a limited amount of available measurements from the north, northeast, and east direction, measurements with lower wind velocities had to be implemented to achieve acceptable results. The lowest wind velocities used to calculate the wind pressure coefficient of the specific cardinal wind direction are given in table 6.1.

**Table 6.1:** The lower limit of wind velocity used to calculate the wind pressure coefficients.

Wind direction [°]	Wind velocity [ $\frac{m}{s}$ ]
0	5.3
45	6
90	6
135	6
180	10
225	10
270	10
315	7.5

During the calculation of the pressure coefficients, the decision was made to exclude extreme values that occurred and affected the averaged coefficients. Specifically, values falling below -2 or exceeding 2 were removed. The reason for removing the values was the assumption that they occurred because of local turbulence or underpressure induced by surrounding buildings and were, therefore, not representable for the pressure coefficient on the facade. Theoretically, the coefficient should be between -1 and 1, hence, it was deemed acceptable to remove the values.

## 6.4 Complications during the measurements and missing data

The measurements were conducted for 10 weeks. After three weeks of measurements, several changes were made in an attempt to improve the observed data. Seven sensors (sensors 2, 5, 6, 7, 13, 14, and 15) were reinstalled because of suspected incorrect installation. In addition, sensors 3 and 4 gave different results, despite being placed on the same floor in a similar area. In an attempt to investigate whether the result was because of errors with one of the sensors or random differences, the two sensors were swapped. Sensors 13, 14, and 15 on the west facades were observed to give a few unreasonable results in pressure. It was decided to reinstall the tube in the window frame, and an observation was made that the tube was sticking out about 2-3 cm outside the window frame in all three cases. The mistake was fixed, and the readings after the correction were improved.

The timing of the measurements from the sensors and the weather station was not coordinated at the beginning of the measuring period. The weather station logs the measurements once a minute. The loggers for the sensors, however, had to be started manually and were not started at the same time. Consequently, the sensors and the weather station did not log measurements simultaneously. Because of the issues that arose with the sensors during the beginning of the measurements, it was decided to exclude the data from the first three weeks of the measurement period.

It was observed that the pressure fluctuated significantly during the period of the day when the mechanical ventilation was turned on. This can be because of the varying air pressure induced by the mechanical fans and the VAV dampers in the building. Because of this, it was initially chosen to exclude the data on weekdays between 8:00 and 18:00. However, because of the missing values to get resulting wind pressure coefficients from the north, northeast, and east wind direction, it was decided to include values in the ventilation period from week 13. During this period, the weather station measures several minutes with wind velocities above  $4 \frac{m}{s}$  from these three cardinal directions.

## 6.5 ZEB Laboratory as IDA ICE model

This chapter will introduce the ZEB Laboratory as an IDA ICE model, including the implementation of the building structure, openings, HVAC system, and usage patterns implemented in the software. Earlier energy simulations and reports, as well as *as-built* documentations of the building and its technical systems, were used to make the model [68, 70, 71]. The location and weather file was set to Værnes, Trondheim because this was the closest location in distance to the ZEB Laboratory.

Due to limitations in IDA ICE, simplifications and modifications were done to make the building geometry. Mainly, the northeast and northwest corner facades were not modeled as inward slopes and therefore did not follow the geometry of the building. The increase this gave in building area is considered minimal and had a negligible effect on the simulation results. The windows placed in these corners were also modified to follow the geometry of the model. Five zones were implemented in the IDA ICE model, including the main staircase and four zones representing the four floors of the building. The staircase on the east side of the building was modeled as one zone that moved from the ground level to the fourth floor. This zone was equipped with openings connected to each floor it passed through to allow free airflow through the model. Each floor was designed with a floor area of  $440m^2$ . The first floor was made with a height of 4.45 m, and the second and third floors were made with a height of 3.85 m. The fourth floor was modeled with a slanted roof. The total height of the building is 22.9 m. All zones except the staircase zone were equipped with an ideal heater with an installed effect of  $160 \frac{W}{m^2}$ , and the set point temperature for heating was  $21^\circ C$ . The U-values in the building components to achieve a level of ZEB-COM are given in table 5.2. Figure 6.12 shows the south and west facades of the ZEB Laboratory model, and figure 6.12 shows the north and east facades of the model.



**Figure 6.12:** The south and west facades of the ZEB Laboratory model in IDA ICE.



**Figure 6.13:** The north and east facades of the ZEB Laboratory model in IDA ICE.

To achieve the most accurate simulation with the found on-site wind pressure coefficients in IDA ICE, the facades were divided into several parts. The division of the facades was done depending on the placement of the sensors used in the differential pressure measurements, so the resulting wind pressure coefficient from each facade was placed in the right area on the IDA ICE model.

### 6.5.1 Openings in the ZEB Laboratory model

The main entrance door of the building has a height of 2.99 m and a width of 2.00 m and allows for two-way airflow. The opening schedule of the entrance door is based on assumptions and expected usage, with a 20% usage pattern in the period where occupants are expected to arrive and leave the building between 07:00 and 09:30 and between 15:00 and 17:00.

Due to extensive computational simulation time, a few of the windows with the same height and identical construction were merged. The windows in the model were a mix of automatic and manual windows. The manual windows were placed 0.8 meters above the floor level, except in the twin rooms, where they were placed 0.85 meters above the floor level. Six of the 14 automatic windows in the twin rooms were placed 0.85 meters above floor level, and the remaining eight were placed 2 meters above floor level. The remaining automatic windows were placed 2.1 meters above floor level, except for two automatic windows on the fourth floor, which were placed 5.3 meters above floor level.

Air leakage through the building body would also occur. The airflows into or out of the building are assumed to occur through small openings in the facade driven by the pressure differences across the envelope. The exfiltration and infiltration driven by wind, buoyancy, and mechanical ventilation were implemented as the airtightness of the modeled building in IDA ICE. A value of  $0.3 \text{ h}^{-1}$  at 50 Pa was used.

## 6.5.2 Internal gains and schedules

The internal gains and schedules from occupancy, equipment, and lighting used in the simulations were based on assessments done by previous students, internal documents regarding the energy usage and standards [9, 70]. The *as-built* document specifies an estimated heat supplement from occupants of  $4.0 \frac{W}{m^2}$ . The specific heat emitted from lighting and equipment was estimated to  $2.4 \frac{W}{m^2}$  and  $3.2 \frac{W}{m^2}$ , respectively. As the IDA ICE model used in this thesis was a simplified model, the schedules for the internal gains were simplified as well. The floor zones featured in the simulation model represent several zones in the ZEB Laboratory that serve varying purposes. Consequently, the schedules utilized in the model may not accurately reflect actual user behavior within the building. The schedules are, however, seen as reasonable to use in the simulations in this thesis.

### Occupancy schedule

Occupancy in the ZEB Laboratory follows the standard opening hours of NTNU from 7:00 to 18:00, with a core time between 8:00 and 16:00. The occupancy in the different parts of the building varies through the day as the building is used for different purposes, such as office work, meetings, and lectures. The number of occupants in each zone was based on the number of chairs in the respective floor zones and the expected usage of the different parts of the zone.

The occupant schedule used in the first floor of the building model is shown in figure 6.14. The maximum occupancy capacity was set to 74 people. The first floor zone included the cafeteria, hence the schedule was mainly based on the predicted user profile in this area. The maximum capacity was set to 75% during lunch, and otherwise, a lower capacity was set as the area is used as a touch-down area. The maximum capacity was set to 75% since it is rarely expected to reach 100%. It was assumed that there were no occupants in the building during the weekend. Hence the occupancy was set to 0 for all building zones.

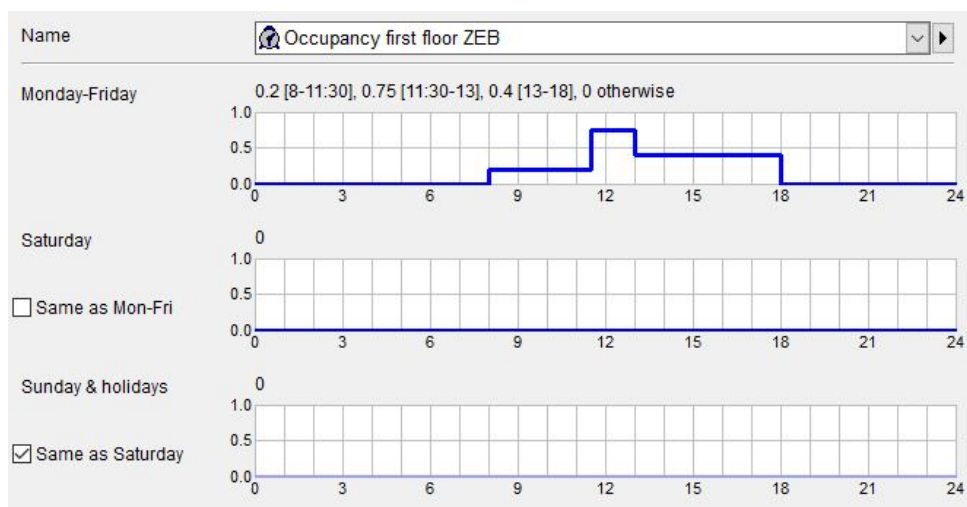
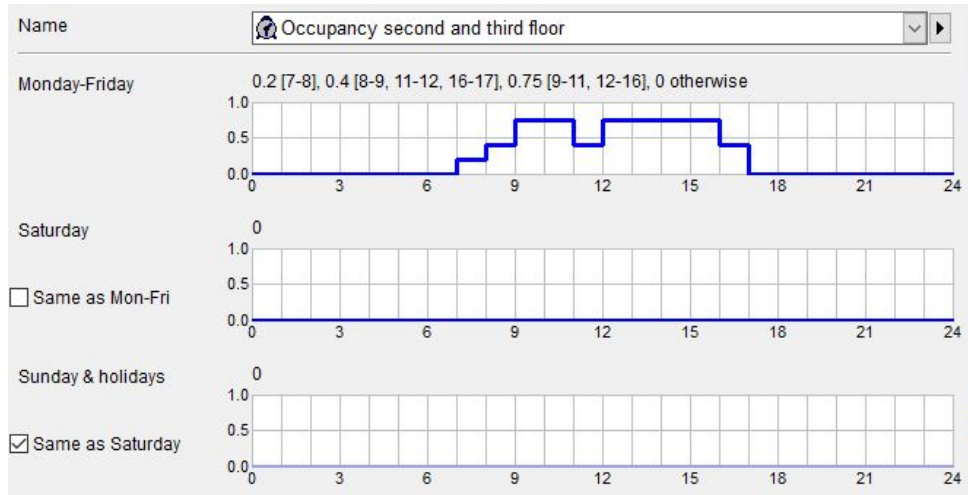


Figure 6.14: Occupant schedule used in the first floor in the IDA ICE model.



The second and third floor zones are mainly office spaces, meeting rooms, and multi-rooms. The maximum occupancy in the two zones was set to 42 and 48 people, respectively. To determine the maximum occupancy capacity, seated office spaces were counted as one person, and the remaining seats were counted as 0,2 people, as the rooms have a lower expected usage. Equivalent to the first floor, it was not expected to reach 100% occupancy in these floors, hence it was reduced to 75%. The occupant schedule for the two zones can be seen in figure 6.15.



**Figure 6.15:** Occupant schedule used in the second and third floor in the IDA IE model.

The fourth floor consists of a classroom and a touch-down area. The maximum occupant capacity was set to 44 people, based on the number of seats in the classroom counted as one person and the number of seats in the touch-down rooms counted as 0.2 persons. The occupancy schedule in the fourth floor zone can be seen in figure 6.16.

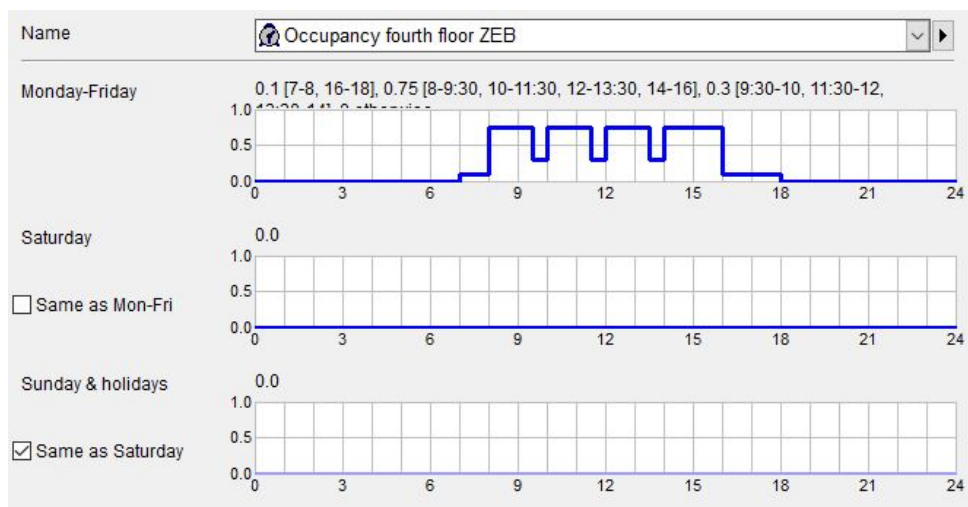


**Figure 6.16:** Occupant schedule used in the fourth floor in the IDA IE model.

### 6.5.3 Mechanical ventilation in the ZEB Laboratory model

The ZEB Laboratory has two ventilation units with a total of  $16\,000 \frac{m^3}{h}$  placed on the fourth floor. In the IDA ICE model, this was modeled as one standard air handling unit. The fans were scheduled to operate at 100% from 08:00 to 18:00 during the weekdays and 0% outside of occupancy hours and during the weekends. The heat exchanger was set to 85% efficiency, and the supply temperature was set to a constant  $19^\circ\text{C}$ . There is no mechanical cooling in the ZEB Laboratory. Hence the cooling coil was changed to 0 to represent this. The modeled AHU in the IDA ICE model is shown in figure 6.17.

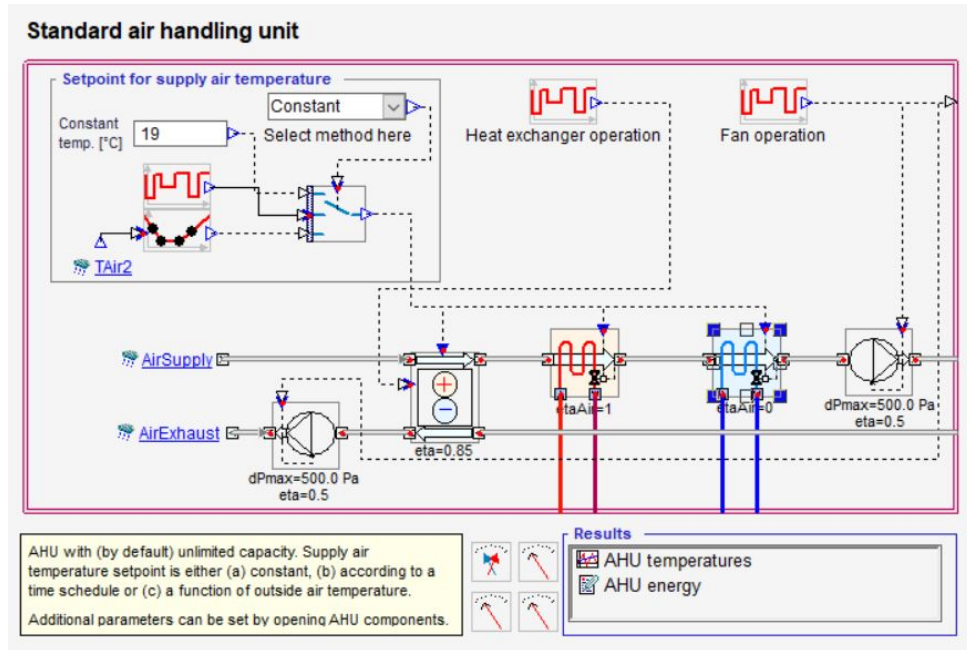


Figure 6.17: The modeled AHU in the ZEB Laboratory model, clipped from IDA ICE.

Two additional ventilation units are also installed for the twin rooms on the second floor, totaling  $2400 \frac{m^3}{h}$ . These units were not implemented in the IDA ICE model as they are only used for research purposes and not building ventilation.

### 6.5.4 Window control algorithm

A window control algorithm was created to implement natural ventilation for cooling purposes in the IDA ICE model. The algorithm was developed by Sande for his Master's thesis [9], and the setpoints were based on his findings for optimal cooling of the building with natural ventilation. The algorithm implemented was a simple on/off algorithm and used automatic heuristic control, mainly based on IF/THEN rules, to open the windows between the chosen setpoints. The setpoint for cooling was  $24^\circ\text{C}$  during occupancy hours and  $26^\circ\text{C}$  during the night. A hysteresis effect was implemented to minimize the number of operations during occupancy hours. When the indoor air temperature exceeded the set limit and the windows opened, the controller would not allow for operation before the temperature fell below  $22^\circ\text{C}$ , which is  $2^\circ\text{C}$  lower than the cooling setpoint.

Further, the maximum CO<sub>2</sub> concentration was set to 900 ppm, and the minimum was set to 700 ppm. However, the windows could stay open if the CO<sub>2</sub> concentrations were below 700 ppm but the indoor temperature was above the setpoint and close earlier if the temperature fell below 22 °C, independent of the CO<sub>2</sub> concentration. The algorithm also included a maximum degree of opening set to 30% of the geometrical area. The algorithm included night cooling, and the controller alternated between day-time and night-time at 7:00 and 18:00. The algorithm was made in a way that the window would automatically close if the ambient temperature fell below 12 °C or if the wind speed exceeded 10<sup>m/s</sup>. A flow diagram of the algorithm can be seen in figure 6.18, and a detailed explanation of the algorithm is given in appendix H.

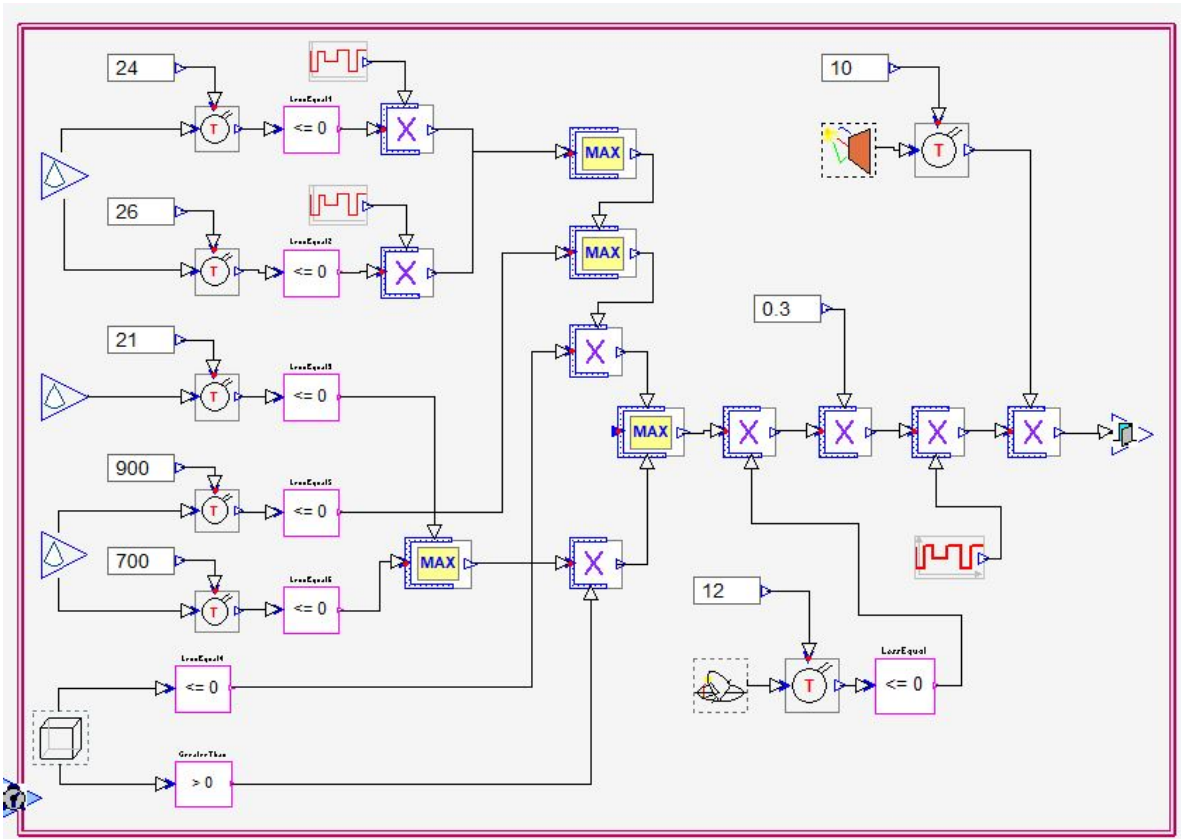


**Figure 6.18:** A flow diagram of the implemented window control algorithm used to allow natural ventilation of the ZEB Laboratory model in IDA ICE.

**6.5.5 Evaluation of simulations in IDA ICE**

Simulations in IDA ICE were done to evaluate the effect of the on-site wind pressure coefficients compared to the standard AIVC coefficients provided in the software. The evaluation was conducted regarding the indoor environment and thermal comfort in the building. Simulations were carried out for a week from 17. July to the 23. July. A week during the summer was chosen because natural ventilation has the biggest potential in the building during this period. The indoor environment was evaluated based on the CO<sub>2</sub> concentrations, age of air, operative temperature, and thermal comfort in the zones.

## 6.6 Evaluation of draught

IDA ICE can not evaluate the air velocity at a given point in a zone, which makes it difficult to evaluate the draught risk in the building. To evaluate this, it was decided to look into a case in the open workspaces placed on the third floor. The air jet evaluated was based on an arbitrary window with automatic control in the zone. The window had an area of  $0.70m^2$  and was placed close to the suspended panels from the roof of the zone. The opening area of the window in the simulated model was set to 30% of the window area, equivalent to  $0.21m^2$ . The airflow rate through the window was read from the ventilation airflow tab in IDA ICE at the given zone, and it was chosen to use  $113\frac{L}{s}$ , or  $0.113\frac{m^3}{s}$ . Equation 4.13 was used to find the throw length from the plane jet with varying values of  $K_2$  and  $\epsilon$ .

To find the throw length,  $U_m$  was set to  $0.2\frac{m}{s}$ , and  $h_0$  was set to  $0.18m$ , based on the window area and the length of the window evaluated.  $\rho_0$  was set to  $1.20\frac{kg}{m^3}$  and  $\rho_r$  was set to  $1.19\frac{kg}{m^3}$ . The relationship  $\frac{\rho_0}{\rho_r}$  is close to 1 because the outdoor and indoor temperatures were relatively similar.

Further, the throw length into the ZEB Laboratory was evaluated both during a day with wind velocities between 2 and  $4\frac{m}{s}$ , or a typical summer day, and during the full simulated week. The throw length in the room was evaluated using the same method as explained above, with values for  $K_2$  and  $\epsilon$  based on conditions in the ZEB Laboratory. The results were presented as a duration curve. The calculations were made based on an occupant located in the open workspaces to the south of the floor. As can be seen on the floor plan in figure 5.3, there is a wall around 5.8 m into the zone, where the air jet will hit if the velocity is high enough. To evaluate the draught risk at this point, the air velocity was calculated by rearranging equation 4.12 to find  $U_m$ . The throw length  $x$  was set to 6.8m, the length of the room before the jet hits the wall, plus a meter where the jet will follow the wall downwards.

## 7 Results

This section contains the results from the differential pressure measurements, calculations of the wind pressure coefficients, and simulations in IDA ICE. The results from the calibration of the sensors are presented first, as well as the calculated pressure acting on the facades based on the differential pressure measurements in the building. Further, the resulting wind pressure coefficients divided into cardinal directions on each facade will be given. Finally, the results from the IDA ICE simulations with both on-site and standard wind pressure coefficients are shown, and an evaluation of the draught risk in the building is presented.

### 7.1 Calibration of the Sensirion sensors

Calibration of the Sensirion sensors was carried out on-site towards the end of the measurement period by following the method described in section 6.2. Equation 7.1 is the general equation used as the trend line describing the relationship between the pressure measured by the Sensirion sensors and the reference VelociCalc pressure logger. The specific value for  $a$  and the  $R^2$  number obtained from the calibrations of each sensor can be found in table 7.1. The coefficient  $b$ , or the point of intersection, is excluded from the table because it was set to zero for all 15 sensors. It should be noted that the wind was approaching from the east, southeast, and east directions during the calibrations.

$$y = a \cdot x + b \tag{7.1}$$

**Table 7.1:** Overview of the  $a$  coefficient and the  $R^2$  number obtained from calibrating the Sensirion sensors against a reference pressure logger.

Sensor	$a$	$R^2$ number
Sensor 1	4.856	0.400
Sensor 2	3.526	0.573
Sensor 3	5.304	0.405
Sensor 4	3.471	0.716
Sensor 5	5.750	0.640
Sensor 6	3.464	0.798
Sensor 7	2.983	0.863
Sensor 8	4.724	0.935
Sensor 9	4.220	0.923
Sensor 10	3.948	0.822
Sensor 11	4.337	0.918
Sensor 12	4.822	0.889
Sensor 13	5.540	0.734
Sensor 14	4.816	0.513
Sensor 15	4.869	0.530

Table 7.1 shows varying coefficients obtained from the calibrations. It is evident that the  $R^2$  number for the sensors placed on the east facade (sensors 6 and 7) and south facade (sensors 8, 9, 10, 11, and 12) are higher than the remaining sensors.

## 7.2 Calculated pressure on the facades

By following the method to calculate the pressure on the building facade by equation 6.5 described in the first half of section 6.3.4, the results in figure 7.1, 7.2, 7.3, and 7.4 was made. The results are the calculated pressure acting on the facades of the ZEB Laboratory and the pressure used in the numerator of equation 4.11 to find the wind pressure coefficients. The x-axis in the graphs is the data points, or measurement points, which were logged once a minute during the measurement period. The data was sorted after time, and data during periods with mechanical ventilation was excluded. Additionally, all data collected during periods with wind velocities below  $4 \frac{m}{s}$  were removed. Because of the excluded data, the graphs do not include all data from the 10 weeks of measurements but rather the specific data used in this thesis.

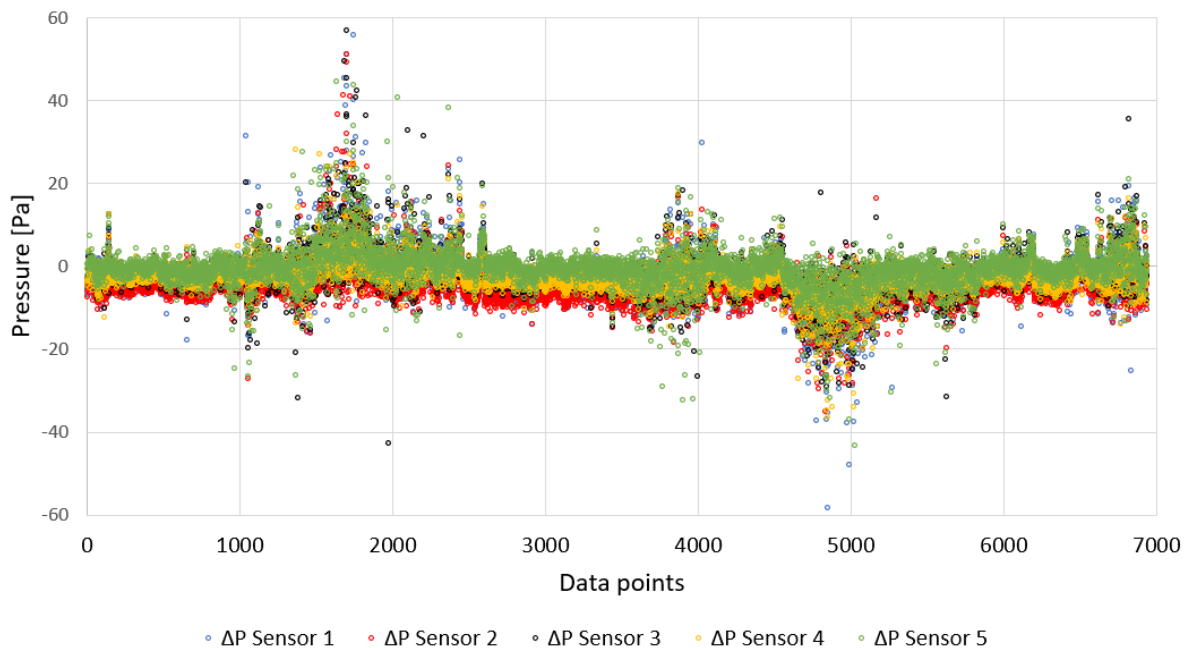


**Figure 7.1:** Calculated wind pressure acting on the north facade of the ZEB Laboratory, based on pressure measurements. The x-axis is given as data points, where one data point represents one minute. The graphs only include the data used for the calculations and not data from the whole measurement period.

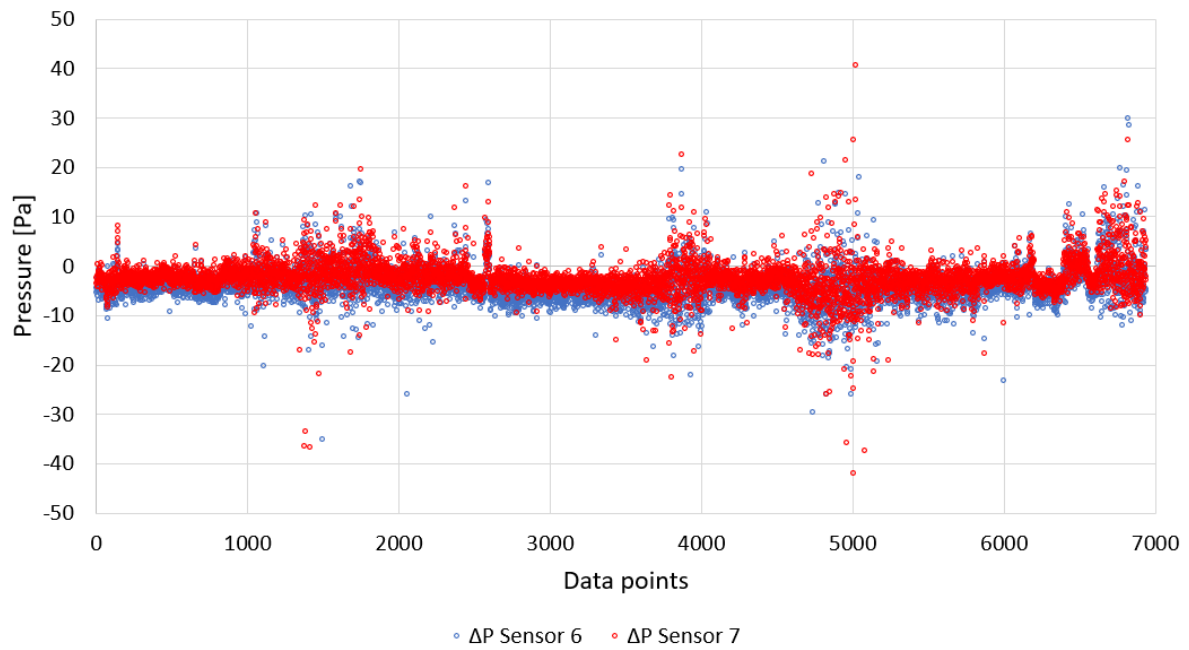


**Figure 7.2:** Calculated wind pressure acting on the east facade of the ZEB Laboratory, based on pressure measurements. The x-axis is given as data points, where one data point represents one minute. The graphs only include the data used for the calculations and not data from the whole measurement period.

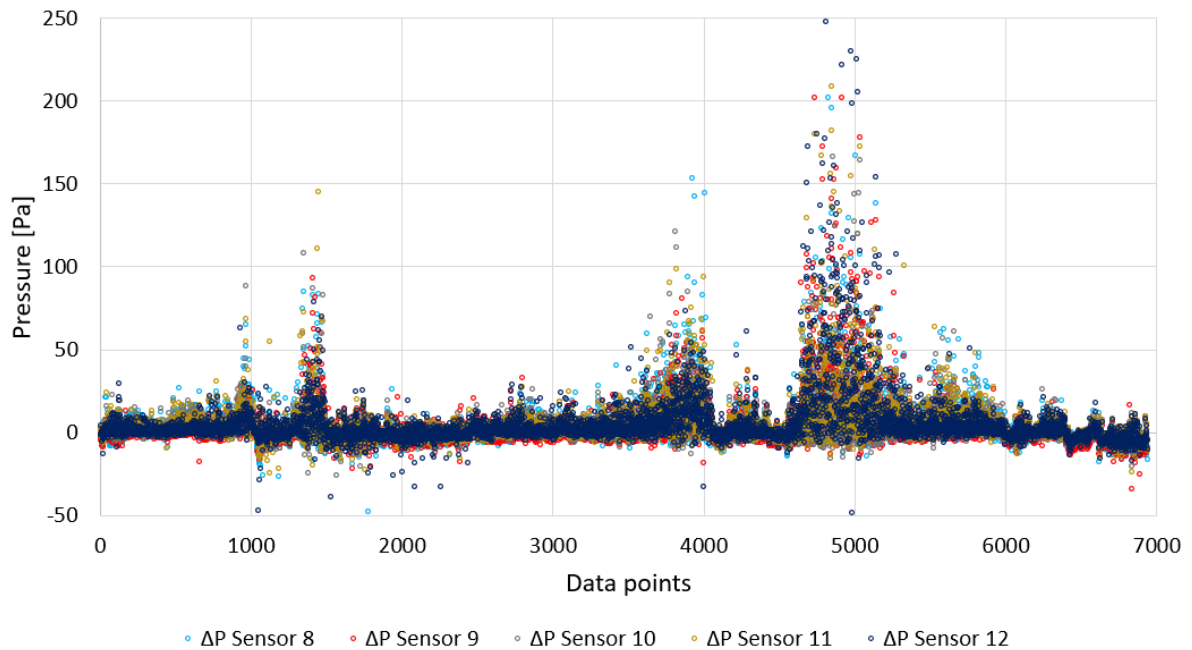


**Figure 7.3:** Calculated wind pressure acting on the south facade of the ZEB Laboratory, based on pressure measurements. The x-axis is given as data points, where one data point represents one minute. The graphs only include the data used for the calculations and not data from the whole measurement period.

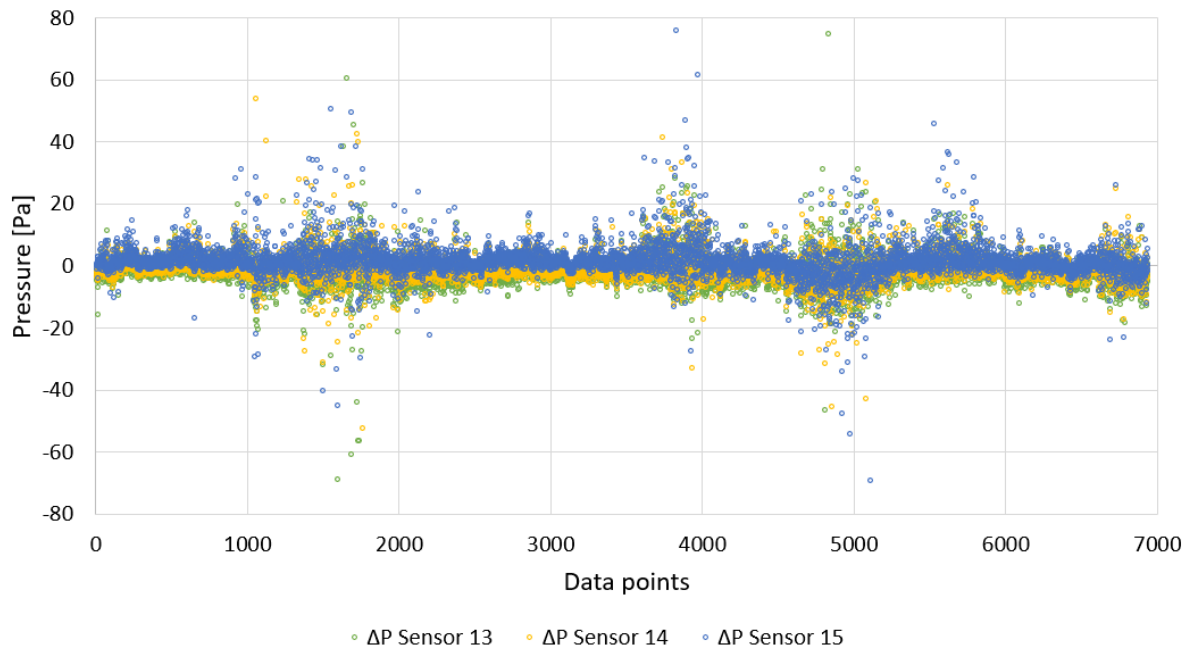


**Figure 7.4:** Calculated wind pressure acting on the west facade of the ZEB Laboratory, based on pressure measurements. The x-axis is given as data points, where one data point represents one minute. The graphs only include the data used for the calculations and not data from the whole measurement period.

It can be observed from figure 7.1, 7.2, 7.3, and 7.4 that the pressure acting on all four facades were normally between -20 Pa to 20 Pa during the measurements, with periods of the pressure exceeding this. The pressures acting on the south facade can generally be observed to be higher than the pressures acting on the remaining facades. Additionally, the pressures acting on the east facades were generally lower than the other facades.

### 7.3 Wind pressure coefficients

The calculated wind pressure coefficients acting on the north, east, south, and west facades of the ZEB Laboratory are given in table 7.2, 7.3, 7.4 and 7.5, respectively. The results were divided into eight cardinal wind directions, with each wind direction being  $\pm 22.5^\circ$ . The pressure coefficients were calculated using the results presented in section 7.2 and equation 4.11, as described in section 6.3.4.  $0^\circ$  represents wind approaching from the north in all tables, and  $180^\circ$  is wind approaching from the south.



**Table 7.2:** Calculated wind pressure coefficients on the north facade, based on the measurements from the five sensors placed on this facade.

North facade					
Wind direction [°]	Sensor 1	Sensor 2	Sensor 3	Sensor 4	Sensor 5
<b>0</b>	0.324	0.096	0.232	0.281	0.218
<b>45</b>	0.137	0.044	0.085	0.085	0.144
<b>90</b>	-0.020	-0.097	-0.002	-0.034	0.044
<b>135</b>	-0.366	-0.270	-0.278	-0.316	-0.214
<b>180</b>	-0.206	-0.165	-0.141	-0.171	-0.140
<b>225</b>	-0.017	-0.054	-0.028	-0.021	-0.031
<b>270</b>	0.073	0.016	0.021	0.039	0.013
<b>315</b>	0.230	0.182	0.248	0.157	0.250

Table 7.2 shows the resulting on-site wind pressure coefficients acting on the north facade. The coefficients were expected to be positive from the northern wind directions and negative from the southern wind directions, which was the case on this facade. The pressure coefficients logged by sensor 5, placed on the fourth floor, were generally slightly higher than the sensors placed on the lower floors. It should be noted that sensor 2 logged values significantly closer to 0 from the north than the other sensors.

**Table 7.3:** Calculated wind pressure coefficients on the east facade, based on the measurements from the two sensors placed on this facade.

East facade		
Wind direction [°]	Sensor 6	Sensor 7
<b>0</b>	0.070	0.235
<b>45</b>	0.162	0.186
<b>90</b>	0.095	0.048
<b>135</b>	-0.072	-0.002
<b>180</b>	-0.093	-0.071
<b>225</b>	-0.026	-0.012
<b>270</b>	-0.008	0.022
<b>315</b>	0.003	0.040

Calculated wind pressure coefficients acting on the east facade are given in table 7.3. All coefficients were relatively close to 0, regardless of the wind direction. It can be observed that the biggest positive value logged from sensor 6 was from the northeast, and from sensor 7, the north. The biggest negative values from both sensors were from the south, or 180°. The values from the west, which is expected to be the biggest negative, were close to 0.

**Table 7.4:** Calculated wind pressure coefficients on the south facade, based on the measurements from the five sensors placed on this facade.

South facade					
Wind direction [°]	Sensor 8	Sensor 9	Sensor 10	Sensor 11	Sensor 12
<b>0</b>	-0.154	-0.208	-0.041	-0.024	-0.088
<b>45</b>	-0.137	-0.124	-0.019	-0.021	-0.036
<b>90</b>	-0.170	-0.212	-0.101	-0.119	-0.140
<b>135</b>	0.174	0.211	0.160	0.401	0.616
<b>180</b>	0.458	0.595	0.281	0.509	0.691
<b>225</b>	0.306	0.247	0.212	0.232	0.258
<b>270</b>	0.039	0.091	0.011	0.040	0.021
<b>315</b>	-0.007	0.012	0.027	0.038	0.040

Table 7.4 includes the calculated pressure coefficients acting on the south facade. The results on this facade were generally as expected, with the biggest and positive values generated by wind approaching from the south and negative values generated by wind approaching from the north. However, the biggest negative coefficients were generated by wind from the east by all five sensors. It can be observed that the pressure coefficients from sensors 8 and 9 were relatively similar. The resulting coefficients from sensors 10, 11, and 12 were relatively similar, with the exception of sensor 10 from 135° and 180°, which were much lower.

**Table 7.5:** Calculated wind pressure coefficients on the west facade, based on the measurements from the three sensors placed on this facade.

West facade			
Wind direction[°]	Sensor 13	Sensor 14	Sensor 15
<b>0</b>	-0.035	-0.020	0.011
<b>45</b>	-0.040	0.071	0.118
<b>90</b>	-0.140	-0.076	0.003
<b>135</b>	-0.169	-0.216	-0.141
<b>180</b>	-0.014	-0.067	-0.065
<b>225</b>	0.054	0.057	0.139
<b>270</b>	-0.046	0.036	0.052
<b>315</b>	0.053	0.056	0.133

The calculated wind pressure coefficients on the west facade are given in table 7.5. The biggest negative pressure coefficients were induced by wind approaching from 135° from all sensors, and the biggest positive coefficients were induced by wind approaching from 225°. All the calculated on-site pressure coefficients were relatively close to zero and deviated significantly from the standard AIVC coefficients. It can be observed that the pressure coefficients from sensor 15 resulted in positive values by the wind from 0°, 45°, and 90°.

## 7.4 Simulations in IDA ICE

Simulations were carried out by implementing the on-site wind pressure coefficients in the IDA ICE model from tables 7.2, 7.3, 7.4 and 7.5 and standard coefficients provided by AIVC, given in table 5.3. This chapter will focus on the resulting indoor environment from the simulations with the different pressure coefficients for wind-induced natural ventilation. The results will focus on the parameters on the first and third floors. Lastly, an evaluation of the draught risk in the building when opening the windows will be presented. Simulations were done for a week in July, from 17. July to the 23. July. All figures in this chapter are results from this time interval.

### 7.4.1 Simulation with on-site wind pressure coefficients

Figure 7.5 and figure 7.6 illustrate the mean air temperature and the operative temperature in the first and third floor during the simulated week with on-site pressure coefficients. The temperatures in the third floor fluctuated more than in the first floor. The operative temperatures were generally higher than the mean air temperature in both zones. It can also be observed that the temperature fluctuated less during the weekend on the 22. July and 23. July, when the occupants were absent. The temperature fluctuated more on the third floor, and it is evident that the windows were opened on this floor during the middle of the day on the 23. July.

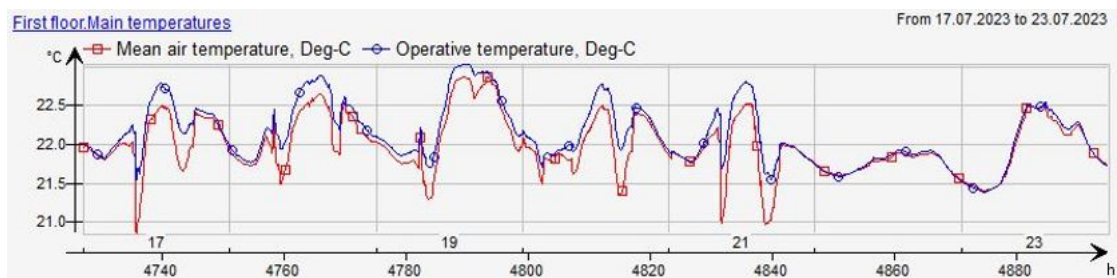


**Figure 7.5:** Resulting indoor temperatures in the first floor during the simulated week with on-site pressure coefficients. The figure is clipped from IDA ICE.

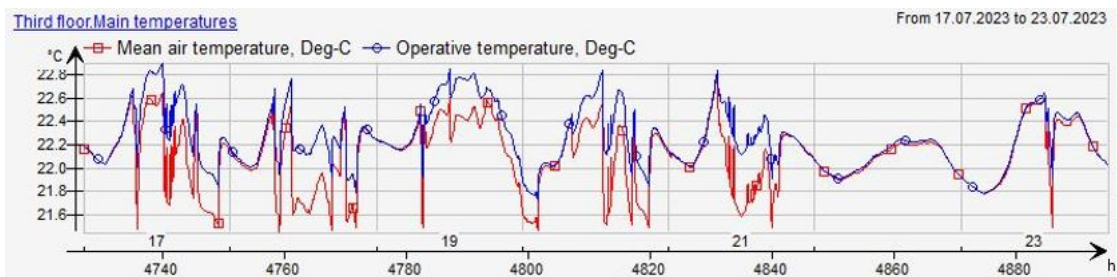


**Figure 7.6:** Resulting indoor temperatures in the third floor during the simulated week with on-site pressure coefficients. The figure is clipped from IDA ICE.

The CO<sub>2</sub> concentrations in the first and third floor during the simulation can be found in figure 7.7 and figure 7.8, respectively. CO<sub>2</sub> concentration in the first floor exceeded 650 ppm during the 20. July around 12:30, and the concentration in the third floor peaked around 13:00 the same day. However, the concentrations remained below 600 ppm in both zones during most of the simulated week.

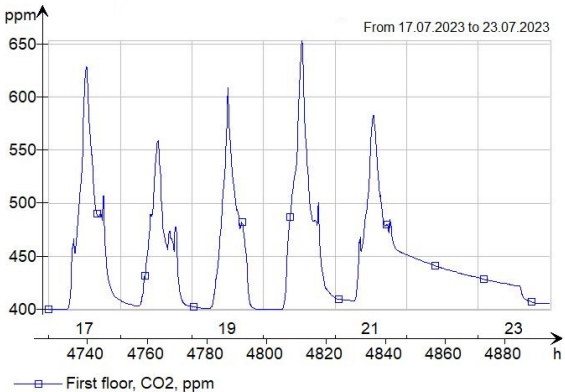


**Figure 7.7:** CO<sub>2</sub> concentrations in the first floor during the simulated week with on-site pressure coefficients. The figure is clipped from IDA ICE.

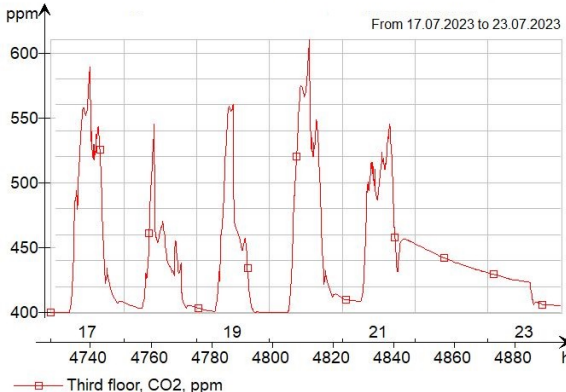


**Figure 7.8:** CO<sub>2</sub> concentrations in the third floor during the simulated week with on-site pressure coefficients. The figure is clipped from IDA ICE.

Results from the simulation with on-site pressure coefficients regarding the age of air in the first and third floor are shown in figure 7.9 and figure 7.10. The age of air reached a peak during the weekend when it exceeded 25 hours in both zones. The results were, however, lower during the weekdays, from 17. July to 21. July, and it is evident that the air in the building was exchanged during the day. The relative humidity fluctuated between 40% and 58% in the first floor and 40% and 60% in the third floor. The relative humidity averaged 49.6% in the first floor and 49.1% in the third floor during the simulated week.

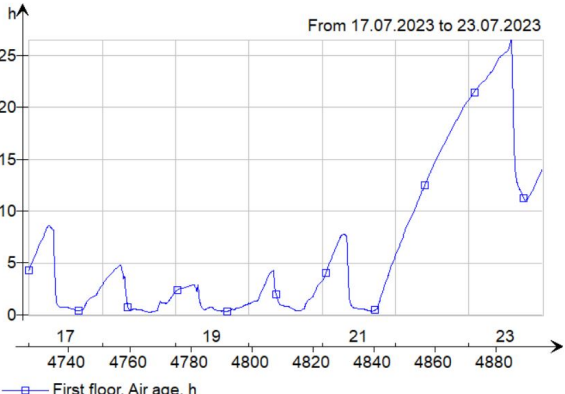


**Figure 7.9:** Resulting age of air in the first floor with simulation using on-site pressure coefficients. The figure is clipped from IDA ICE.

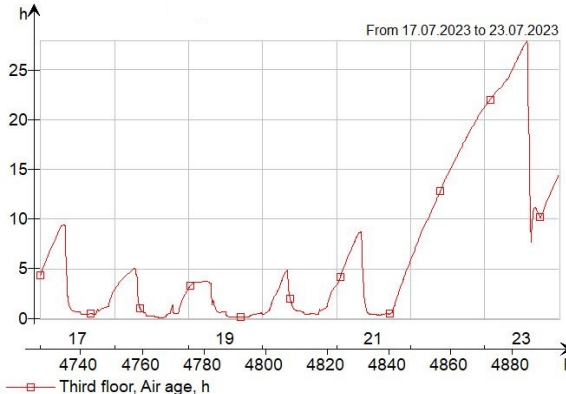


**Figure 7.10:** Resulting age of air in the third floor with simulation using on-site pressure coefficients. The figure is clipped from IDA ICE.

The number of occupancy hours within four comfort categories evaluated according to EN-15251 is shown in table 7.6. All hours were within the best category, and there were no unacceptable hours with temperatures exceeding 26°C in the two zones.

**Table 7.6:** Number of occupancy hours within four comfort categories evaluated according to EN-15251. The simulation was done with on-site pressure coefficients.

Comfort category	First floor [h]	Third floor [h]
Best	50	50
Good	50	50
Acceptable	50	50
Unacceptable	0	0

The PPD and PMV in the first and third floor zones are shown in figure 7.11 and 7.12. The PPD in the first floor can be observed to be slightly higher than the third floor, with certain values above 8. The PMV in both zones was around -0.3, indicating that the occupants were relatively comfortable with the thermal environment.

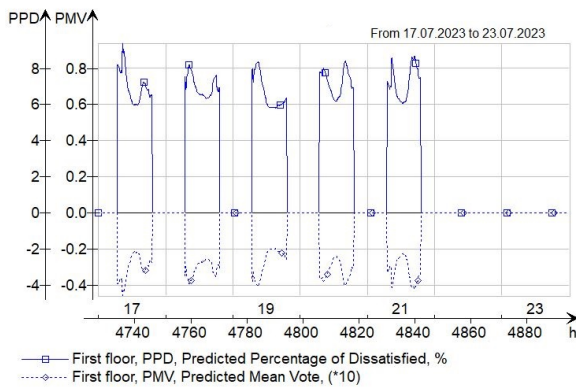


**Figure 7.11:** PPD and PMV in the first floor from simulation with on-site pressure coefficients. The figure is clipped from IDA ICE.

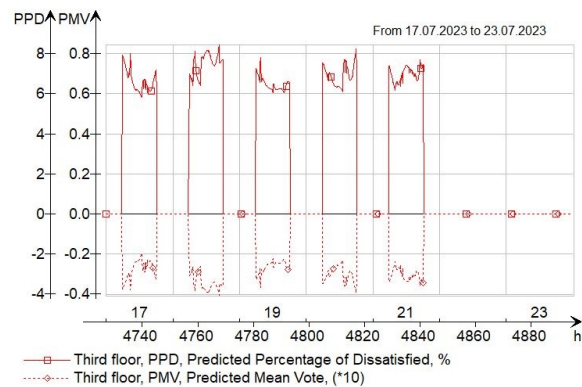


**Figure 7.12:** PPD and PMV in the third floor from simulation with on-site pressure coefficients. The figure is clipped from IDA ICE.

#### 7.4.2 Simulation with standard wind pressure coefficients

The mean air temperatures and the operative temperatures in the first and third floors in the simulation with standard pressure coefficients can be seen in figure 7.13 and figure 7.14, respectively. It can be observed that the temperature fluctuated more in the third floor than in the first floor. Additionally, the temperatures were more stable during the weekend.

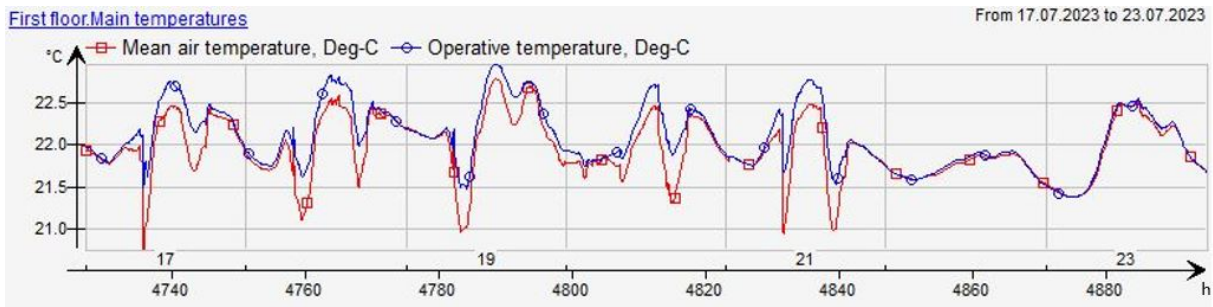


**Figure 7.13:** Resulting indoor temperatures in the first floor during the simulated week with standard pressure coefficients. The figure is clipped from IDA ICE.

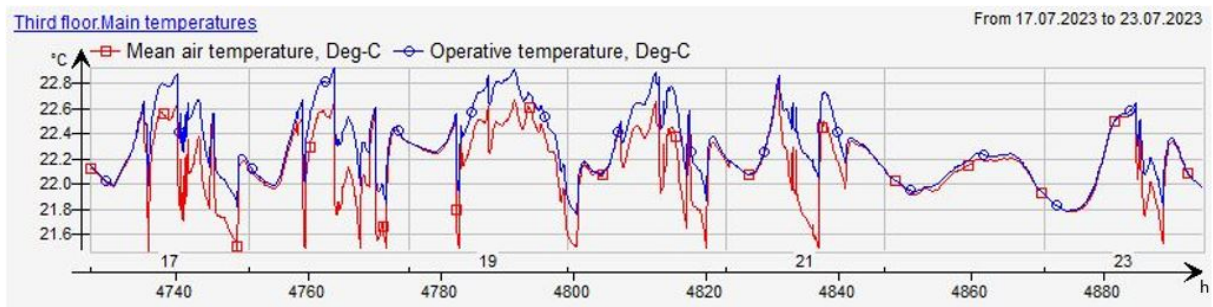


**Figure 7.14:** Resulting indoor temperatures in the third floor during the simulated week with standard pressure coefficients. The figure is clipped from IDA ICE.

Figures 7.15 and 7.16 show the CO<sub>2</sub> concentrations in the first and third floor, respectively, during the simulated week. The observed CO<sub>2</sub> concentrations were generally higher in the first floor. It can also be observed that the accumulated CO<sub>2</sub> concentrations during the day were removed during the night. Additionally, the CO<sub>2</sub> concentrations did not exceed 650 ppm in either zones during the week.

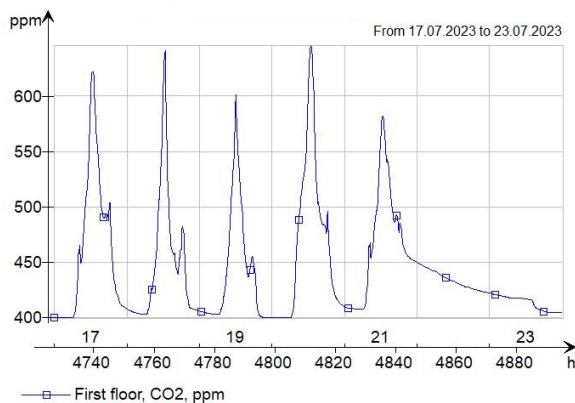


**Figure 7.15:** CO<sub>2</sub> concentrations in the first floor during the simulated week with standard pressure coefficients. The figure is clipped from IDA ICE.

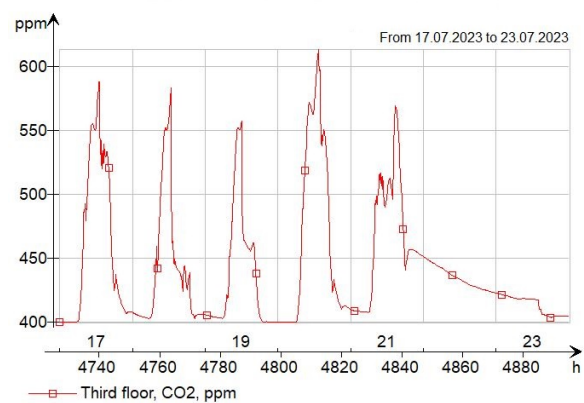


**Figure 7.16:** CO<sub>2</sub> concentrations in the third floor during the simulated week with standard pressure coefficients. The figure is clipped from IDA ICE.

Relative humidity in the first floor zone fluctuated between 40% and 58% throughout the week and averaged at around 49.5%. In the third floor, the relative humidity was between 40% and 60%, and averaged at 48.9%. The relative humidity in both zones was, therefore, within the acceptable range. The age of air on the first and third floors are shown in figure 7.17 and 7.18. It can be observed that the age of air increased in both zones during the night and decreased once the windows opened during the day. During the weekend, the age of air increased to reach 25 hours in both zones.

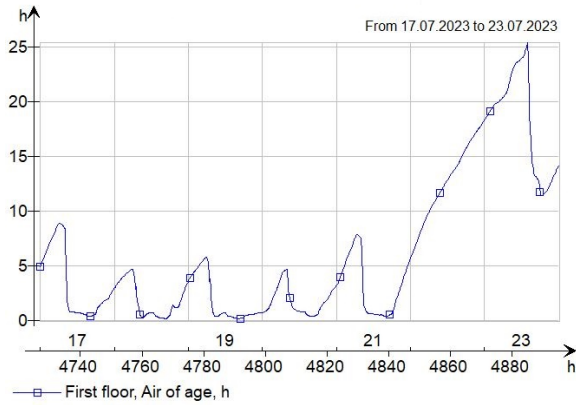


**Figure 7.17:** Resulting age of air in the first floor with simulation using standars pressure coefficients. The figure is clipped from IDA ICE.

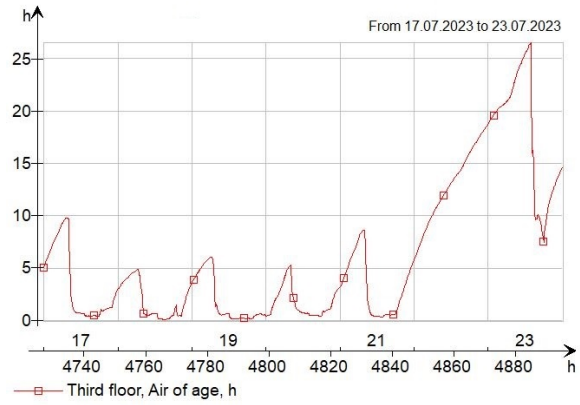


**Figure 7.18:** Resulting age of air in the third floor with simulation using standars pressure coefficients. The figure is clipped from IDA ICE.

Table 7.7 shows the number of occupancy hours within four comfort categories evaluated according to EN-15251 in both the first and third floor zones. The table shows that all occupancy hours were within the best category, and there were no hours in the unacceptable category, meaning no hours above 26°C.

**Table 7.7:** Number of occupancy hours within four comfort categories evaluated according to EN-15251. The simulation was done with on-site pressure coefficients.

Comfort category	First floor [h]	Third floor [h]
Best	50	50
Good	50	50
Acceptable	50	50
Unacceptable	0	0

The PMV and PPD during the simulated week in the first and third floor zones are shown in figures 7.19 and 7.20. The parameters in both zones followed the same patterns. The PMV parameter was between -0.2 and -0.4 during the occupancy hours, suggesting that the occupants perceived the thermal environment as mostly comfortable. The PPD parameter indicates that around 7% of the occupants were dissatisfied with the environment

in the first floor, and that fewer people were predicted to be dissatisfied with the thermal environment in the third floor.

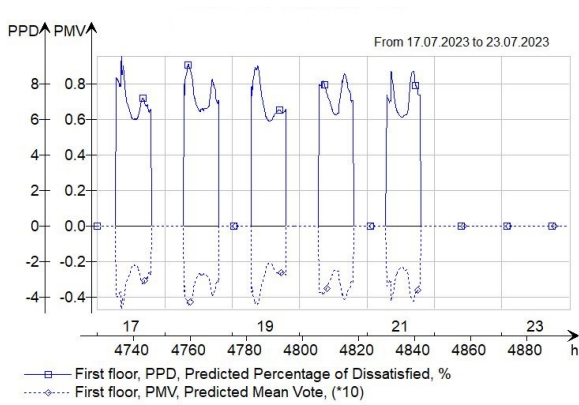


**Figure 7.19:** PPD and PMV in the first floor from simulation with standard pressure coefficients. The figure is clipped from IDA ICE.

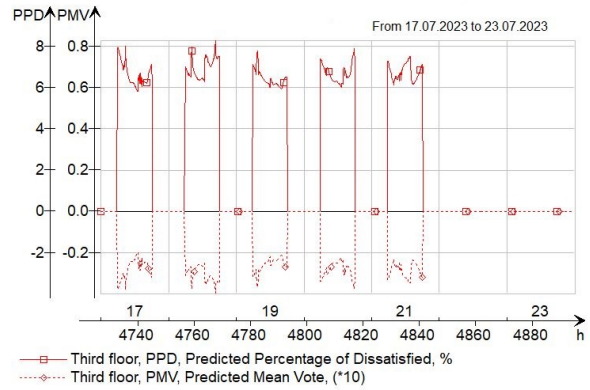


**Figure 7.20:** PPD and PMV in the third floor from simulation with standard pressure coefficients. The figure is clipped from IDA ICE.

## 7.5 Evaluation of draught

To evaluate the draught risk, it was chosen to evaluate the draught from one arbitrary window in the open workspace on the third floor. Using equation 4.12 and the set values described in section 6.6, the throw length of the air jet, given in table 7.8, were calculated with different values of  $K_2$  and  $\epsilon$ . The air velocity,  $U_0$  was calculated to  $0.538 \frac{m}{s}$ , based on the airflow rate and the area of the window opening.

**Table 7.8:** Calculated throw length of the air entering an arbitrary window on the third floor. The throw length was calculated with different values of  $K_2$  and  $\epsilon$ .

	$\epsilon = 0.7$	$\epsilon = 0.8$	$\epsilon = 0.9$
$K_2 = 3$	11.3 m	9.9 m	8.8 m
$K_2 = 4$	15.0 m	13.1 m	11.7 m
$K_2 = 5$	18.8 m	16.4 m	14.6 m
$K_2 = 6$	22.5 m	19.7 m	17.5 m

The throw lengths with different values for  $K_2$  and  $\epsilon$  are shown in table 7.8. It can be observed that with the chosen parameters, the air jet would penetrate relatively far into the room. Based on the conditions in the ZEB Laboratory, it was chosen to do further evaluations using the coefficients  $K_2 = 4$ , based on the irregular shape of the opening, and  $\epsilon = 0.9$ , because the opening does not have sharp edges. A duration curve of the air jet throw length entering the same window during a typical day with wind velocity between 2 and  $2.5 \frac{m}{s}$  is shown in figure 7.21. The ambient wind velocity corresponding



to the calculated throw length can be seen in figure 7.22. The velocity of the air as it reached the wall in the room was calculated to be below  $0.1 \frac{m}{s}$ , meaning it is insignificant. It can be observed that the throw length was relatively short and did not exceed 1.2 m.

It should be noted that the x-axis in the presented results in this section are in data points imported from IDA ICE. One data point is approximately equal to 5 minutes. During the processing of the data, all negative values of airflow were removed, as this means the air was exiting out of the building.

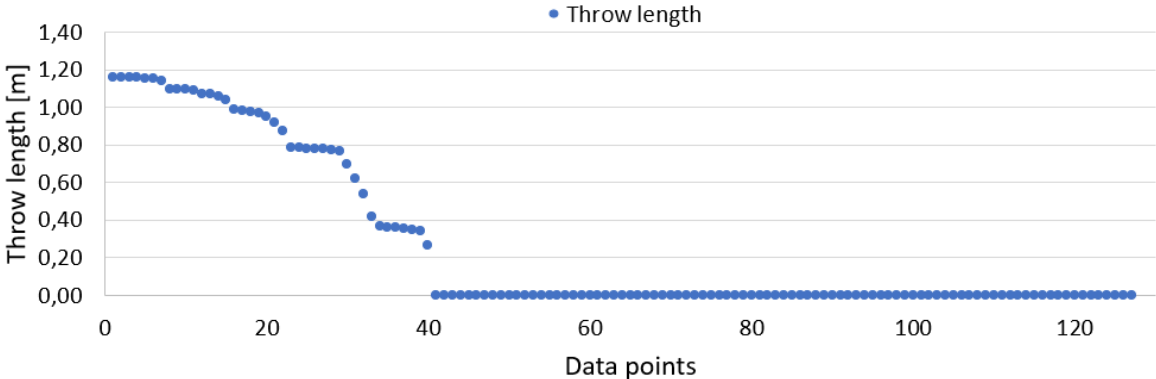


**Figure 7.21:** Duration curve of the air throw length into the zone during one typical day. The x-axis represents data points imported from IDA ICE, where one data point is equal to approximately 5 minutes.

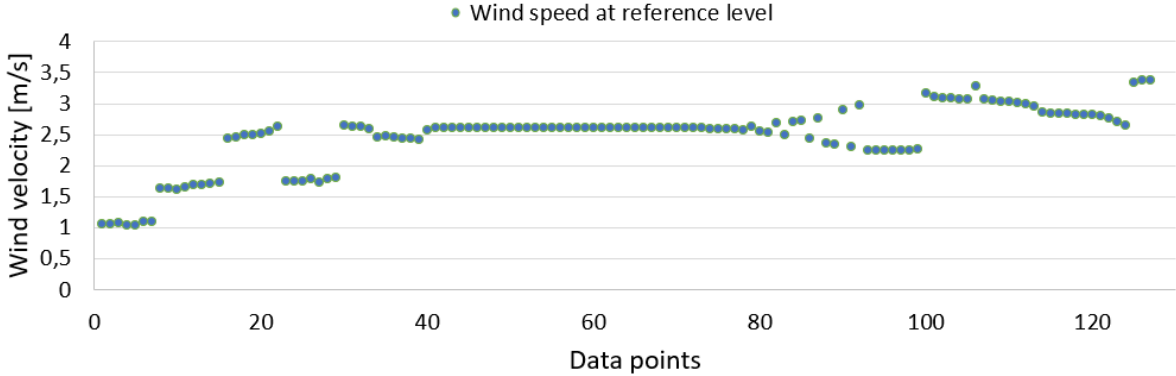


**Figure 7.22:** Wind velocity at reference level during the simulated day. The x-axis represents data points imported from IDA ICE, where one data point is equal to approximately 5 minutes.

The throw length of the air jet during the simulated week is given in figure 7.23, and the air velocity at 6.8 m into the room and the ambient wind speed are given in figure 7.24 and 7.25, respectively. It can be observed that the throw length of the air jet exceeded 10 m on several occasions when the wind velocity exceeded around  $7 \frac{m}{s}$ . Additionally, the velocity of the air jet as it reached the wall was around  $0.3 \frac{m}{s}$  during the highest wind velocities.

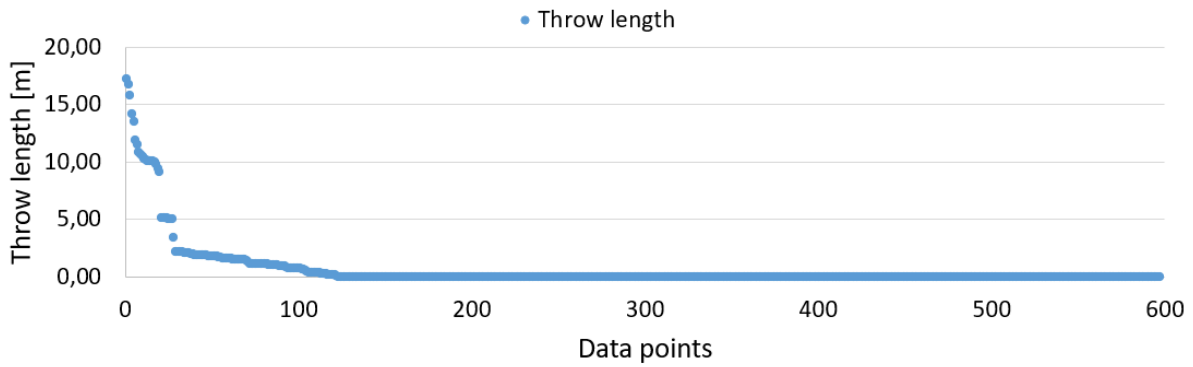


**Figure 7.23:** Duration curve of the air throw length into the zone during the simulated week. The x-axis represents data points imported from IDA ICE, where one data point is equal to approximately 5 minutes.

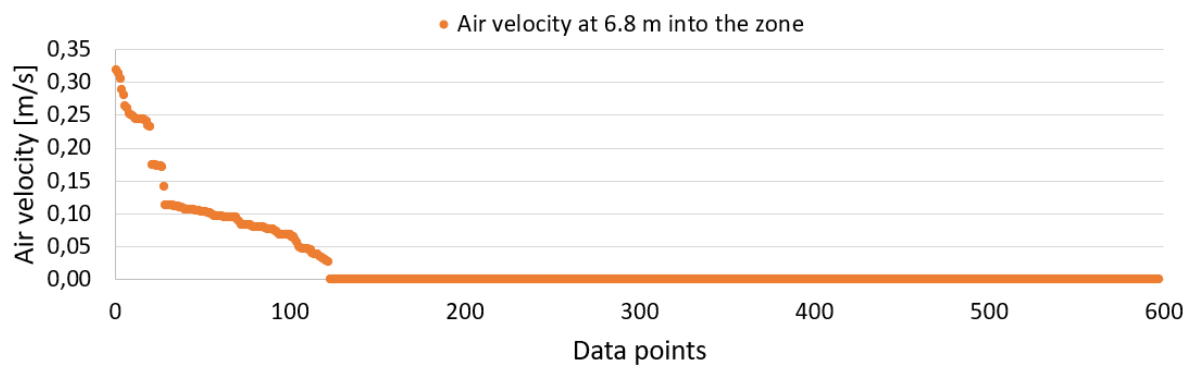


**Figure 7.24:** The calculated velocity of the air jet at 6.8 m into the room during the simulated week. The x-axis represents data points imported from IDA ICE, where one data point is equal to approximately 5 minutes.

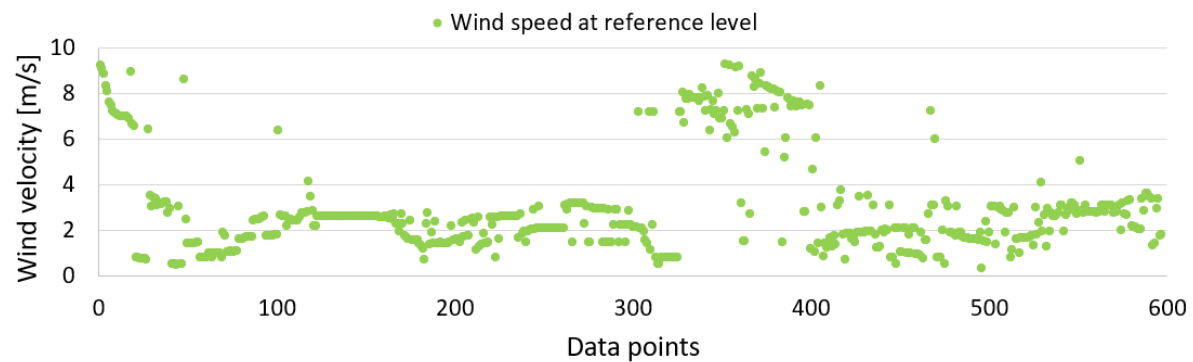


**Figure 7.25:** Wind velocity at reference level during the simulated week. The x-axis represents data points imported from IDA ICE, where one data point is equal to approximately 5 minutes.

## 8 Discussion

This section will discuss the results presented in section 7. The section begins by reflecting on the wind pressure coefficients and possible reasons for any deviations, as well as discussing the complications during the measurements. Further, the simplified model of the ZEB Laboratory is discussed, along with the results from the two simulations with on-site and standard wind pressure coefficients. Lastly, a discussion around the draught risk is presented, and a reflection on the improvement of the window control algorithm to allow natural ventilation of the building.

### 8.1 Weather data used for calculations

The weather station, placed on the roof of the ZEB Laboratory, measured the ambient conditions utilized in this thesis. Additionally, the intake of the tube connected to the reference sensor, measuring the static freestream pressure induced by the wind, was placed halfway on the weather station pole. Ideally, these parameters should be measured in freestream. It is, however, a possibility that the measurements at the height of the weather station were affected by turbulent air from the building itself and the surrounding buildings. The weather station was placed 2 meters above the roof, which might not be high enough to ensure free air without any impact from turbulent air. This increased the uncertainty of the data. As explained in section 4.2.3, using wind velocities that are affected by local surroundings and, therefore, not in freestream can create biases in the wind pressure coefficient calculations.

### 8.2 Pressure on the facades

The calculated pressures acting on the facades of the ZEB Laboratory based on the pressure measurements are presented in figure 7.1, 7.2, 7.3, and 7.4. In theory, positive pressure acting on one facade should result in negative pressure on the opposite facade, but due to a significant amount of measurements, it is difficult to conclude if this was the case based on the resulting graphs. For example, positive pressure on the east facade, shown in figure 7.2, should result in negative pressure acting on the west facade, shown in figure 7.4. Because of fluctuations in the results in the two graphs, it is difficult to evaluate if this is the case without looking at single values or very short periods of measurement. However, several data points with high positive pressure can be observed on the south facade, in figure 7.3, around data point 5000, and in the same period, the pressure acting on the north facade, in figure 7.1, is observed to be negative. This indicates that the measurements agree with the theory.

### 8.3 Wind pressure coefficients

In this section, the resulting wind pressure coefficients given in table 7.2, 7.3, 7.4, and 7.5 will be discussed and compared to the standard coefficients given by AIVC. It is important to note that the on-site pressure coefficients are specific to the building, and deviations from the standard coefficients will occur due to factors like underpressure and turbulence from nearby structures and topography. Issues and complications that occurred during the measuring periods will be discussed in this section as well.

The wind pressure coefficients on the north facade, presented in table 7.2, were mostly as expected. Sensor 2 did, however, log a very small pressure coefficient from the north direction, or  $0^\circ$ . This sensor was placed close to the northwest corner of the building on the second floor, and underpressure from the Nina building or turbulence around the corner could have impacted the results. Overall, the on-site pressure coefficients on this facade were relatively similar to the standard pressure coefficients given in table 5.3 from the north and northeast wind directions. From the northwest direction, or  $315^\circ$ , the on-site coefficients were significantly higher. From the remaining cardinal wind directions, the on-site pressure coefficients were much closer to zero compared to the AIVC coefficients.

Wind pressure coefficients on the east facade, provided in table 7.3 were not as expected. Firstly, all values were relatively close to 0. There are limited buildings and vegetation towards the east of the building, hence it was expected that the results would be better due to more stable wind conditions. In addition, it was expected that the pressure coefficients would be the greatest from  $90^\circ$  and the values from  $135^\circ$  would be positive. This was not the case, and it is unsure if this was because of issues with the equipment or if the surroundings had an unexpected effect on the measured pressure.

Wind pressure coefficients on the south facade are given in table 7.4. The table shows that the coefficients on the second floor (sensors 8 and 9) and on the third floor (sensors 10, 11, and 12) gave relatively similar results, which was expected. The exception was two values from sensor 10 at  $135^\circ$  and  $180^\circ$ , which were significantly lower than the results from sensors 11 and 12 from the same wind directions. The deviation could be because sensor 10 was placed close to the southeast corner of the building during the measurements and could have been affected by turbulence around the corner. The biggest negative coefficient was expected to be induced by wind approaching from the north. This was, however, not the case, as the lowest value was induced by wind approaching from the east. This could be because of turbulent air from buildings located to the north of the ZEB Laboratory, resulting in fluctuating pressure on the facade from the north, and more undisturbed wind approaching from the east resulting in more stable measurements.

The west facade of the ZEB Laboratory has a slight tilt and is not oriented directly toward the west, but rather around  $240^\circ$ . This would explain why the biggest pressure coefficients, shown in table 7.5, inducing the biggest inflow were from  $225^\circ$ , and the biggest outflow of air was by the wind from  $135^\circ$ . The pressure coefficients deviated significantly from the

standard pressure coefficients. Firstly, all on-site coefficients were relatively close to zero. Secondly, it was expected that the wind approaching from  $0^\circ$ ,  $45^\circ$ , and  $90^\circ$  would result in negative pressure coefficients. This was not the case for sensor 15, and additionally, the values from sensor 14 were very close to zero. The pressure coefficient from sensor 13 and  $270^\circ$  was expected to provide a positive value. However, this is negative. One possible explanation for the discrepancies could be the underpressure induced by the Nina building situated to the west of the ZEB Laboratory.

In general, all measurements with wind from the west, northwest, and southwest were most likely affected by an underpressure induced by the Nina-building. In addition, NTNU has several buildings located to the north of the ZEB Laboratory, which could create turbulence or underpressure and affect the results as well. Furthermore, the extension of the ZEB Laboratory, where the solar panels are placed at ground level of the south facade, could generate turbulence and local peaks in the measured pressure.

There are general uncertainties with the calculated on-site wind pressure coefficients. In order to attain the most accurate results, it was desirable to use wind velocities of the highest magnitude available. Nevertheless, due to a limited amount of available measurements from the northern, northeastern, and eastern directions, it became necessary to utilize lower wind velocities in order to gather a sufficient quantity of measurements to estimate the coefficients. Consequently, there are greater uncertainties with the calculated coefficients from these wind directions. These uncertainties arise as a result of increased fluctuating wind associated with lower wind velocities, generating localized regions of higher or lower pressure on the building facades.

### 8.3.1 Calibration of the sensors

The measured pressure from the Sensirion sensors was calibrated against a reference pressure logger to ensure their accuracy and reliability. Table 7.1 presents the coefficients that arose after the calibrations and a notably better  $R^2$  number can be observed for the sensors positioned on the east and south facades. This implies a higher level of correlation between the data collected from the sensors and the reference pressure logger. The reason for the better values can be attributed to the direction of the wind, primarily originating from the east and south during the calibration period. This wind pattern led to more stable measurements on the east and south facades, resulting in more precise outcomes. The north and west facades could have been subjected to turbulence induced by the wind, which negatively impacted the data quality.

Calibration of the sensors was necessary to get the resulting wind pressure coefficients, and it is evident from table 7.1 that the measured pressure from the sensors deviated significantly from reality. For optimal results, the calibration of the sensors could be carried out in a laboratory with controlled conditions. Additionally, calibrations should be conducted multiple times under the same conditions to evaluate the stability of the

sensors. However, the calibrations were done on-site in the ZEB Laboratory. Doing the calibrations on-site means the results were affected by turbulence around the building and local pressure differences. On the other hand, conducting the calibrations on-site compared to in a laboratory can have an effect related to the installation of the sensors. By conducting calibrations in a laboratory, the sensors would have to be reinstalled, which could again result in uncertainties with the setup. There is also a significant uncertainty with the manual readings of the pressure logger used for the calibrations. It can not be guaranteed that the values were read from the reference pressure logger simultaneously as the data logger connected to the Sensirion sensors did readings. In addition, there are uncertainties with regard to the lack of values to make the equations for calibrations. The measurements to gather data to calibrate against were only completed for a limited time, hence giving a limited number of values.

### **8.3.2 Complications during the measurements**

Several problems were discovered during the measurement period. Firstly, there are general uncertainties with the setup of the sensors. The tubes used in the setup, as shown in figure 6.1, were relatively stiff, but there is still a possibility that they may have been pinched, resulting in restricted airflow through them. Additionally, as described in section 6.4, it was discovered that several of the sensors were not installed correctly after a short period. For best results, the tube should be parallel to the outer window frame, but it was discovered that sensors 13, 14, and 15 stuck out around three centimeters from the window. This meant the pressure could be affected by more turbulent air and no longer measured only the static pressure at the facade. The results were improved after the reinstallation of the sensors, but there are still uncertainties related to the installation of the sensors.

As mentioned in section 6.4, the timing of the measurements from the sensors and the weather station was not coordinated during the first three weeks of the measurements. As a consequence of this, the inaccuracy of the data was increased as the logging of the measurements was not happening at the same time. Because of this, in addition to the reinstallation of the sensors, it was deemed acceptable to exclude the data from this period from the calculations to improve the accuracy of the resulting wind pressure coefficients.

The calculations required data from periods with high wind velocities due to issues with the reliability of the results under low wind velocity conditions. The presence of local wind gusts and varying distances between the sensors and the weather station resulted in challenges when considering wind pressure coefficients under these conditions. Local wind gusts can create relatively big pressure differences on one facade yet not be recorded by the weather station due to the distance between the two points of measurement. Consequently, the calculated wind pressure coefficient may be inaccurate because the measurements were not coordinated. As a result of the uncertainties with low wind velocities for the calculation, the wind velocities provided in table 6.1 were used as the lower limits.

To improve the results of the on-site wind pressure coefficients, the pressure measurements over the facades could be conducted for a longer period of time. By doing this, the extreme values due to local wind gusts and turbulence could be excluded from the data base, resulting in more reliable and accurate pressure coefficients. By conducting the measurements for a longer period, more data could be gathered during periods with high wind, improving the inaccuracies in the results.

## **8.4 IDA ICE model of the ZEB Laboratory**

Simulations of the ZEB Laboratory were done in IDA ICE with a simplified model. The model used simplified zones where one zone represented the whole floor. The ZEB Laboratory consists of several open zones, but the building also includes closed rooms with only mechanical ventilation. Because the closed rooms were not implemented in the model, the airflows through the building were not representative of the real building. In addition, a few of the windows were merged to limit the simulation time, but the areas are still correct, and this should not affect the results.

Simplifications in the IDA ICE model were additionally done to the internal gains, such as the occupancy and equipment. The occupancy in the building will vary during the day and during the week. The occupancy implemented in the four floor zones was, however, considered to be representable for an arbitrary day. The occupancy in the staircase moving from the first floor to the fourth floor was set to zero. This is not realistic, as occupants will stay in this zone for short periods of time while moving between the floors. It is also challenging to predict the heat emitted heat from the equipment in the building. Therefore, the results from the simulations are, therefore, an estimate, and differences in the internal gains can impact the indoor environment in the building.

The climate and weather file used in the IDA ICE simulations was from Værnes, Trondheim. This was considered acceptable since it was the location closest in distance to the ZEB Laboratory. However, it is possible to implement a weather file with data gathered from the weather station located on the roof of the building, but this was not done because of limited time. Using a local weather file could improve the simulations, as it would be a better representation of the local parameters, like the temperature, wind velocity, and wind direction. By using more accurate parameters of the ambient conditions around the building, the simulations would be a better representation of the pressure and airflows affecting the indoor climate in the building.

### **8.4.1 Simulations with on-site and standard wind pressure coefficients**

Simulations were done with standard and on-site wind pressure coefficients during a warm week in July. As discussed in section 3.3, natural ventilation is difficult to implement in Nordic climates and window operation should often be limited to avoid draught and high heating demands in the building during the heating season. The indoor climate and energy

demand of the ZEB Laboratory during the winter were not explored in this thesis, and the developed algorithm might not be applicable during this period. To use the algorithm for window operations during the winter, the setpoints may have to be adjusted, and it is possible to implement different criteria than the ones used for opening and closing the windows. For example, it is possible to implement an algorithm for opening the windows mainly when the CO<sub>2</sub> exceeds a set value, but it is important with a good controller included so the indoor temperature is not lowered too much, resulting in a bigger heating demand and, consequently, no energy savings.

In the on-site pressure measurements, the surrounding buildings and vegetation of the ZEB Laboratory were taken into account by the pressure coefficients due to the pressure that arises from the wind effects because of the surroundings. Consequently, it was considered acceptable to exclude site shading in the simulation. However, the site shading is not taken into account in the standard pressure coefficients. This is a weakness in using the standard coefficients and one of the reasons on-site coefficients should be used as far as possible.

The implemented algorithm for window operations does not consider relative humidity in the zone or the noise associated with the motor when opening the windows. It was observed during the simulations that the windows alternated between opening and closing when the ambient temperature was around 22°C, the setpoint for closing the window. This could create a lot of noise and be perceived as disturbing by the occupants in the zone. This phenomenon also indicates that the algorithm does not work optimally and that improvements can be made to it.

## **8.5 Comparison of the on-site and standard wind pressure coefficients**

The results from the simulations, presented in section 7.4, indicate that using both standard and on-site pressure coefficients resulted in an acceptable indoor environment. The operative temperatures were within the acceptable range with no hours exceeding 26°C, and there were no big accumulation of CO<sub>2</sub> concentrations as it remained below 650 ppm during both simulations. The small accumulation of CO<sub>2</sub> concentrations during the weekdays in occupational hours was removed during the nights. The concentrations were not removed as quickly during the weekend, indicating that the windows were not opening as frequently during this period. The mechanical ventilation system was additionally turned off during the weekends and did not contribute to removing the concentrations.

Simulations resulted in PPD below 10, and PMV averaged around -0.3 during both simulations. The values were within the expected limits for a building in building category II, where the ZEB Laboratory can be found, described in section 2.2. The age of air was relatively similar during the two simulations. However, the age of air was lower during the night to 19. July in both floor zones in the on-site pressure coefficient simulation,



indicating a bigger ventilation rate during this period. The age of air during the weekends in both simulations reached around 25 hours. The age of air during this period indicates that the ventilation system is not efficient, with limited natural ventilation of the area and no mechanical ventilation. This could be perceived as uncomfortable by the occupant. In cases like this, it is important to have manual windows in the building to give the occupant the opportunity to regulate the air quality.

In general, the results presented limited differences between the indoor climate in the ZEB Laboratory when using on-site and standard wind pressure coefficients. The operative temperature in the two building zones evaluated during the two simulations showed minimal differences, and the CO<sub>2</sub> concentrations were very similar. However, the CO<sub>2</sub> concentrations were lower during the second day in both floors when the on-site pressure coefficients were simulated. Additionally, the third floor concentrations were lower during the fifth day in the same simulation. This indicates a bigger ventilation airflow rate into the zones during these periods when the on-site pressure coefficients were used.

It is difficult to conclude what effect the on-site wind pressure coefficients have on the indoor environment of the ZEB Laboratory compared to standard coefficients, based on the model and simulations utilized in this thesis. However, it is possible that the results would differ if a more realistic model of the ZEB Laboratory were implemented in IDA ICE, including the closed zones with only mechanical ventilation. Implementing these zones could affect the airflow rate and airpath inside the building and, consequently, the resulting indoor environment parameters. A possible explanation for the small differences in the two simulations can be that the simulated week does not include longer periods with high wind velocities. Therefore, the buoyancy effect is the main contributor to natural ventilation in the building. The effect of wind-induced natural ventilation, and therefore the wind pressure coefficients, would be greater during periods of higher wind velocities.

Giving the occupants the ability to control their thermal environment is important. Occupants that are able to interact with the building and its systems are generally found to be more satisfied with the indoor environment. However, concerns could occur with giving the occupants the ability to override and close the automatic windows. This could cause a decrease in the quality of the thermal environment as the temperature in the building increases and the air movement in the building decreases.

## 8.6 Draught risk in the ZEB Laboratory

IDA ICE can not evaluate the air velocity at a specific point in the zone, making it difficult to evaluate the draught risk in the zone, such as at a specific desk. To evaluate the draught risk in the ZEB Laboratory, the method explained in section 6.6 was followed. There is a higher draught risk closer to the open windows, as the air velocity is the highest near the opening. The air velocity does, however, decrease as it reaches further into the zone.

Because of the Coanda effect, described in section 4.3, the air can reach even further into the zone before it releases from the roof.

The throw length of the air jet through the window, shown in figure 7.21 was found to evaluate the draught risk in the ZEB Laboratory during one of the simulated days. The graph indicates that for this specific day, the risk for draught was relatively low, as the air velocity in the room was low. The air would only penetrate 1.20 m into the room and release from the surface at this distance. This means that the occupant placed here might feel a slight draught, but it is important to remember that draught is highly dependent on the occupant's thermal sensation as well as the indoor temperature of the zone.

The wind velocity during a typical summer day is around 3 to 4  $\frac{m}{s}$ . From figure 7.22 it can be seen that the wind velocities during this day were slightly lower than this, at around 2.5  $\frac{m}{s}$ . Given that the throw length of the air jet was relatively low, and the velocity of the air was insignificant as the air jet hit the wall in the zone, it can be concluded that there is a generally low risk of draught that can be perceived as uncomfortable by the occupants in the building during low wind velocities in the summer.

When evaluating the draught risk during the simulated week, in figures 7.23, 7.24, and 7.25, it is evident that higher wind velocities resulted in higher inflow through the windows and greater throw length of the air. It can be observed from the results that the air jet hit the wall placed 6.8 m into the room during the simulated week, and the air velocity was found to be around 0.3  $\frac{m}{s}$  during the periods of the week as the jet hit the wall. This indicates that there is a higher risk of draught near the wall and turbulence that can be perceived as uncomfortable for the nearby occupants in this area during these conditions.

As can be observed from the results in chapter 7.5, there are periods with no airflow through the window, meaning the window is closed, even though the wind velocity is around 3  $\frac{m}{s}$ . This indicates that the window is closed due to other reasons, like the ambient temperature being too low or because the indoor parameters are within the acceptable range.

## 8.7 Improvement of the window control algorithm

The window control algorithm was found to achieve an acceptable indoor environment during the simulated week with the implementation of natural ventilation. However, the algorithm is a simple on-off algorithm with heuristic control. A more complex automatic control algorithm using feed-forward control or machine learning systems could, in theory, anticipate the indoor environment and the need for ventilation based on previous data. Such a system could possibly predict the best possible action with regard to the indoor climate and thermal environment and evaluate the possibility of utilizing natural ventilation instead of mechanical ventilation. This could result in reduced fan power of the mechanical system and reduce the energy needed in the building.

It is also possible to modify the control algorithm used in this thesis to follow other criteria or setpoints for opening the windows. For example, it is possible to implement variable opening of the windows instead of the set 30% opening used in this thesis. Variable openings can result in a smaller opening that can be used during periods with high airflow rates through the windows and contribute to lowering the draught risk. The setpoints in the algorithm could be changed as well, for example, use 21°C as the minimum value for air temperature in the zone and use night cooling between 22:00 and 06:00 to investigate the effects this has on the indoor environment.

## 9 Conclusion

The aim of this Master's thesis was to conduct pressure measurements on the facades of the ZEB Laboratory and use the measurements to calculate on-site wind pressure coefficients specific to the building. The resulting wind pressure coefficients were implemented in IDA ICE, and simulations were done with a window control algorithm to allow natural ventilation of the building. The aim was to investigate the effect of using on-site wind pressure coefficients compared to standard coefficients and the effect they had on the indoor environment.

Pressure measurements over the facades of the ZEB Laboratory were conducted for 10 weeks with 15 Sensirion differential pressure sensors and an additional reference sensor. A distinct amount of the gathered data from the pressure measurements were removed due to low wind velocities or fluctuation in pressure because of the mechanical ventilation system. The remaining data were used to calculate on-site wind pressure coefficients specific to the building. There are general uncertainties with the setup of the sensors regarding pinching of the tube connected to the sensors and whether the sensors only measured the static pressure on the building facades.

The resulting on-site wind pressure coefficients had varying degrees of reliability. The coefficients were generally affected by an underpressure that occurred from the Nina building located to the west of the ZEB Laboratory and NTNU located to the north of the building. There were several uncertainties with the results. Firstly there are general inaccuracies associated with the distance between the 15 sensors measuring the differential pressure over the facades and the placement of the reference sensor, resulting in missing coordination between the two measurements. Additionally, it was desirable to use the highest wind velocities possible, but because of a limited amount of values available during periods with high wind velocities approaching from the north, northeast, and east direction, lower wind velocities were used. Consequently, this resulted in bigger inaccuracies with the wind pressure coefficient associated with these directions. To improve the results, the pressure measurements should be carried out for a longer period of time.

Simulations in IDA ICE were carried out during a week in July, and natural ventilation was implemented in the model by a window control algorithm. The simulations, including both calculated on-site and standard wind pressure coefficients, resulted in an acceptable indoor environment with acceptable operative temperatures and no occupational hours above 26°C. Additionally, the CO<sub>2</sub> concentrations did not exceed 650 ppm, and the PPD and PMV were found to be within the acceptable range for such a building. The differences between the two simulations were minimal, which can be attributed to the fact that the wind velocity during the simulated week was relatively low, resulting in the buoyancy effect being the main contributor to natural ventilation of the building. Additionally, the ZEB Laboratory model in IDA ICE was a simplified model with simplified zones, and a more complicated and realistic model could impact the results.

The results from the simulations indicate that the window control algorithm incorporated in the model work as intended to allow natural ventilation of the building. However, the algorithm was developed for use during the cooling season, and modifications to the algorithm could be necessary to use the algorithm to incorporate natural ventilation in the building during the heating season.

## 10 Further work

To improve the results of the on-site wind pressure coefficients, pressure measurements over the facades should be conducted for a longer period to achieve more stable and reliable readings. By conducting the results for a longer period, extreme values due to local wind gusts and turbulence could be excluded. Additionally, it could result in an increase in the number of values during periods of high wind velocities to use in the calculations.

In general, more extensive testing should be done to eliminate uncertainties with the equipment, including calibrating the sensors in a laboratory with controlled conditions. In addition, a method to coordinate the time delay between the sensors measuring the differential pressure over the facades and the reference sensor could be developed.

Development of the ZEB Laboratory model in IDA ICE could be done to improve the reliability of the simulations of the indoor environment with on-site wind pressure coefficients. A weather file with data collected from the local weather station at the ZEB Laboratory could be implemented in the model to achieve a more realistic simulation with local ambient parameters. The window control algorithm could additionally be developed and modified to be able to implement natural ventilation during the heating season.

## References

- [1] European Commission. *Energy performance of buildings directive*. en. URL: [https://energy.ec.europa.eu/topics/energy-efficiency/energy-efficient-buildings/energy-performance-buildings-directive\\_en](https://energy.ec.europa.eu/topics/energy-efficiency/energy-efficient-buildings/energy-performance-buildings-directive_en) (visited on 05/31/2023).
- [2] *Energy performance of buildings directive*. en. URL: [https://energy.ec.europa.eu/topics/energy-efficiency/energy-efficient-buildings/energy-performance-buildings-directive\\_en](https://energy.ec.europa.eu/topics/energy-efficiency/energy-efficient-buildings/energy-performance-buildings-directive_en) (visited on 12/18/2022).
- [3] Laurence Gibbons and Saqib Javed. “A review of HVAC solution-sets and energy performance of nearly zero-energy multi-story apartment buildings in Nordic climates by statistical analysis of environmental performance certificates and literature review”. eng. In: *Energy (Oxford)* 238 (2022). Place: Oxford Publisher: Elsevier Ltd, p. 121709. ISSN: 0360-5442.
- [4] Vinh Van Tran, Duckshin Park, and Young-Chul Lee. “Indoor air pollution, related human diseases, and recent trends in the control and improvement of indoor air quality”. eng. In: *International journal of environmental research and public health* 17.8 (2020). Place: Switzerland Publisher: MDPI AG, p. 2927. ISSN: 1661-7827.
- [5] Zitao Jiang, Tomohiro Kobayashi, Mats Sandberg, Toshio Yamanaka, Noriaki Kobayashi, Narae Choi, Kayuki Sano, and Kota Toyosawa. “Analysis of single-sided ventilation flows of a generic isolated building using particle tracking method in LES simulation”. eng. In: *Building and environment* 235 (2023). Publisher: Elsevier Ltd. ISSN: 0360-1323.
- [6] Yujiao Chen, Leslie K. Norford, Holly W. Samuelson, and Ali Malkawi. “Optimal control of HVAC and window systems for natural ventilation through reinforcement learning”. eng. In: *Energy and buildings* 169 (2018). Place: LAUSANNE Publisher: Elsevier B.V, pp. 195–205. ISSN: 0378-7788.
- [7] Selamawit Mamo Fufa, Reidun Dahl Schlanbusch, Kari Sørnes, Marianne Rose Inman, and Inger Andresen. *A Norwegian ZEB Definition Guideline*. eng. Accepted: 2016-07-26T10:46:16Z. Trondheim: SINTEF Academic Press, 2016. ISBN: 978-82-536-1513-4. URL: <https://ntnuopen.ntnu.no/ntnu-xmlui/handle/11250/2401097> (visited on 11/06/2022).
- [8] Berit Time, Alessandro Nocente, Hans Martin Mathisen, Arne Førland-Larsen, Anders Ramberg Myhr, Terje Jacobsen, and Arild Gustavsen. *ZEB Laboratory - Research Possibilities*. eng. Accepted: 2019-09-02T07:37:52Z ISSN: 1894-2466 Publication Title: 16. SINTEF akademisk forlag, 2019. ISBN: 978-82-536-1633-9. URL: <https://sintef.brage.unit.no/sintef-xmlui/handle/11250/2611934> (visited on 12/11/2022).
- [9] Martin Sande. *Ventilative Cooling Potential of the ZEB Laborator: Based on simulations performed with IDA ICE*. Master’s thesis. Trondheim: Norwegian University of Science and Technology, June 2021.
- [10] Ingebjørg Eggen Skarbøvik. *Evaluating the Method for Measuring and Calculating Wind Pressure Coefficients - A Case Study of the ZEB Laboratory*. Tech. rep. Trondheim, Dec. 2022.

- [11] Yousef Al horr, Mohammed Arif, Martha Katafygiotou, Ahmed Mazroei, Amit Kaushik, and Esam Elsarrag. “Impact of indoor environmental quality on occupant well-being and comfort: A review of the literature”. eng. In: *International journal of sustainable built environment* 5.1 (2016). Publisher: Elsevier B.V, pp. 1–11. ISSN: 2212-6090. (Visited on 10/12/2022).
- [12] Standard Norge. *Ergonomics of the thermal environment - Analytical determination and interpretation of thermal comfort using calculation of the PMV and PPD indices and local thermal comfort criteria (ISO 7730:2005)*. eng. Standard. Mar. 2006. URL: <https://www.standard.no/no/Nettbutikk/produktkatalogen/Produktpresentasjon/?ProductID=158329> (visited on 11/22/2022).
- [13] Jan Vincent Thue. *Bygningsfysikk : grunnlag*. nob. Place: Bergen. Fagbokforlaget, 2016. ISBN: 978-82-450-1994-0. (Visited on 12/10/2022).
- [14] Sturla Ingebrigtsen. *Ventilasjonsteknikk : Del 1*. nob. 3. oppl. Vol. Del 1. Place: Oslo. Oslo: Skarland press, 2016. ISBN: 978-82-90033-34-2.
- [15] Direktoratet for byggkvalitet. *Veiledning om tekniske krav til byggverk*. no. 2017. URL: <https://dibk.no/regelverk/byggteknisk-forskrift-tek17/> (visited on 11/22/2022).
- [16] Silje Kathrin Asphaug, Berit Time, Jan Vincent Thue, Stig Geving, Arild Gustavsen, Hans Martin Mathisen, and Sivert Uvsløkk. *Kunnskapsstatus – Fuktbufring i materialer og påvirkning på energibehov*. norsk. Tech. rep. ISBN: 978-82-536-1448-9. SINTEF akademisk forlag, 2015. URL: <http://hdl.handle.net/11250/2387052> (visited on 11/08/2022).
- [17] Rune Becher, Marianne Bjerke, Finn Martinsen, and Johan Øvrevik. *Inneklima i skoler og barnehager: Helsemessig betydning for barn og unge*. nob. ISBN: 978-82-8082-778-4 Place: Oslo. 2016. (Visited on 11/08/2022).
- [18] Francis Allard. *Natural ventilation in buildings: a design handbook*. London: James & James, 1998. ISBN: 1 873936 72 9. (Visited on 10/05/2022).
- [19] Runming Yao, Baizhan Li, and Jing Liu. “A theoretical adaptive model of thermal comfort – Adaptive Predicted Mean Vote (aPMV)”. eng. In: *Building and environment* 44.10 (2009). Place: OXFORD Publisher: Elsevier Ltd, pp. 2089–2096. ISSN: 0360-1323. (Visited on 11/09/2022).
- [20] Alexandre Soares dos Reis, Petra Vaquero, Marta Ferreira Dias, and Alice Tavares. “Passive Discomfort Index as an alternative to Predicted Mean Vote and Predicted Percentage of Dissatisfied to assess occupant’s thermal discomfort in dwellings”. eng. In: *Energy reports* 8 (2022). Publisher: Elsevier Ltd, pp. 956–965. ISSN: 2352-4847. (Visited on 11/09/2022).
- [21] Standard Norge. *Indoor environmental input parameters for design and assessment of energy performance of buildings addressing indoor air quality, thermal environment, lighting and acoustics (NS-EN 15251:2007+NA:2014)*. norsk. Standard. Sept. 2007. URL: <https://www.standard.no/no/Nettbutikk/produktkatalogen/Produktpresentasjon/?ProductID=703200> (visited on 05/20/2023).
- [22] *Inneklima og luftkvalitet på arbeidsplassen*. no. URL: <https://www.arbeidstilsynet.no/tema/inneklima/> (visited on 02/03/2023).



- [23] Wenjuan Wei, Pawel Wargocki, Johann Zirngibl, Jana Bendžalová, and Corinne Mandin. “Review of parameters used to assess the quality of the indoor environment in Green Building certification schemes for offices and hotels”. eng. In: *Energy and buildings* 209 (2020). Place: Lausanne Publisher: Elsevier B.V, p. 109683. ISSN: 0378-7788.
- [24] Sverre Holøs and Mads Mysen. *Krav til ventilasjon og termisk inneklima i TEK10*. Tech. rep. SINTEF, 2016.
- [25] Alberto Meiss, Jesús Feijó-Muñoz, and Miguel A. García-Fuentes. “Age-of-the-air in rooms according to the environmental condition of temperature: A case study”. eng. In: *Energy and buildings* 67 (2013). Place: LAUSANNE Publisher: Elsevier B.V, pp. 88–96. ISSN: 0378-7788.
- [26] David Etheridge and Mats Sandberg. *Building ventilation : theory and measurement*. eng. Place: Chichester. Wiley, 1996. ISBN: 0-471-96087-X.
- [27] Jiajia Gao, Xinhua Xu, Xiuming Li, Jili Zhang, Yuan Zhang, and Gongda Wei. “Model-based space temperature cascade control for constant air volume air-conditioning system”. eng. In: *Building and environment* 145 (2018). Place: OXFORD Publisher: Elsevier Ltd, pp. 308–318. ISSN: 0360-1323. (Visited on 11/20/2022).
- [28] Mads Mysen and Peter Schild. *Behovsstyrt ventilasjon, DCV - forutsetninger og utforming*. Tech. rep. ISBN: 978-82-536-1372-7. Oslo: Sintef, 2014, p. 68. (Visited on 10/17/2022).
- [29] David (David W.) Etheridge. *Natural ventilation of buildings : theory, measurement and design*. eng. Edition: 2nd ed. ISBN: 1-283-28006-X Place: Hoboken, N.J. 2012.
- [30] Camille Allocca, Qingyan Chen, and Leon R. Glicksman. “Design analysis of single-sided natural ventilation”. In: *Energy and Buildings* 35.8 (2003), pp. 785–795. ISSN: 0378-7788. DOI: [https://doi.org/10.1016/S0378-7788\(02\)00239-6](https://doi.org/10.1016/S0378-7788(02)00239-6). URL: <https://www.sciencedirect.com/science/article/pii/S0378778802002396>.
- [31] J.S. Park. “Long-term field measurement on effects of wind speed and directional fluctuation on wind-driven cross ventilation in a mock-up building”. eng. In: *Building and environment* 62 (2013). Place: OXFORD Publisher: Elsevier Ltd, pp. 1–8. ISSN: 0360-1323.
- [32] Steven Emmerich, William Dols, and James Axley. *Natural Ventilation Review and Plan for Design and Analysis Tools*. en. Aug. 2001. URL: [https://tsapps.nist.gov/publication/get\\_pdf.cfm?pub\\_id=860854](https://tsapps.nist.gov/publication/get_pdf.cfm?pub_id=860854).
- [33] Pei-Chun Liu, Hsien-Te Lin, and Jung-Hua Chou. “Evaluation of buoyancy-driven ventilation in atrium buildings using computational fluid dynamics and reduced-scale air model”. eng. In: *Building and environment* 44.9 (2009). Place: OXFORD Publisher: Elsevier Ltd, pp. 1970–1979. ISSN: 0360-1323.
- [34] Risto Kosonen, Juha Jokisalo, Ilari Ranta-aho, and Esa-Pekka Koikkalainen. “Methods to Reduce Stack Effect and Improve Energy Efficiency in a Nordic High Rise Residential Building”. eng. In: *Procedia Engineering* 205 (2017). Publisher: Elsevier Ltd, pp. 2311–2317. ISSN: 1877-7058.
- [35] GR Hunt and PP Linden. “The fluid mechanics of natural ventilation—displacement ventilation by buoyancy-driven flows assisted by wind”. eng. In: *Building and en-*

- vironment : the international journal of building science and its applications* 34.6 (1999). Place: Oxford Publisher: Pergamon, pp. 707–720. ISSN: 0360-1323. (Visited on 11/19/2022).
- [36] O. Seppänen and W.J. Fisk. “Association of ventilation system type with SBS symptoms in office workers”. eng. In: *Indoor air* 12.2 (2002). Edition: Received for review 12 February 2001. Accepted for publication 5 March 2001. © Indoor Air (2002) Place: Oxford, UK Publisher: Blackwell Publishers, pp. 98–112. ISSN: 0905-6947. (Visited on 10/12/2022).
- [37] Per Heiselberg. *Principles of Hybrid Ventilation*. Tech. rep. IEA Energy Conservation in Buildings and Community Systems Programme, 2002.
- [38] Ritesh Wankhade, Giovanni Pernigotto, and Michele Larcher. “A Literature Review on Methods and Metrics for the Analysis of Outdoor Air Displacement Conditions in the Urban Environment”. eng. In: *Energies (Basel)* 16.6 (2023). Place: Basel Publisher: MDPI AG, p. 2577. ISSN: 1996-1073.
- [39] V Heide, L Georges, A G Lien, and H M Mathisen. “Review of HVAC strategies for energy renovation of detached houses towards nZEB in cold climates”. eng. In: *IOP Conference Series: Earth and Environmental Science* 352.1 (2019). Place: Bristol Publisher: IOP Publishing, p. 12048. ISSN: 1755-1307.
- [40] Zhonghua Gou, Wajishani Gamage, Stephen Siu-Yu Lau, and Sunnie Sing-Yeung Lau. “An investigation of thermal comfort and adaptive behaviors in naturally ventilated residential buildings in tropical climates: A pilot study”. eng. In: *Buildings (Basel)* 8.1 (2018). Place: BASEL Publisher: Mdpi, p. 5. ISSN: 2075-5309.
- [41] John Kaiser Calautit, Dominic O’Connor, and Ben Richard Hughes. “A natural ventilation wind tower with heat pipe heat recovery for cold climates”. eng. In: *Renewable energy* 87 (2016). Place: OXFORD Publisher: Elsevier Ltd, pp. 1088–1104. ISSN: 0960-1481.
- [42] Iliia Kravchenko, Risto Kosonen, Juha Jokisalo, and Simo Kilpeläinen. “Performance of Modern Passive Stack Ventilation in a Retrofitted Nordic Apartment Building”. In: *Buildings*. 12.2 (2022). Place: Basel, Switzerland : Publisher: MDPI AG, p. 96. ISSN: 2075-5309.
- [43] Rakesh Khanal and Chengwang Lei. “Solar chimney—A passive strategy for natural ventilation”. eng. In: *Energy and buildings* 43.8 (2011). Place: LAUSANNE Publisher: Elsevier B.V, pp. 1811–1819. ISSN: 0378-7788.
- [44] Sabrina Barbosa and Kenneth Ip. “Perspectives of double skin façades for naturally ventilated buildings: A review”. eng. In: *Renewable & sustainable energy reviews* 40 (2014). Place: OXFORD Publisher: Elsevier Ltd, pp. 1019–1029. ISSN: 1364-0321.
- [45] Jorge S. Carlos and Helena Corvacho. “Ventilated Double Window for the Pre-heating of the Ventilation Air Comparison of Its Performance in a Northern and a Southern European Climate”. eng. In: *Journal of Renewable Energy (Hindawi)* 2013 (2013). Publisher: Hindawi Publishing Corporation, pp. 1–11. ISSN: 2314-4386.
- [46] Peter Engelmann, Doreen Kalz, and Graziano Salvalai. “Cooling concepts for non-residential buildings: A comparison of cooling concepts in different climate zones”. eng. In: *Energy and buildings* 82 (2014). Place: LAUSANNE Publisher: Elsevier B.V, pp. 447–456. ISSN: 0378-7788.

- [47] Yujiao Chen, Zheming Tong, Holly Samuelson, Wentao Wu, and Ali Malkawi. “Realizing natural ventilation potential through window control: The impact of occupant behavior”. eng. In: *Energy Procedia* 158 (2019). Publisher: Elsevier Ltd, pp. 3215–3221. ISSN: 1876-6102.
- [48] Rune Andersen, Valentina Fabi, Jorn Toftum, Stefano P. Corgnati, and Bjarne W. Olesen. “Window opening behaviour modelled from measurements in Danish dwellings”. eng. In: *Building and environment* 69 (2013). Place: OXFORD Publisher: Elsevier Ltd, pp. 101–113. ISSN: 0360-1323.
- [49] Vegard Heide, Silje Skyttern, and Laurent Georges. “Indoor air quality in natural-ventilated bedrooms in renovated Norwegian houses”. eng. In: *E3S Web of Conferences*. Vol. 246. ISSN: 2555-0403. Les Ulis: EDP Sciences, 2021, p. 1001.
- [50] Yujiao Chen, Zheming Tong, Wentao Wu, Holly Samuelson, Ali Malkawi, and Leslie Norford. “Achieving natural ventilation potential in practice: Control schemes and levels of automation”. eng. In: *Applied energy* 235 (2019). Publisher: Elsevier Ltd, pp. 1141–1152. ISSN: 0306-2619.
- [51] Bo Gao, Xiaoyue Zhu, Jing Ren, Jingyu Ran, Moon Keun Kim, and Jiying Liu. “Multi-objective optimization of energy-saving measures and operation parameters for a newly retrofitted building in future climate conditions: A case study of an office building in Chengdu”. eng. In: *Energy reports* 9 (2023). Publisher: Elsevier Ltd, pp. 2269–2285. ISSN: 2352-4847.
- [52] Rajinder Jagpal. *Annex 35 Control Strategies for Hybrid Ventilation in New and Retrofitted Office and Education Buildings (HYBVENT)*. Tech. rep. Energy Conservation in Buildings and Community Systems, 2015.
- [53] Center for the Built Environment (CBE). *About Mixed-Mode*. 2013. URL: <https://cbe.berkeley.edu/mixedmode/aboutmm.html> (visited on 09/23/2022).
- [54] Arman Ameen, Mathias Cehlin, Ulf Larsson, and Taghi Karimipناه. “Experimental investigation of ventilation performance of different air distribution systems in an office environment-heating mode”. eng. In: *Energies (Basel)* 12.10 (2019). Backup Publisher: Avdelningen för byggnadsteknik, energisystem och miljövetenskap Place: Basel Publisher: MDPI AG, p. 1835. ISSN: 1996-1073. (Visited on 10/25/2022).
- [55] U. Larsson and B. Moshfegh. “Comparison of ventilation performance of three different air supply devices: a measurement study”. In: *International Journal of Ventilation* 16.3 (2017). Publisher: Taylor & Francis reprint: <https://doi.org/10.1080/14733315.2017.1299519>, pp. 244–254. ISSN: 2044-4044. DOI: 10.1080/14733315.2017.1299519. URL: <https://doi.org/10.1080/14733315.2017.1299519> (visited on 10/25/2022).
- [56] Nikhil Kumar, Ronita Bardhan, Tetsu Kubota, Yoshihide Tominaga, and Mohammadreza Shirzadi. “Parametric study on vertical void configurations for improving ventilation performance in the mid-rise apartment building”. eng. In: *Building and environment* 215 (2022). Place: Oxford Publisher: Elsevier Ltd, p. 108969. ISSN: 0360-1323.
- [57] Xiaohai Zhou, Aytac Kubilay, Dominique Derome, and Jan Carmeliet. “Comparison of wind-driven rain load on building facades in the urban environment and open

- field: A case study on two buildings in Zurich, Switzerland”. eng. In: *Building and environment* 233 (2023). Publisher: Elsevier Ltd, p. 110038. ISSN: 0360-1323.
- [58] Xiaoxiong Xie, Zhiwen Luo, Sue Grimmond, and Lewis Blunn. “Use of wind pressure coefficients to simulate natural ventilation and building energy for isolated and surrounded buildings”. eng. In: *Building and environment* 230 (2023). Publisher: Elsevier Ltd, p. 109951. ISSN: 0360-1323.
- [59] Ambar Tariq, Jagbir Singh, and Sushil Kumar Singh. “Wind Load Analysis on Gable Roof of Low-Rise Building”. eng. In: *IOP Conference Series: Earth and Environmental Science* 1110.1 (2023). Place: Bristol Publisher: IOP Publishing, p. 12093. ISSN: 1755-1307.
- [60] Alberto Meiss, Miguel A. Padilla-Marcos, and Jesús Feijó-Muñoz. “Methodology applied to the evaluation of natural ventilation in residential building retrofits: A case study”. eng. In: *Energies (Basel)* 10.4 (2017). Place: BASEL Publisher: MDPI AG, p. 456. ISSN: 1996-1073.
- [61] Yuguo Li, Angelo Delsante, and Jeff Symons. “Prediction of natural ventilation in buildings with large openings”. eng. In: *Building and environment* 35.3 (2000). Place: OXFORD Publisher: Elsevier Ltd, pp. 191–206. ISSN: 0360-1323. (Visited on 11/17/2022).
- [62] Stergiani Charisi, Thomas K. Thiis, and Tormod Aurlen. “Full-scale measurements of wind-pressure coefficients in twin medium-rise buildings”. eng. In: *Buildings (Basel)* 9.3 (2019). Place: Basel Publisher: MDPI AG, p. 63. ISSN: 2075-5309.
- [63] Lars Gullbrekken, Sivert Uvsløkk, Tore Kvande, Kaj Pettersson, and Berit Time. “Wind pressure coefficients for roof ventilation purposes”. eng. In: *Journal of wind engineering and industrial aerodynamics* 175 (2018). Place: AMSTERDAM Publisher: Elsevier Ltd, pp. 144–152. ISSN: 0167-6105.
- [64] Hans Martin Mathisen. *Air jets*. Lecture given in the subject TEP4315 - Indoor environment. NTNU, Oct. 2022.
- [65] Xin Nie, Zhihang Chen, and Zehui Zhu. “Assessment of Low-Reynolds Number  $k-\epsilon$  Models in Prediction of a Transitional Flow with Coanda Effect”. eng. In: *Applied sciences* 13.3 (2023). Place: Basel Publisher: MDPI AG, p. 1783. ISSN: 2076-3417.
- [66] Amit Bardia, Rabya Saraf, Andrew Maslow, Kamal Khabbaz, and Feroze Mahmood. “The Coanda Effect”. eng. In: *Anesthesia and analgesia* 123.3 (2016). Place: PHILADELPHIA Publisher: International Anesthesia Research Society, pp. 582–584. ISSN: 0003-2999.
- [67] *About the ZEB Centre*. URL: <http://www.zeb.no/index.php/en/about-zeb/about-the-zeb-centre> (visited on 11/06/2022).
- [68] Thomas L. L. Baxter and Arne Frøland-Larsen. *ZEB Flexible lab - Energikonsept*. Unpublished internal document. June 2020.
- [69] A Nocente, B Time, HM Mathisen, T Kvande, and A Gustavsen. “The ZEB Laboratory: the development of a research tool for future climate adapted zero emission buildings”. eng. In: *Journal of Physics: Conference Series* 2069.1 (2021). Publisher: IOP Publishing, p. 12109. ISSN: 1742-6588.
- [70] Arne Frøland-Larsen. *ZEB FLEXIBLE LAB Status ZEB-COM Målpris 2 - Dokumentasjon*. Unpublished internal document. Nov. 2017.

- [71] Bravida. *Leveransebeskrivelse - ZEB flexible lab*. Unpublished internal document. Dec. 2018.
- [72] IDA ICE - Simulation Software | EQUA. URL: <https://www.equa.se/en/ida-ice> (visited on 12/18/2022).
- [73] SENSIRION. *Datasheet SDP8xx-Analog: Differential Pressure Sensor with Analog Output*. Mar. 2018. URL: [https://sensirion.com/media/documents/68DF0025/6167E542/Sensirion\\_Differential\\_Pressure\\_Datasheet\\_SDP8xx\\_Analog.pdf](https://sensirion.com/media/documents/68DF0025/6167E542/Sensirion_Differential_Pressure_Datasheet_SDP8xx_Analog.pdf) (visited on 11/22/2022).
- [74] Voltcraft. *Operating instructions: Data logger Item No. 2203101 (DL-250V: Voltage)*. URL: <https://asset.conrad.com/media10/add/160267/c1/-/gl/002203098ML00/manual-2203101-voltcraft-dl-250v-voltage-data-logger-unit-of-measurement-voltage-001-up-to-30-v-pdf-generator.pdf> (visited on 11/22/2022).
- [75] HK instruments. *Differential Pressure Transmitters: DPT-Priima\_MOD: Multifunctional high accuracy differential pressure transmitters*. 2022. URL: [https://hkstruments.fi/wp-content/uploads/2022/06/DPT-Priima-MOD\\_Series\\_Datasheet-1.0.pdf](https://hkstruments.fi/wp-content/uploads/2022/06/DPT-Priima-MOD_Series_Datasheet-1.0.pdf) (visited on 11/22/2022).
- [76] SENSIRION. *Application Note for SDP800 Series differential pressure sensors: Compensation of pressure drop in a hose*. Feb. 2019. URL: [https://sensirion.com/media/documents/E2B13D4F/6166C422/Sensirion\\_Differential\\_Pressure\\_Datasheet\\_SDP800\\_Pressure\\_drop\\_in\\_ho.pdf](https://sensirion.com/media/documents/E2B13D4F/6166C422/Sensirion_Differential_Pressure_Datasheet_SDP800_Pressure_drop_in_ho.pdf) (visited on 11/22/2022).

# A Facade drawings of the ZEB Laboratory



Figure A.1: Facade drawings of the ZEB Laboratory of the north facade

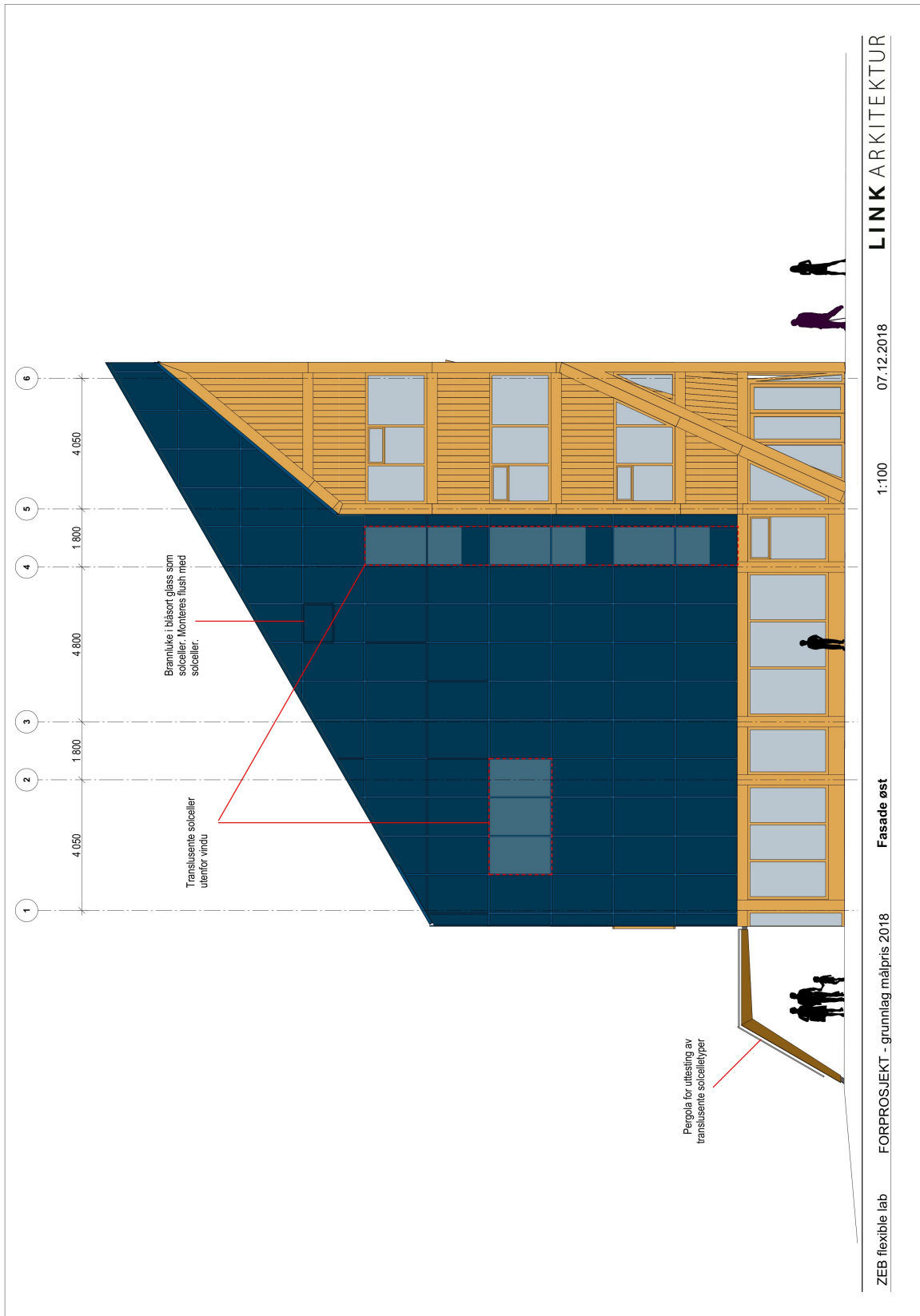
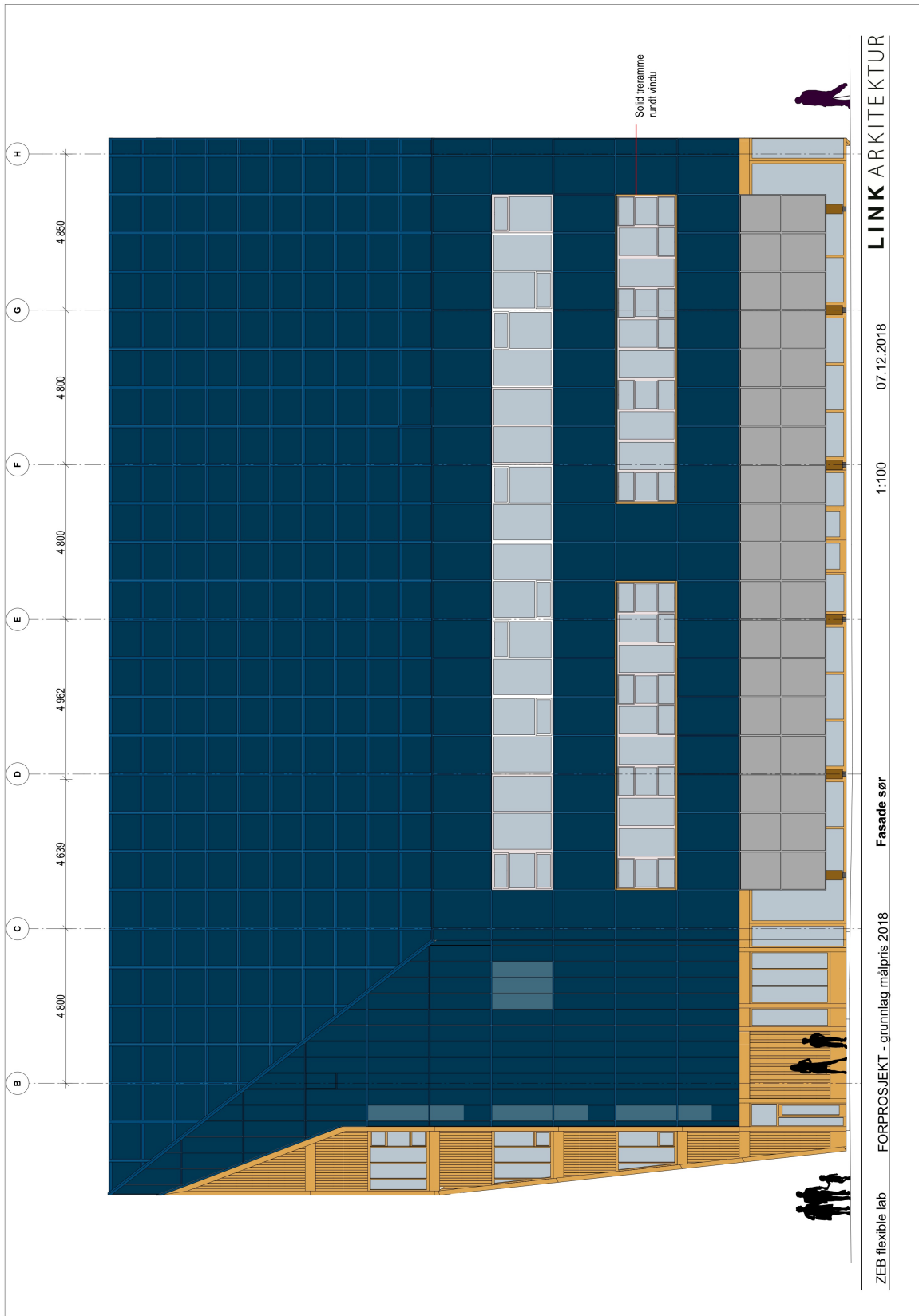
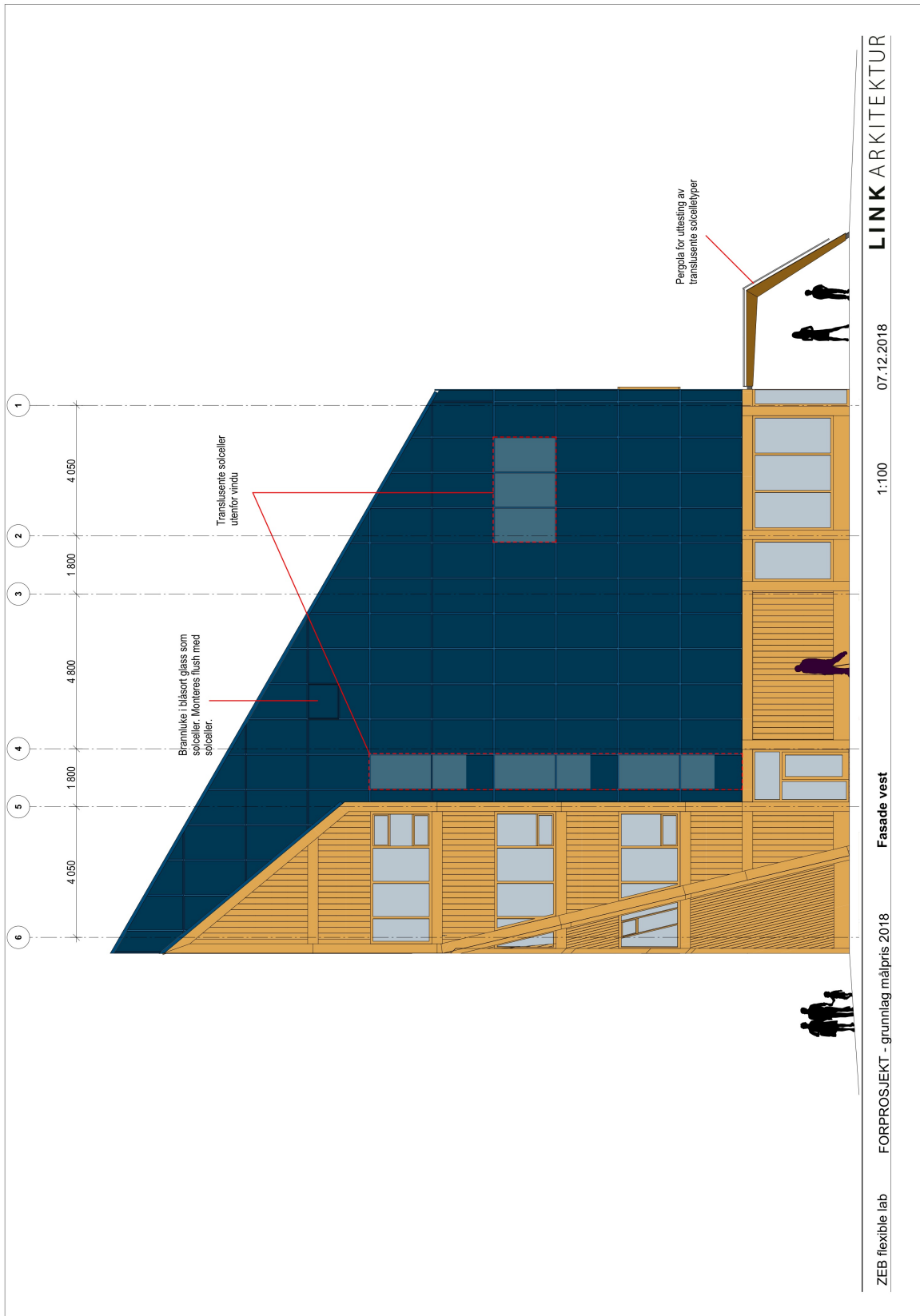


Figure A.2: Facade drawings of the ZEB Laboratory of the east facade



**Figure A.3:** Facade drawings of the ZEB Laboratory of the south facade





**Figure A.4:** Facade drawings of the ZEB Laboratory of the west facade

# B ZEB Laboratory floor plans



Figure B.1: Floor plan of the first floor of the ZEB Laboratory.



Figure B.2: Floor plan of the second floor of the ZEB Laboratory.



Figure B.3: Floor plan of the third floor of the ZEB Laboratory

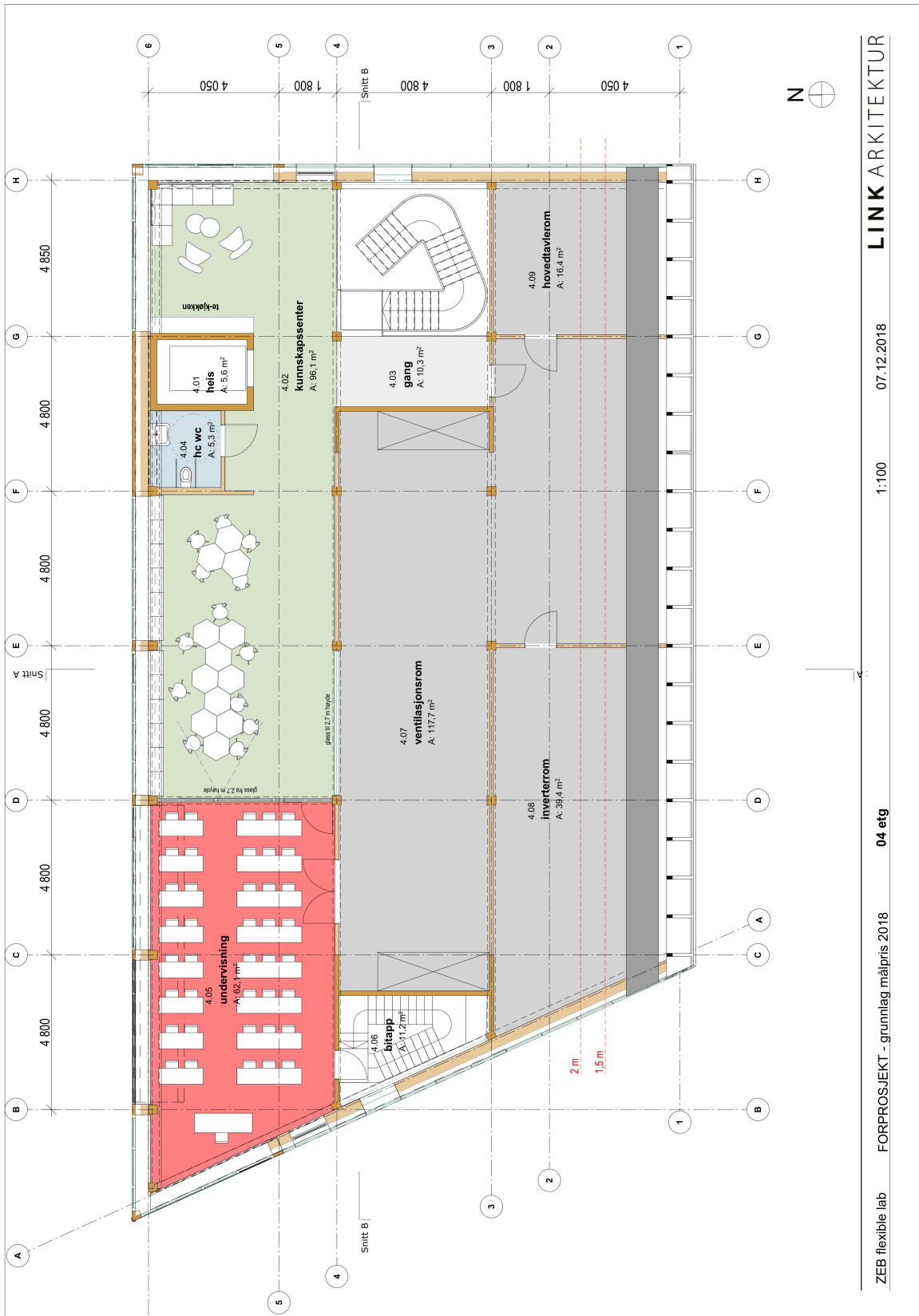
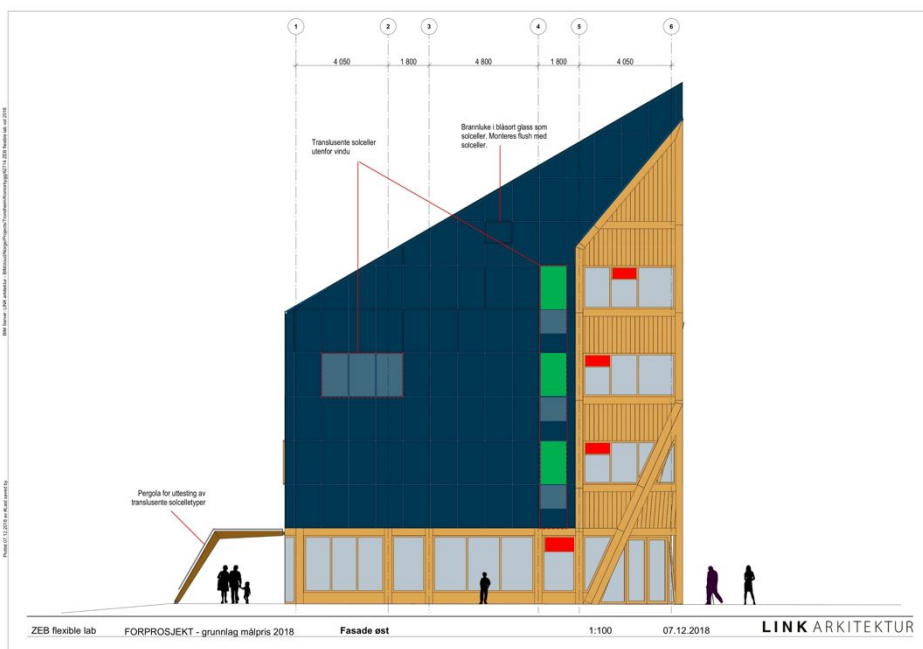


Figure B.4: Floor plan of the fourth floor of the ZEB Laboratory

## C Placement of the manual and automatic windows in the ZEB Laboratory



**Figure C.1:** Placement of the manual and automatic windows on the north facade. The manual windows are illustrated in green, and the automatic windows are illustrated in red. The real placement of the windows, shown in the figure, deviates slightly from the architectural facade drawings.



**Figure C.2:** Placement of the manual and automatic windows on the east facade. The manual windows are illustrated in green, and the automatic windows are illustrated in red. The real placement of the windows, shown in the figure, deviates slightly from the architectural facade drawings.

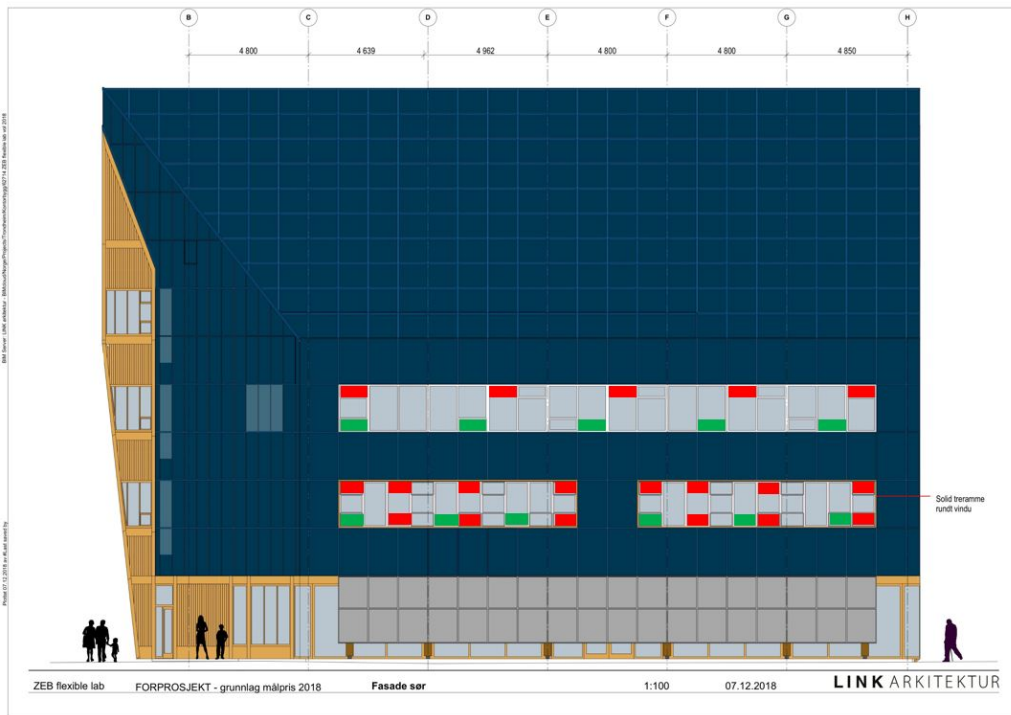


**Figure C.3:** Placement of the manual and automatic windows on the south facade. The manual windows are illustrated in green, and the automatic windows are illustrated in red. The real placement of the windows, shown in the figure, deviates slightly from the architectural facade drawings.

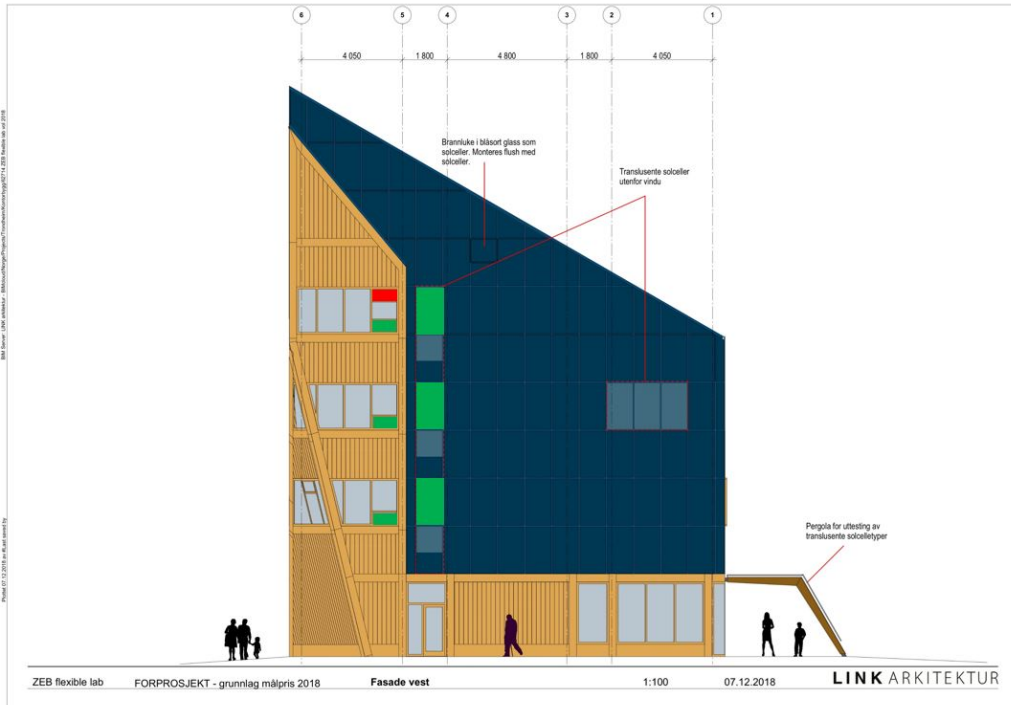


**Figure C.4:** Placement of the manual and automatic windows on the north facade. The manual windows are illustrated in green, and the automatic windows are illustrated in red. The real placement of the windows, shown in the figure, deviates slightly from the architectural facade drawings.

# D Raw output data from the differential pressure measurements

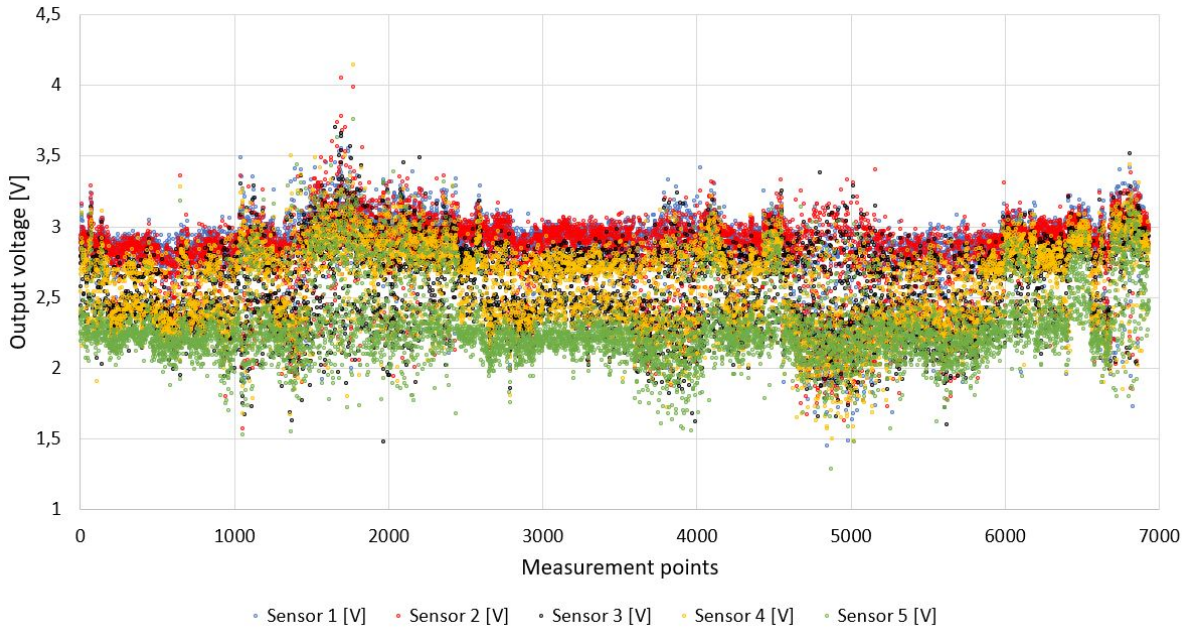


Figure D.1: Raw data from sensors 1, 2, 3, 4, and 5 placed on the north facade.

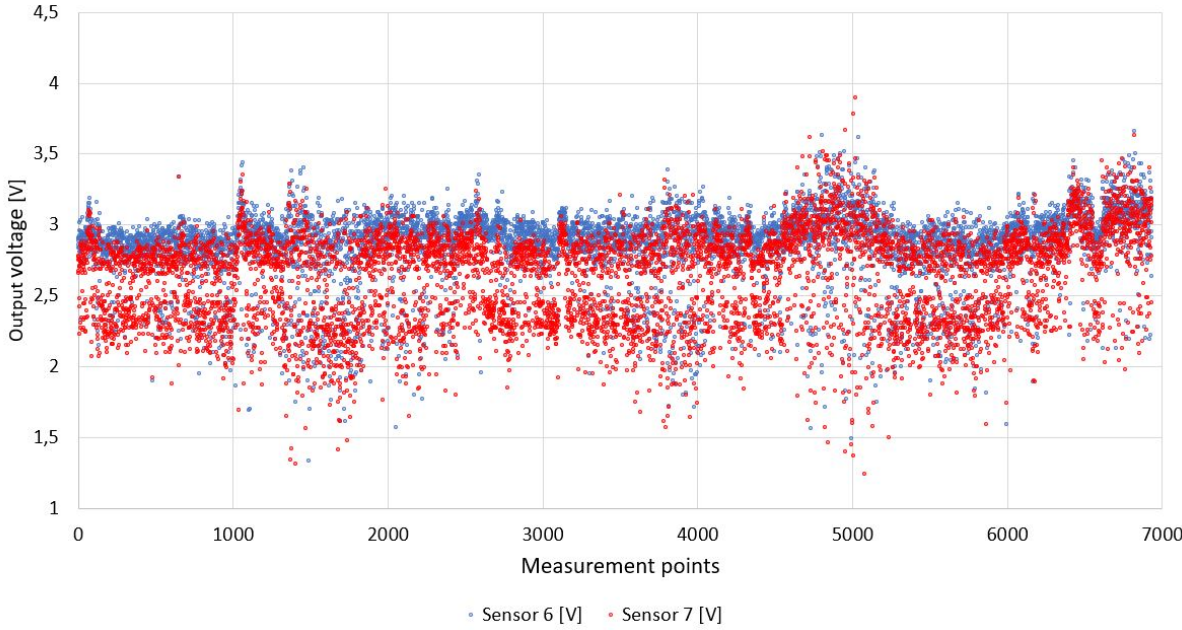
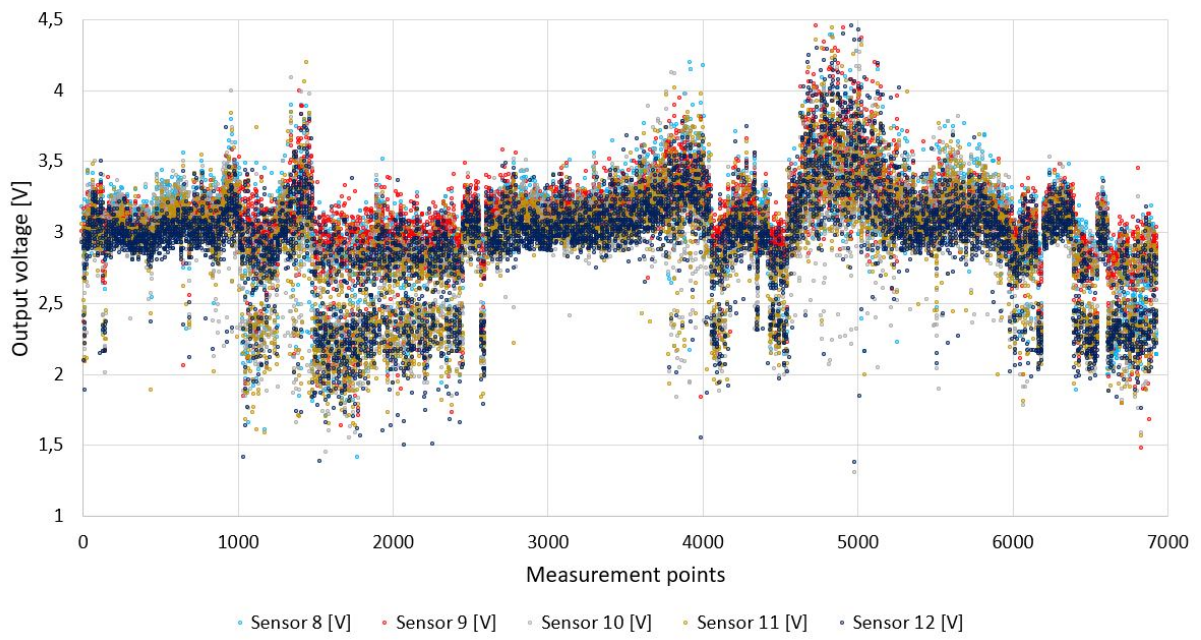
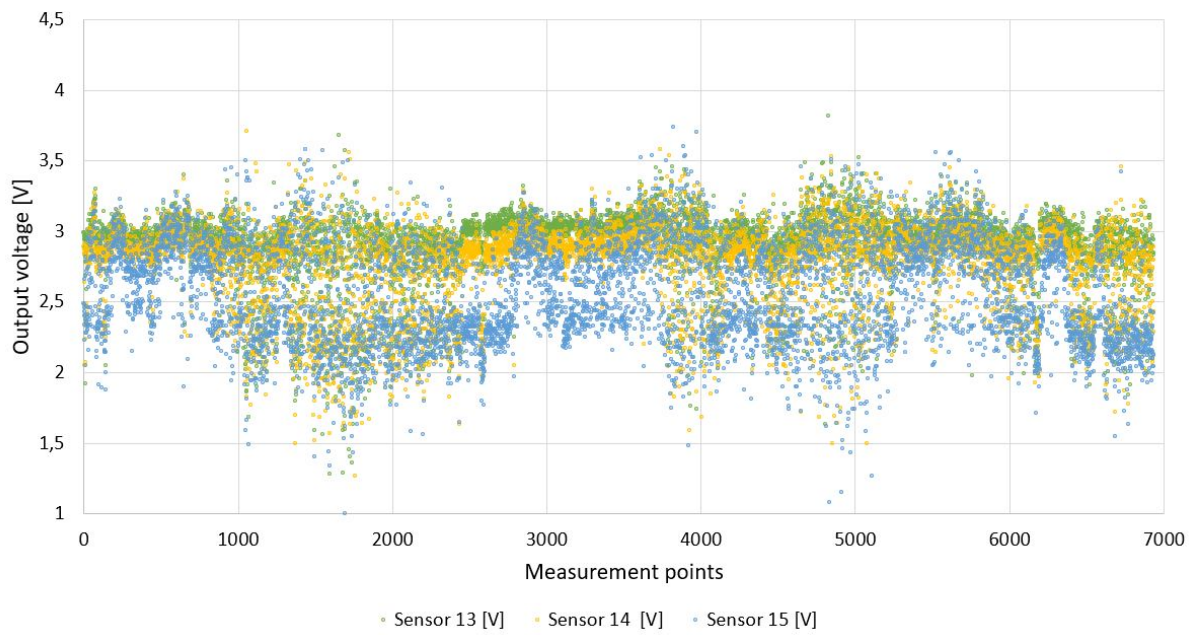


Figure D.2: Raw data from sensors 6 and 7 placed on the east facade.





**Figure D.3:** Raw data from sensors 8, 9, 10, 11, and 12 placed on the south facade.



**Figure D.4:** Raw data from sensors 13, 14, and 15 placed on the west facade

# E Raw output data from the reference sensor

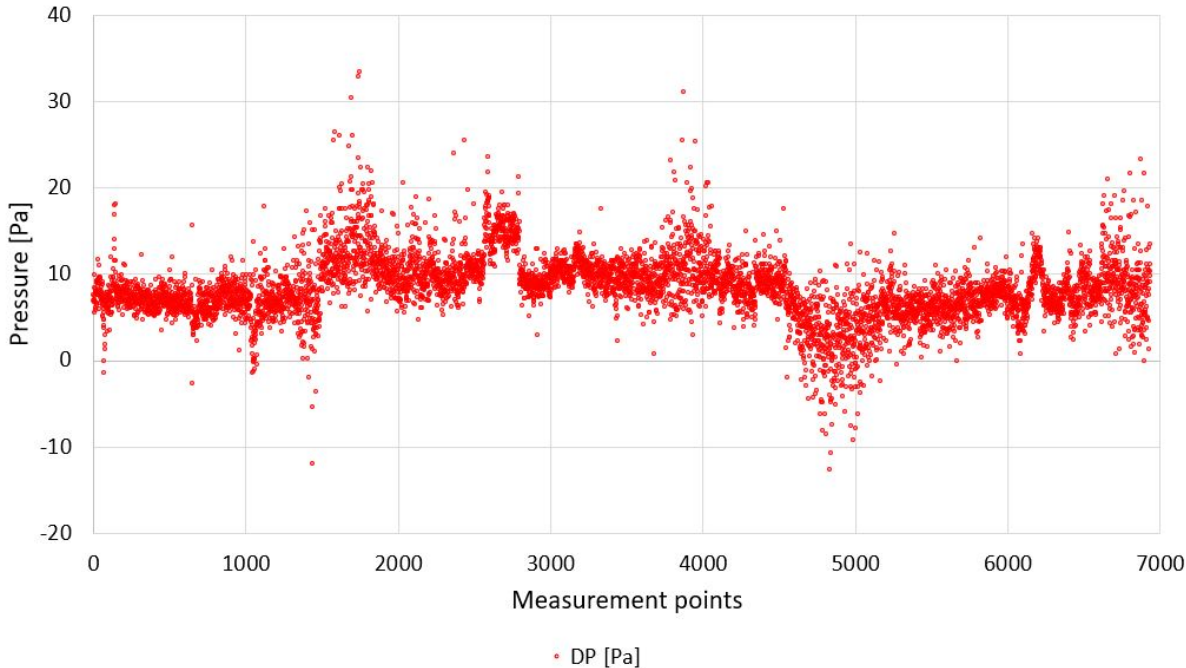
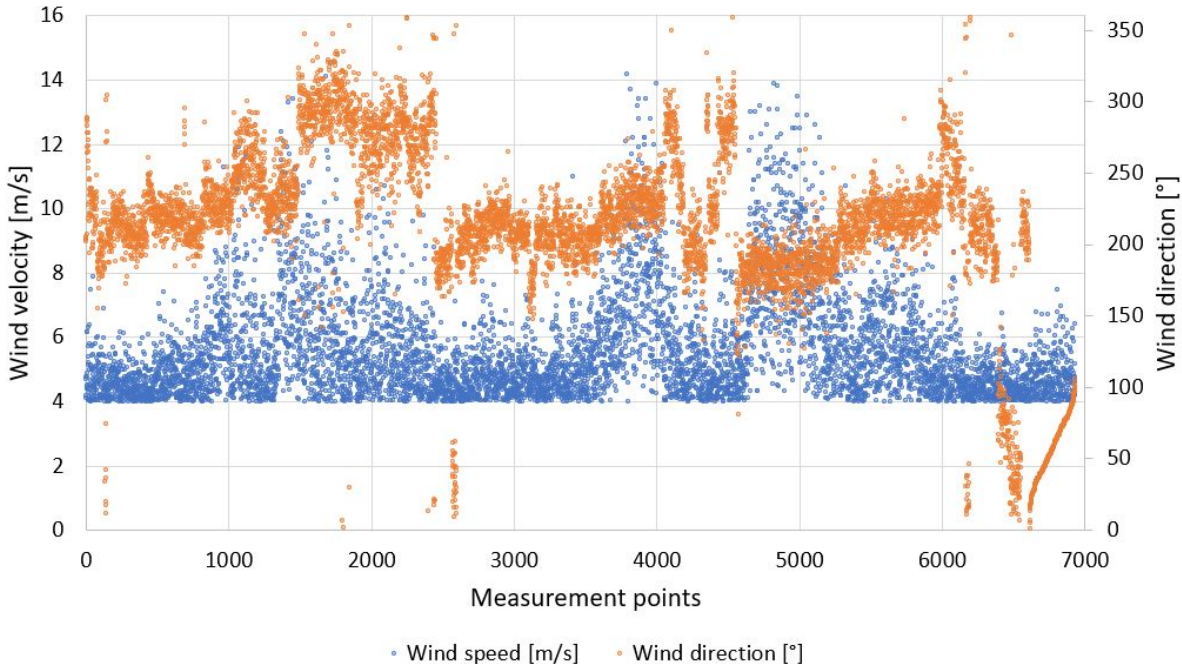
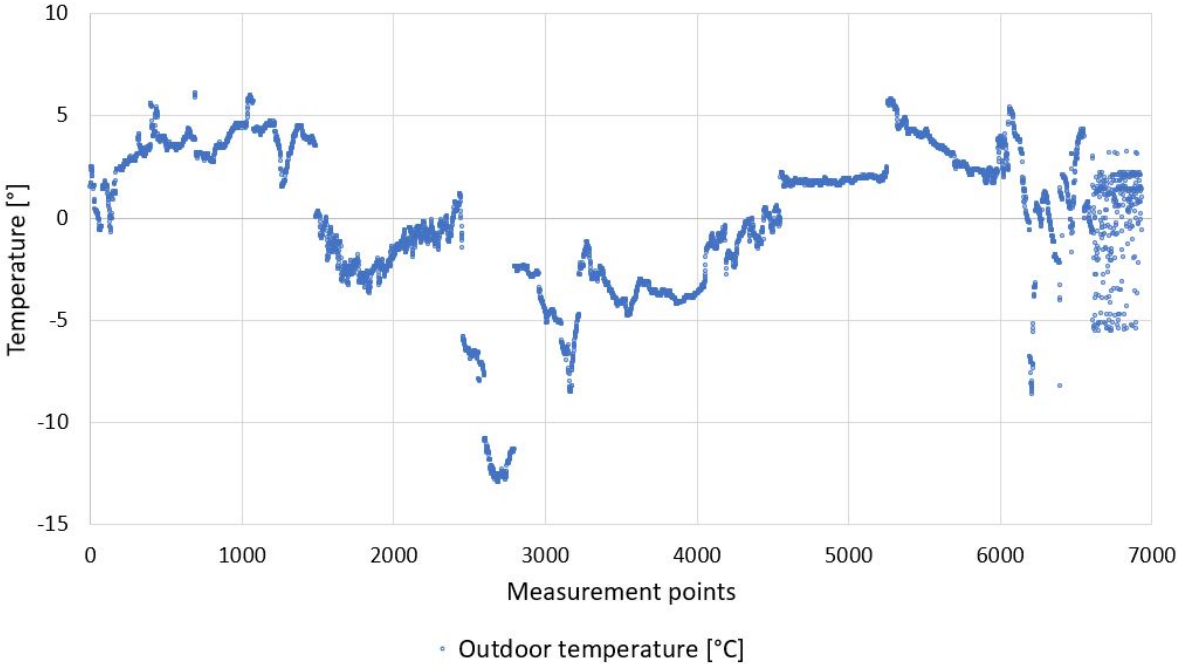


Figure E.1: Raw data from the reference sensor

# F Raw output data from weather station



**Figure F.1:** Raw data of the wind velocity and wind direction obtained from the weather station.



**Figure F.2:** Raw data of the outdoor temperature obtained from the weather station.

## G Calculation of differential pressure

This part will show the equations used to derive equation 6.5 used to calculate the pressure coefficients. Where the different points used are placed is illustrated in figure 6.11.

Firstly, equation G.1 can be rearranged into equation G.2 to find the pressure against the window,  $P_v$ .

$$\Delta P_{m,v} = P_v - P_i \quad (\text{G.1})$$

$$P_v = \Delta P_{m,v} + P_i \quad (\text{G.2})$$

Then, equation G.3 can be rearranged into equation G.4. Here, the height compensation over the tube is included as well, and  $P_{i,s}$  is the indoor pressure and is defined in equation G.5.

$$\Delta P_{m,t} = P_{i,s} - P_t - \Delta P_{tube} \quad (\text{G.3})$$

$$P_t = -\Delta P_{m,t} + P_{i,s} - \Delta P_{tube} \quad (\text{G.4})$$

$$P_{i,s} = P_i - \Delta P_i \quad (\text{G.5})$$

Further, the freestream pressure,  $P_f$ , is calculated in equation G.6 by implementing equations G.4 and G.5.

$$P_f = P_t + \Delta P_{out} = -\Delta P_{m,t} + P_i - \Delta P_i - \Delta P_{tube} + \Delta P_{out} \quad (\text{G.6})$$

Equations G.2 and G.6 are used to calculate the differential pressure and find the pressure coefficient, derived in equation G.7.

$$\begin{aligned} \Delta P &= P_v - P_f \\ &= \Delta P_{m,v} + P_i - (-\Delta P_{m,t} + P_i - \Delta P_i - \Delta P_{tube} + \Delta P_{out}) \\ &= \Delta P_{m,v} + P_i + \Delta P_{m,t} - P_i + \Delta P_i + \Delta P_{tube} - \Delta P_{out} \\ &= \Delta P_{m,v} + \Delta P_{m,t} + \Delta P_i + \Delta P_{tube} - \Delta P_{out} \end{aligned} \quad (\text{G.7})$$

## H Description of the window control algorithm

The window control algorithm, in figure H.1, is marked with letters. The description of the mechanism for the respective controllers is described below.

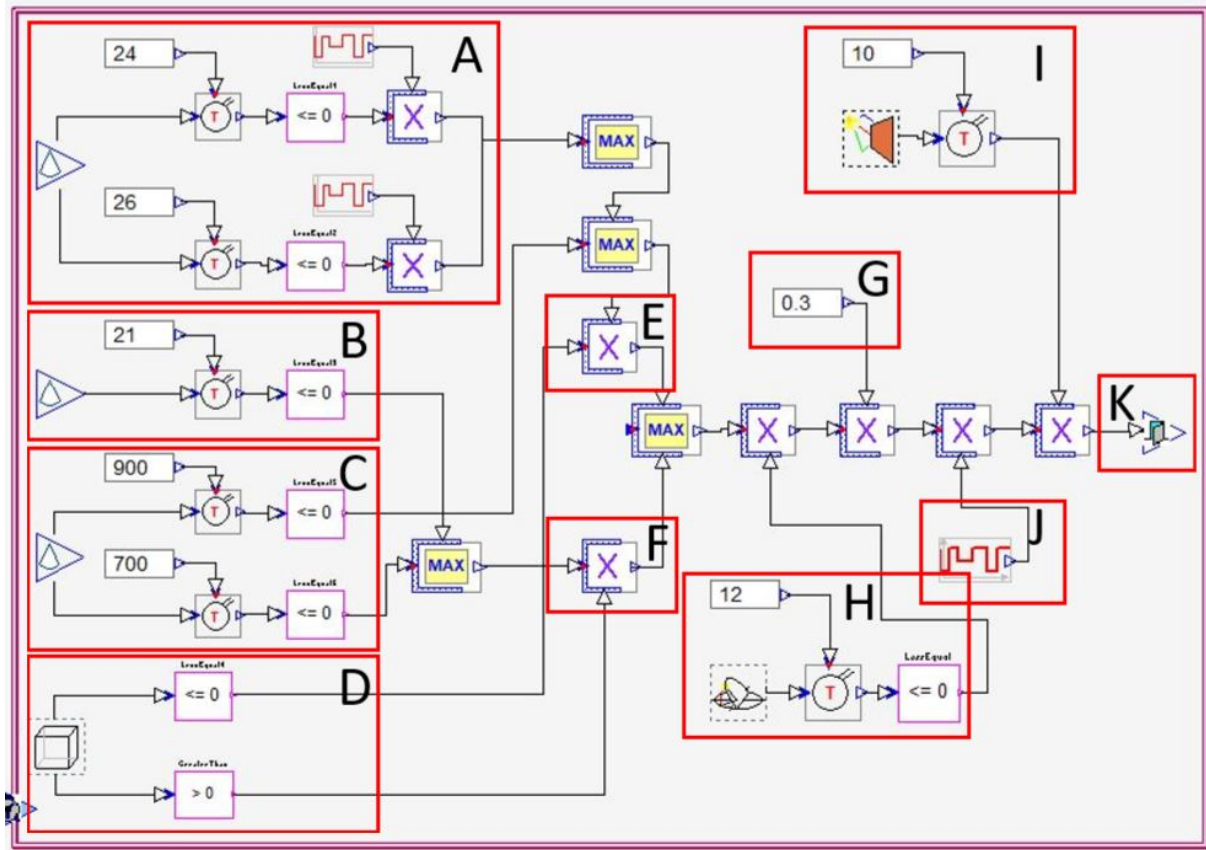


**Figure H.1:** Detailed description of the window control algorithm.

- A Sends the maximum air temperature of the specific zone
- B Sends the minimum air temperature of the specific zone
- C Sends the limits for CO<sub>2</sub> concentrations of the specific zone
- D Sends 1 if the window is open and 0 if the window is closed
- E Sends 1 if the air temperature in the specific zone exceeds 24° during the daytime and 26° during the nighttime, or if the CO<sub>2</sub> concentration exceeds 900 ppm, given that the window was closed
- F Sends 1 if the air temperature is above 21° or the CO<sub>2</sub> concentration exceeds 700 ppm, given that the window is open
- G The maximum percentage of opening set to 30%
- H Sends 1 if the ambient temperature is above 12°

- I Sends 1 if the wind velocity is below  $10\frac{m}{s}$
- J Changes between daytime and nighttime ventilation at 07:00 and 18:00
- K Opens the window if the resulting signal is 1 and closes the window if the resulting signal is 0


# Risk Assessment Report

## [ZEB-Laboratory]

<b>Project name</b>	Master - Mechanical, Natural and Hybrid Ventilation for the ZEB Laboratory
<b>Facility name</b>	ZEB-Laboratory
<b>Building and room number</b>	ZEB-Laboratory
<b>Project leader</b>	Hans Martin Mathisen
<b>Facility responsible</b>	Tore Kvande, IBM
<b>HES coordinator</b>	Morten Grønli
<b>HES responsible</b>	Terese Løvås
<b>Risk assessment performed by</b>	Ingebjørg Eggen Skarbøvik

### *Approval:*

<b>Apparatur kort (UNIT CARD) valid for:</b>	
<b>Forsøk pågår kort (EXPERIMENT IN PROGRESS) valid for:</b>	

Role	Name	Date	Signature
Project leader	Hans Martin Mathisen	2023-01-24	
HES coordinator	Morten Grønli		
HES responsible	Terese Løvås		



 **NTNU**

Norwegian University of  
Science and Technology